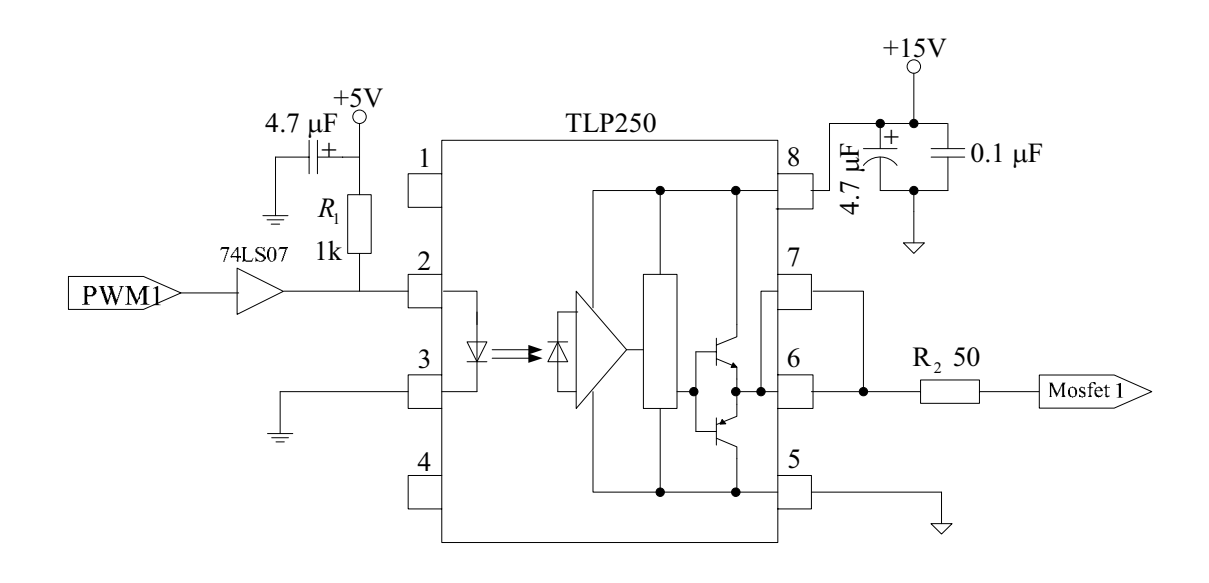
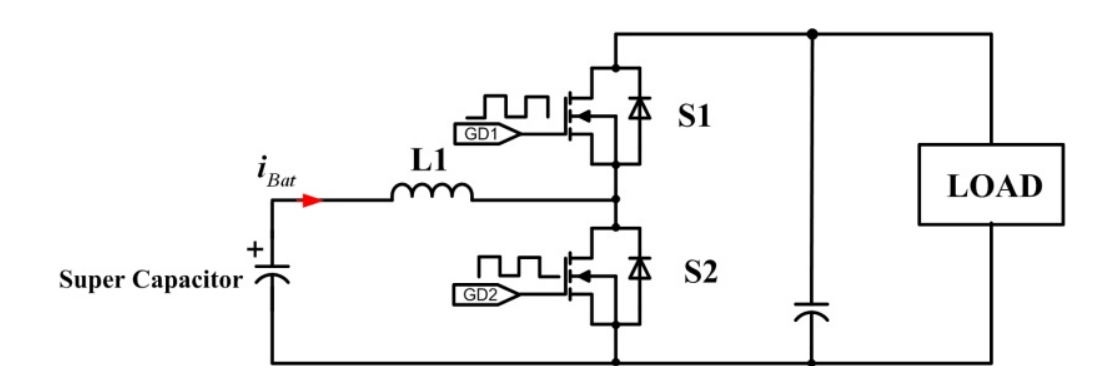
2.2.2.4 วงจรขับเกต (Gate Driver) เพื่อความสะดวกในการต่อใช้งานและให้วงจรขับมีขนาดเล็ก จึงใช้ ไอซีสำเร็จรูปเบอร์ TLP 250 ขนาด 8 ขา ซึ่งในวงจรทบแรงดันขนาด 2 เฟส จะต้องทำการสร้างวงจรขับ เกตขึ้นมาทั้งหมด 2 วงจรเพื่อทำหน้าที่ขับเกตของมอสเฟตทั้ง 2 ตัว จากภาพที่ 2-18 สัญญาณอินพุต จากไมโครคอนโทรลเลอร์เข้ามายังขา 2 และขา 3 ของ TLP250 เพื่อจัดไบอัสให้แก่โฟโต้ไดโอดที่ต่ออยู่ ภายในตัวไอซี TLP250 ระหว่างขา 2 และขา 3 โดยที่ขา 2 ของ TLP250 ต่อเข้ากับ Vcc (+5 V) เพื่อ รักษาระดับของแรงดันให้คงที่ ทำให้โฟโต้ไดโอดทำงานได้อย่างเต็มที่ ซึ่งจะต่อ Pull up ตัวต้านทาน 1 $\mathbf{k}\Omega$ ทำหน้าที่ควบคุมกระแสที่ไหลผ่านออปโต้คัปเปอร์ โดยสัญญาณเอาต์พุตจะได้ตามคุณสมบัติของไอซี ชึ่ง TLP 250 มีลักษณะเป็นไปตามสัญญาณอินพุตที่ป้อนเข้ามา แต่มอสเฟตกำลังเป็นอุปกรณ์สวิตช์ กำลังที่ต้องการแรงดันควบคุมให้มอสเฟตกำลังทำงาน ดังนั้นสัญญาณที่เข้ามาควบคุมจะต้องเป็น สัญญาณพัลส์ที่สามารถทำให้มอสเฟตกำลังทำงานได้และหยุดทำงานได้รวดเร็วตามความต้องการซึ่ง จะต้องเป็นสัญญาณพัลส์แบบสี่เหลี่ยม โดยที่ไอซี TLP 250 ถูกจัดวงจรตามคุณสมบัติของไอซีคือจะ ได้รับการป้อนแรงดันไฟตรง 15 V เข้าที่ขา 8 และต่อกราวด์เข้าที่ขา 5 ของไอซี โดยสัญญาณเอาต์พุตที่ จะออกมาจากขา 6 และขา 7 ของไอซีเมื่อเทียบกับกราวด์ที่ขา 5 ของไอซี สัญญาณที่ได้ออกมาเป็นพัลส์ จะมีระดับของสัญญาณอยู่ที่ +15 V ตามแหล่งจ่ายไฟที่ป้อนให้กับไอซีและความถี่ที่ได้จะเท่ากับความถึ่ ของสัญญาณอินพุตที่ป้อนให้กับไอซีและ R2 จะเป็นตัวควบคุมกระแสที่ ที่จะไหลผ่านไปยังขา G ของ เพาเวอร์มอสเฟตและเมื่อทำการวัดระดับสัญญาณที่ได้ที่ขา G และขา S ของเพาเวอร์มอสเฟตสัญญาณ ที่ได้เหมาะสมกับความต้องการของมอสเฟตกำลังที่สามารถทำงานเป็นสวิตช์ได้



ภาพที่ 2-18 วงจรขับเกต

2.3 ตัวแปลงไฟสำหรับแบตเตอรื่ชนิดซุปเปอร์คาปาซิเตอร์

2.3.1 การออกแบบวงจรกำลังของวงจรทบแรงดันไฟฟ้ากระแสตรง (2-Quadrant Converter)



ภาพที่ 2-19 วงจรบูสต์คอนเวอร์เตอร์ 2 ทิศทาง

จากภาพที่ 2-19 เป็นส่วนของวงจรทบแรงดันแบบ 2 ทิศทาง มีมอสเฟตกำลังทำหน้าที่เป็น สวิตช์รับคำสั่งการสวิตช์มาจากตัวขับเกตต่อเข้าที่จุด GD1 และ GD2 ในวงจรกำลังจะประกอบไปด้วย การออกแบบส่วนต่างๆ ดังนี้

2.3.1.1 การคำนวณหาค่าตัวเหนี่ยวนำความถี่สูง ในวงจรทบแรงดันไฟฟ้ากระแสตรง ตัวเหนี่ยวนำเป็น อุปกรณ์ที่สำคัญมาก เนื่องจากมีหน้าที่ในการเก็บและคายพลังงานเป็นผลให้ระดับแรงดันทางเอาต์พุตมี ค่าสูงกว่าระดับแรงดันที่อินพุตการคำนวณหาค่าของตัวเหนี่ยวนำสามารถหาได้จากสมการ

$$L_{\min} = \frac{D(1-D)^2 R}{2f}$$
 (2-16)

เมื่อ $L_{
m min}$ คือค่าตัวเหนี่ยวนำต่ำสุดที่สามารถใช้งานได้ในวงจร

f คือความถี่ที่ใช้ในวงจร มีค่า 25 kHz

R คือค่าความต้านทานโหลดของวงจรหาได้จาก

$$R = \frac{V_{bus}^2}{Po_{\min}} \tag{2-17}$$

เมื่อ V_{bus} คือแรงดันด้านออกของวงจรที่ต้องการมีค่า 60 V Po_{\min} คือกำลังทางด้านเอาต์พุตที่ให้ประสิทธิภาพต่ำสุดหาได้จากสมการที่ (2-18)

$$\eta_{\min} = \frac{Po_{\min}}{Pi_{\max}} \tag{2-18}$$

 η_{\min} คือประสิทธิภาพต่ำสุดของวงจรที่ต้องการคือ 80 เปอร์เซ็นต์ Pi_{\max} คือกำลังทางด้านอินพุตที่ให้ประสิทธิภาพต่ำสุด หาได้จากสมการที่ (2-19)

$$Pi_{\max} = V_{bat \max} i_{bat \max}$$
 (2-19)

 $V_{bat
m max}$ คือแรงดันของแบตเตอรี่สูงสุดคือ 24 V $i_{bat
m max}$ คือกระแสของแบตเตอรี่สูงสุดคือ 20 A แทนค่าลงในสมการที่ (2-19)

$$Pi_{\text{max}} = 24 \times 20 = 480 \,\text{W}$$

แทนค่า $\mathit{Pi}_{\mathrm{max}}$ ลงในสมการที่ (2-18) เพื่อหา $\mathit{Po}_{\mathrm{min}}$

$$Po_{\min} = \eta_{\min} Pi_{\max}$$

$$Po_{\min} = \frac{80}{100} \times 480 = 384 \,\text{W}$$

แทนค่า Po_{\min} ลงในสมการที่ (2-17)

$$R = \frac{V_{bus}^{2}}{Po_{min}} = \frac{60^{2}}{384} = 9.357\Omega$$

จากสมการที่ (2-1) $\,D\,$ คือดิวตี้ไซเคิล หาได้จาก

$$D = 1 - \frac{V_{bat}}{V_{bus}} \tag{2-20}$$

เมื่อ V_{bat} คือ แรงดันอินพุต มีค่า 24 V แทนค่าลงในสมการที่ (2-20)

$$D = 1 - \frac{24}{60} = 0.6$$

แทนค่าลงในสมการที่ (2-16) เพื่อหาค่าตัวเหนี่ยวนำ

$$L_{\min} = \frac{0.6(1-0.6)^2 \times 9.375}{2 \times 25 \times 10^3} = 18 \mu H$$

ดังนั้นจึง เลือกใช้ขดลวดพันบนแกน EE55 คำนวณหาจำนวนรอบของขดลวดได้จาก

$$N = \frac{LI_{peak}}{B_{\text{max}}S}$$

เมื่อ N คือจำนวนรอบของขดลวด

 $I_{\it peak}$ คือกระแสสูงสุดที่ใหลในขดลวด มีค่า 10 A

 $B_{
m max}$ คือความเข้มฟลักซ์สูงสุดได้จากกราฟ BH Curve มีค่า 0.025 T

S คือพื้นที่ของแกน EE55 มีค่า 354 mm 2

$$N = \frac{18 \times 10^{-6} \times 10}{0.012 \times 10^{-6} \times 354} = 42.37$$
 รอบ

2.3.1.2 การเลือกอุปกรณ์สวิตซิ่ง อุปกรณ์สวิตซิ่งในวงจรทบแรงดันไฟฟ้ากระแสตรงควรเลือกอุปกรณ์ที่ ทำงานได้ดีที่ความถี่สูง เวลาในการเปลี่ยนสถานะค่อนข้างสั้น ในการวิจัยนี้ได้เลือกใช้มอสเฟตกำลังทำ หน้าที่เป็นอุปกรณ์สวิตซิ่ง เพราะนอกจากสามารถทำงานที่ความถี่สูงได้ตั้งแต่ 30 kHz ไปจนถึง 400 kHz เวลาในการสวิตซ์อยู่ในช่วงนาโนวินาที และในวงจรขับมอสเฟตกำลังนั้นทำได้ง่ายเพราะควบคุม ด้วยแรงดันและต้องการกระแสอินพุตค่าต่ำๆ เท่านั้น

โดยใด้เลือกใช้เพาเวอร์มอสเฟตเบอร์ IRFP264 ของบริษัท International Rectifier IR มี คุณลักษณะสมบัติต่าง ๆ ที่สำคัญดังนี้ ความต้านทานระหว่างขาเดรนและซอร์ส ขณะนำกระแส $R_{DS(on)}=0.075\Omega$ ซึ่งมีค่าต่ำมาก แรงดันตกคร่อมระหว่างขาเดรนและขาซอร์ส (V_{DS}) ที่ทนได้ 250 V กระแสเดรน (I_D) สูงสุดที่สามารถไหลผ่านได้ 38 A เวลาคืนสภาพของเพาเวอร์มอสเฟต $t_{rr}=620\,ns$

2.3.1.3 การคำนวณหาค่าตัวเก็บประจุด้านเอาต์พุต ในวงจรกำลังของวงจรทบแรงดันไฟฟ้าตัวเก็บประจุ ด้านเอาต์พุตของวงจรมีหน้าที่ในการเก็บพลังงานในรูปของประจุไฟฟ้าและทำการจ่ายแรงดันออกให้กับ เอาต์พุตหรือภาระ (Load) หรือคายประจุไฟฟ้าเมื่ออุปกรณ์สวิตชิ่ง Turn on และทำการเก็บประจุ เมื่อ อุปกรณ์สวิตชิ่ง Turn off ดังนั้นจำเป็นต้องเลือกตัวเก็บประจุที่สามารถทนแรงดันได้เท่ากับหรือมากกว่า แรงดันเอาต์พุต หากเลือกตัวเก็บประจุที่มีขนาดใหญ่จะมีส่วนช่วยในการลดแรงดันกระเพื่อมทางด้าน เอาต์พุต สามารถคำนวณหาค่าตัวเก็บประจุทางด้านเอาต์พุตได้จากสมการที่ (2-21)

$$\frac{\Delta V_{bus}}{V_{bus}} = \frac{D}{RCf}$$
 (2-21)

เมื่อ $rac{\Delta V_{bus}}{V_{bus}}$ คือค่า Ripple Factor กำหนดให้มีค่าไม่เกิน 1 เปอร์เซ็นต์

 ΔV_{bus} คือแรงดันกระเพื่อมทางด้านเอาต์พุต

 V_{bus} คือแรงดันเอาต์พุต มีค่า 60 V

C คือค่าตัวเก็บประจุทางด้านเอาต์พุต

D คือดิวตี้ไซเคิล หาได้จากสมการที่ (2-5) มีค่า 0.6

R คือค่าความต้านทานโหลดของวงจร

f คือความถี่ที่ใช้ในวงจร มีค่า 25 kHz

แทนค่าในสมการที่ (2-21) เพื่อหา ΔV_{bus}

$$\frac{\Delta V_{bus}}{60} = 0.01$$

ดังนั้น

$$\Delta V_{bus} = 0.01 \times 60 = 0.6 \text{V}$$

หาค่าตัวเก็บประจุทางด้านเอาต์พูตจากสมการที่ (2-21)

$$C = \frac{D}{Rf \frac{\Delta V_{Bus}}{V_{Bus}}}$$

แทนค่า

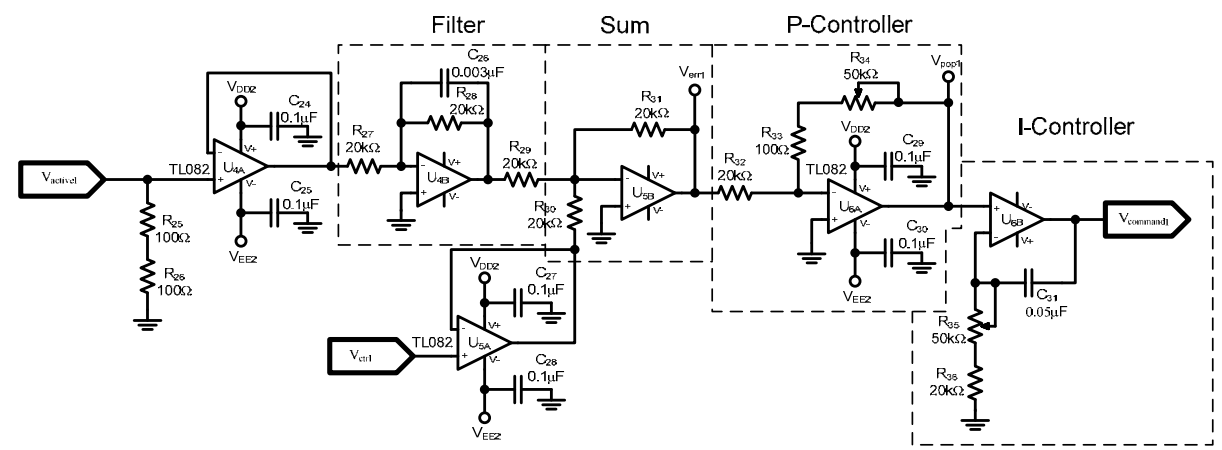
$$C = \frac{0.6}{9.375 \times 25 \times 10^3 \times 0.01} = 256 \mu F$$

ดังนั้นควรเลือกตัวเก็บประจุทางด้านเอาต์พุตของวงจรที่มีค่าสูงกว่า 256 µF และแรงดันที่ทนได้ ต้องไม่ต่ำกว่าแรงดันเอาต์พุตที่ 60 V

2.3.2 การออกแบบวงจรควบคุม

วงจรควบคุมกระแสเป็นวงจรที่ทำหน้าที่ควบคุมให้ระดับการจ่ายกระแสคงที่ถึงแม้ว่าภาระจะมี การเปลี่ยนแปลง การจัดวงจรควบคุมแสดงดังภาพที่ 2-20 จุดต่ออินพุต V_{ctr} เป็นจุดรับสัญญาณคำสั่ง จาก dSPACE เพื่อควบคุมการจ่ายกระแสของคอนเวอร์เตอร์ทั้งหมด จุดต่ออินพุต $V_{active1}$ เป็นจุดต่อรับ สัญญาณป้อนกลับค่ากระแสจากเซนเซอร์กระแสที่ได้รับการแปลงให้เป็นแรงดันแล้ว จากวงจรตรวจจับ กระแสและจุดต่อเอาต์พุต $V_{command1}$ เป็นจุดต่อสัญญาณออกจากตัวควบคุมไปให้วงจรกำเนิดสัญญาณ PWM เพื่อควบคุมการสวิตช์ต่อไป จัดเป็นวงจรกันชนเพื่อป้องกันไม่ให้วงจรดึงกระแสที่จุด $V_{active1}$ และ V_{ctr} ซึ่งอาจทำให้แรงดันทั้ง 2 จุดลดลงจนการทำงานของคอนเวอร์เตอร์ผิดพลาดได้ U1B จัดเป็นวงจรกรองแรงดันเพื่อกรองแรงดัน $V_{active1}$ จากเซนเซอร์กระแสให้มีความเรียบมากที่สุด เพราะสัญญาณที่ได้ จากเซนเซอร์กระแสยังมีการกระเพื่อมตามลักษณะของกระแสจากตัวเหนี่ยวนำความถี่สูงอยู่ ส่วน U2B

เป็นวงจรเป็นวงจรรวมสัญญาณระหว่างสัญญาณคำสั่ง V_{ctrl} กับสัญญาณ $V_{active1}$ แต่เนื่องจาก $V_{active1}$ ถูก กลับเฟสสัญญาณเพราะเป็นการป้อนกลับค่ากระแสแบบลบ ทำให้เอาต์พุตที่จุด V_{errl} เป็นผลต่างของ V_{ctrl} - $V_{active1}$ ส่งต่อไปยังตัวควบคุมกระแสแบบ PI



ภาพที่ 2-20 วงจรควบคุมกระแสของตัวแปลงไฟสำหรับแบตเตอร์รี่

จากการคำนวนทำให้ได้ค่า K_p ของ P-Controller และค่า T_i ของ I-Controller ในภาพที่ 2-20 ที่ ทำให้ได้การตอบสนองต่อคำสั่ง V_{ctr} ได้ในเวลาที่ต้องการ ณ จุดที่ค่า $K_p=0.285$ และค่า $T_i=2.085$ ms ดังนั้นสามารถคำนวณหาค่าอุปกรณ์ต่างๆ ได้ดังนี้

จากสมการโอนย้ายของวงจรควบคุมแบบ PI แบบอิสระต่อกัน

$$\frac{V_{command1}(s)}{V_{err1}(s)} = K_P \left(1 + \frac{1}{T_i s} \right)$$
 (2-22)

เมื่อ $V_{command1}(s)$ คือแรงดันเอาต์พุตของตัวควบคุมแบบ PI

 $V_{\it err1}(s)$ คือแรงดันผลต่างของ $V_{\it ctrl}$ - $V_{\it active 1}$

โดยที่อัตราขยายของ $K_{\scriptscriptstyle P}$ หาได้จากสมการ

$$K_P = \frac{R_{33} + R_{34}}{R_{32}} \tag{2-23}$$

ในการออกแบบเลือกค่าความต้านทาน R_{32} = 20 k Ω และ R_{33} = 100 Ω หาค่า R_{34} โดยแทนค่า ลงสมการที่ (2-23)

$$R_{34} = 0.285 \times 20 \text{k}\Omega - 100\Omega = 5.6 \text{k}\Omega$$

เพื่อลดความผิดพลาดที่อาจเกิดขึ้นจากตัวอุปกรณ์ในการใช้งานจริงเลือกใช้ R_{34} เป็นตัวต้านทาน ปรับค่าที่สามารถปรับค่าครอบคลุมค่าความต้านทาน 5.6 k Ω เพื่อปรับให้ได้ค่าที่ใกล้เคียงที่สุด โดย เลือกใช้ตัวต้านทานปรับค่า 50 k Ω

ในส่วนของ I-Controller คำนวณหาค่าอุปกรณ์ได้จากสมการ

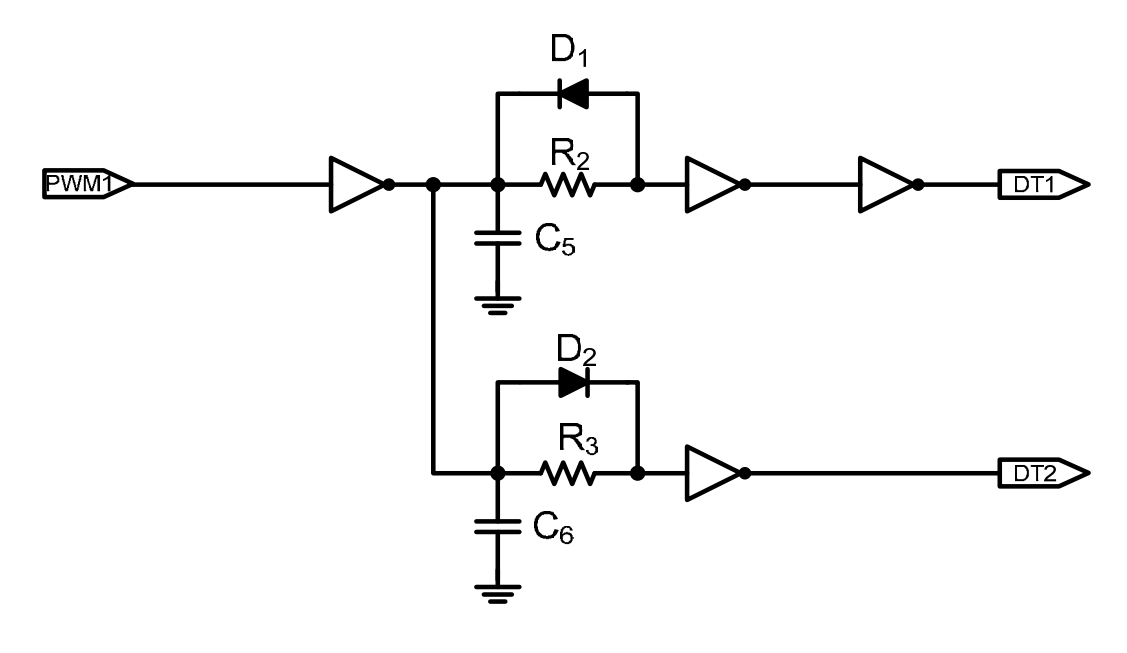
$$T_i = (R_{35} + R_{36})C_{31} (2-24)$$

การออกแบบในงานวิจัยเลือกใช้ค่าความต้านทาน R_{36} = 20 k Ω และค่าของตัวเก็บประจุ C_{31} = 0.05 μ F คำนวณหาค่า R_{35} โดยแทนค่าลงในสมการที่ (2-24)

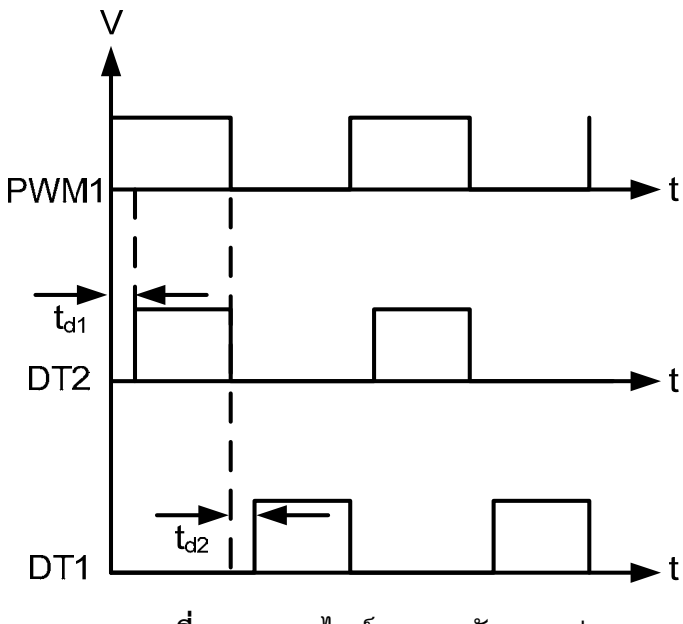
2.085ms=
$$(R_{35}+20k\Omega)0.05\mu F$$

 $R_{35} = \frac{2.085ms}{0.05\mu F} -20k\Omega = 21.7k\Omega$

2.3.2.1 วงจรเดดไทม์ (Dead time circuit) วงจรดังภาพที่ 2-21 ทำหน้าที่ในการหน่วงสัญญาณคำสั่ง สวิตช์เพื่อป้องกันไม่ให้ชุดสวิตช์ทั้ง 2 ตัวในแต่ละเฟสทำงานพร้อมกัน โดยสัญญาณคำสั่งสวิตช์จะถูก หน่วงด้วยตัวต้านทานและตัวเก็บประจุในขอบขาขึ้นเท่านั้น ก็เพียงพอที่จะป้องกันไม่ให้เกิดการลัดวงจร ของสวิตช์ทั้ง 2 ชุด และเมื่อสัญญาณอินพุตเป็น High หลังจากผ่าน NOT GATE ก็จะเปลี่ยนสถานะเป็น Low ตัวเก็บประจุตึ่งมีแรงดันสูงอยู่ก็จะคายประจุผ่านตัวต้านทาน เมื่อระดับแรงดันที่ตัวเก็บประจุต่ำถึง ระดับที่ NOT GATE มองเป็นสถานะ Low สัญญาณเอาต์พุตเป็น High ช่วงนี้จะไม่มีการหน่วงเวลา เพราะกระแสไหลผ่านไดโอดมาชาร์จตัวเก็บประจุแล้วเต็มทันที ทำให้เอาต์พุตของ NOT GATE อีกตัว เป็น Low การปรับค่าความต้านทานจะทำให้ระยะการหน่วงเวลาเปลี่ยนไปลักษณะการหน่วงของ Dead time แสดงดังภาพที่ 2-22



ภาพที่ 2-21 วงจรเดดไทม์ (Dead time circuit)



ภาพที่ 2-22 เดดไทม์ของการขับมอสเฟต

จากภาพที่ 2-21 เป็นวงจรเดดไทม์ จุดต่อ PWM1 เป็นจุดรับสัญญาณที่ได้จากวงจรกำเนิด สัญญาณ PWM ส่วนทางด้านเอาต์พุตจุดต่อ DT1 และ DT2 เป็นส่วนที่ได้ถูกกำหนดเดดไทม์แล้วเพื่อส่ง ต่อไปยังวงจรขับเกตต่อไป

จากข้อมูลของไอซี NOT GATE เบอร์ 74LS14 ที่ใช้ในวงจรเดดไทม์ สัญญาณอินพุตที่ทำให้ เอาต์พุตเป็นลอจิก "1" คือแรงดันอินพุต 1.6 V มอสเฟตกำลังที่ใช้มีเวลาในการคืนสภาพ (t_n) 620 นาโน วินาที คิดเวลาที่อีกตัวหนึ่งทำงานได้เต็มที่และอีกตัวหนึ่งหยุดทำงานสนิท ควรหน่วงเวลาทั้งหมด 2 t_n ดังนั้นเวลาหน่วงมีค่า 620 นาโนวินาที x 2 = 1,240 นาโนวินาที หรือ1.24 ไมโครวินาที ในวงจรเดด ไทม์นี้คิดเวลาหน่วงประมาณ 2 ไมโครวินาที เลือกใช้ค่า C_5 = 3 nF คำนวณหาค่า R_2 ได้จาก

$$V_{\rm C5} = V_{CC} \left(1 - e^{-t_{d2}/R_2 C_5} \right)$$

เมื่อ V_{C5} คือ แรงดันที่ตกคร่อม $\mathbf{C_5}$ ที่ทำให้อินพุตเป็นสถานะ high คือ 1.6 V V_{CC} คือ แรงดันไฟเลี้ยงวงจรมีค่า 5 V

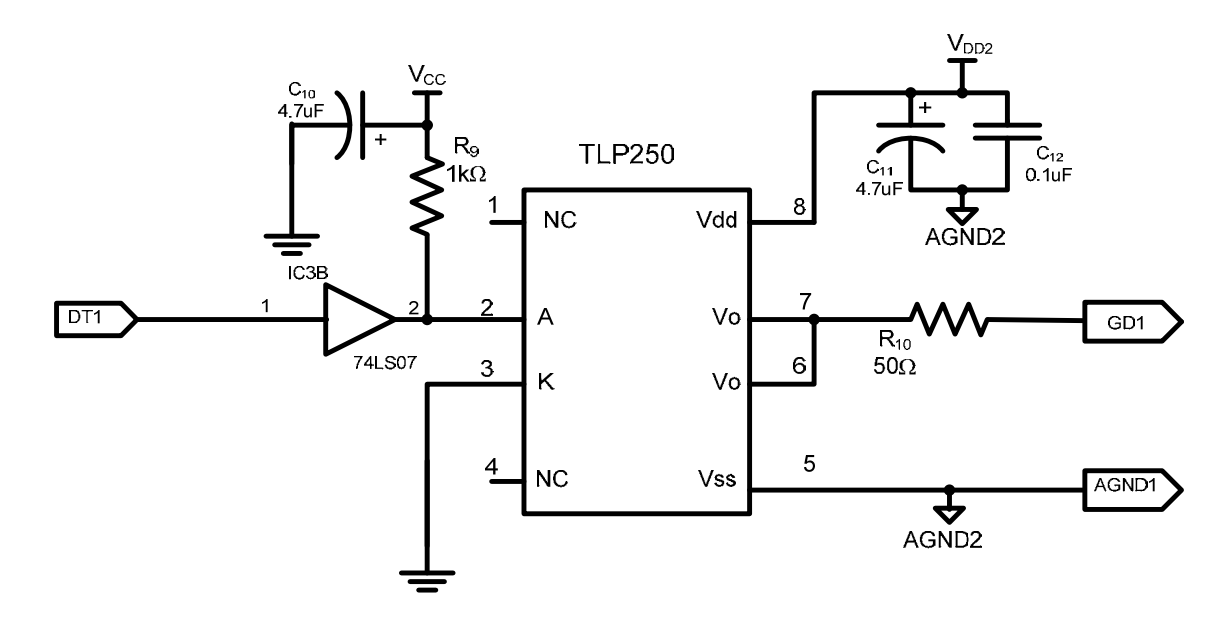
แทนค่าลงในสมการด้านบน

$$1.6 = 5\left(1 - e^{-2 \times 10^3 / R_2 \times 3 \times 10^{-9}}\right)$$

$$R_2 = -0.67 \times 10^3 \frac{\log e}{\log 0.68} = 1.74 \text{k}\Omega$$

ในการใช้งานจริง เลือกใช้งาน R_2 มีค่า 2 Ω ซึ่งทำให้ค่าเดดไทม์ที่ได้จริงมีค่า 2.31 ไมโครวินาที

2.3.2.2 วงจรชับนำเกต ด้วยไอซี TLP250 สัญญาณที่ผ่านการมอดูเลตตามความกว้างของพัลล์หรือ สัญญาณ PWM มีลักษณะเป็นสัญญาณพัลล์สี่เหลี่ยม สัญญาณนี้ถูกส่งไปยังวงจรชับนำเกตด้วยไอซีสร้าง สัญญาณขับนำเกตเบอร์ TLP250 เพื่อควบคุมการทำงานของมอสเฟต วงจรสร้างขับนำเกตแสดงดัง ภาพที่ 2-23 จากวงจรสัญญาณด้านเข้าเป็นสัญญาณที่ถูกส่งมาจากวงจรกำเนิดสัญญาณ PWM มีนาด แรงดัน 0 V ถึง 5 V สัญญาณนี้ถูกส่งเข้าไปไบแอสให้ LED ใน TLP250 นำกระแสโดยมีความต้านทาน R_9 ทำหน้าที่จำกัดกระแสในการไบแอสและใช้ไอซีบัฟเฟอร์ 74LS07 เป็นตัวป้องกันไฟ 5 V ที่จะเกิดการ ใหลย้อนกลับของแรงดันเข้าไปในวงจรกำเนิดสัญญาณ PWM เมื่อ LED นำกระแส ส่งผลทำให้ ทรานซิสเตอร์ซนิด NPN ทางด้านเอาต์พุตของ TLP250 นำกระแส แรงดันที่ขา 7 ของ TLP250 เทียบ กับกราวน์เท่ากับ VDD2 (15 V) เพียบกับกราวน์ เมื่อแรงดัน V_{GS} มีค่าเป็นบวกสามารถทำให้มอสเพตนำกระแสได้ ส่วนในกรณีที่แรงดันอินพุตน้อยกว่า 0.7 V LED ภายใน TLP250 หยุดนำกระแสส่งผลให้ทรานซิสเตอร์ซนิด NPN ทางด้านเอาต์พุตของ TLP250 หยุดนำกระแสเช่นเดียวกัน แต่ทรานซิสเตอร์ซนิด PNP จะนำกระแสส่งผลให้ ที่สภาวะนี้แรงดัน ที่ขา 7 ของ TLP250 เทียบกับกราวน์มีค่าประมาณ 0 V เมื่อแรงดันที่ V_{GS} มีค่าเป็น 0 V ก็จะทำให้มอส เฟตหยุดนำกระแสได้



ภาพที่ 2-23 วงจรขับนำเกตโดยใช้ไอซีเบอร์ TLP250

จากภาพที่ 2-23 จุดต่ออินพุตของวงจร จุด DT1 เป็นจุดรับสัญญาณจากวงจรเดดไทม์และที่ เอาต์พุตของวงจร จุด GD1 เป็นจุดต่อสัญญาณไปยังสวิตช์แต่ละตัวโดยจุดนี้จะเทียบกับจุด AGND1 ต่อ จุด GD1 เข้าที่ขาเกตของ S1 และจุด AGND1 เข้าที่ขาซอร์สจากภาพเป็นวงจรขับเกตจำนวน 1 ชุด ดังนั้นในการใช้งานต้องสร้างวงจรลักษณะเดียวกันนี้ทั้งหมด 2 ชุด

2.4 การบริหารจัดการพลังงานในระบบจ่ายไฟฟ้ากระแสตรงแบบผสมด้วยเซลล์เชื้อเพลิง เซลล์แสงอาทิตย์และแบตเตอร์รี่ชนิดซุปเปอร์คาปาซิเตอร์

2.4.1 วงจรกำลังสำหรับแหล่งจ่ายไฟแบบผสม

โครงสร้างการต่อวงจรกำลังของแหล่งจ่ายไฟแบบผสมนี้แสดงได้ดังภาพที่ 2-24 [24] ตัวแปลงไฟ สำหรับเซลล์เชื้อเพลิงคือวงจรบูสที่ขนานกัน 4 ชุด (หัวข้อ 2.1) ตัวแปลงไฟสำหรับเซลล์แสงอาทิตย์คือ วงจรบูสที่ขนานกัน 2 ชุด (หัวข้อ 2.2) ตัวแปลงไฟสำหรับซุปเปอร์คาปาซิเตอร์คือวงจรแปลงไฟแบบ 2 ทิสทาง (2-Quadrant Converter) ที่ขนานกัน 4 ชุด (หัวข้อ 2.3)

เพื่อเป็นการป้องกันและการทำงานที่มีความเร็วสูง ตัวแปลงไฟของเซลล์เชื้อเพลิง เซลล์ แสงอาทิตย์และซุปเปอร์คาปาซิเตอร์จะถูกควบคุมด้วยวงปิดของการควบคุมกระแสของแต่ละตัว ดัง อธิบายไปแล้วในหัวข้อ 2.1 2.2 และ 2.3 เพื่อแน่ใจว่าระบบทำงานที่มีเสถียรภาพ (Stability) ความเร็ว ของวงปิดระบบควบคุมกระแสซึ่งเป็นระบบควบคุมวงในสุด (inner current regulation loops) จะต้อง ทำงานที่ความเร็วสูงกว่าระบบควบคุมวงปิดของระบบคุมควบวงนอก (outer control loops) [25] ระบบ ควบคุมกระแสนี้จะรับคำสั่งอ้างอิง (References) สามสัญญาณคือกระแสคำสั่งของซุปเปอร์คาปาซิเตอร์ i_{SCREF} กระแสคำสั่งของเซลล์เชื้อเพลิง i_{FCREF} และกระแสคำสั่งของเซลล์แสงอาทิตย์ i_{PVREF} กระแสคำสั่ง ทั้งสามนี้จะถูกกำเนิดมาจากตัวควบคุมบริหารจัดการพลังงานทั้งระบบ ซึ่งจะนำเสนอดังต่อไปนี้

2.4.2 แบบจำลองทางคณิตศาสตร์ของแหล่งจ่ายไฟแบบผสม

เราพิจารณาให้กระแสของเซลล์เชื้อเพลิง กระแสของเซลล์แสงอาทิตย์และกระแสของซุปเปอร์คา ปาซิเตอร์ทำงานตามกระแสคำสั่งอย่างรวดเร็ว ดังนั้น

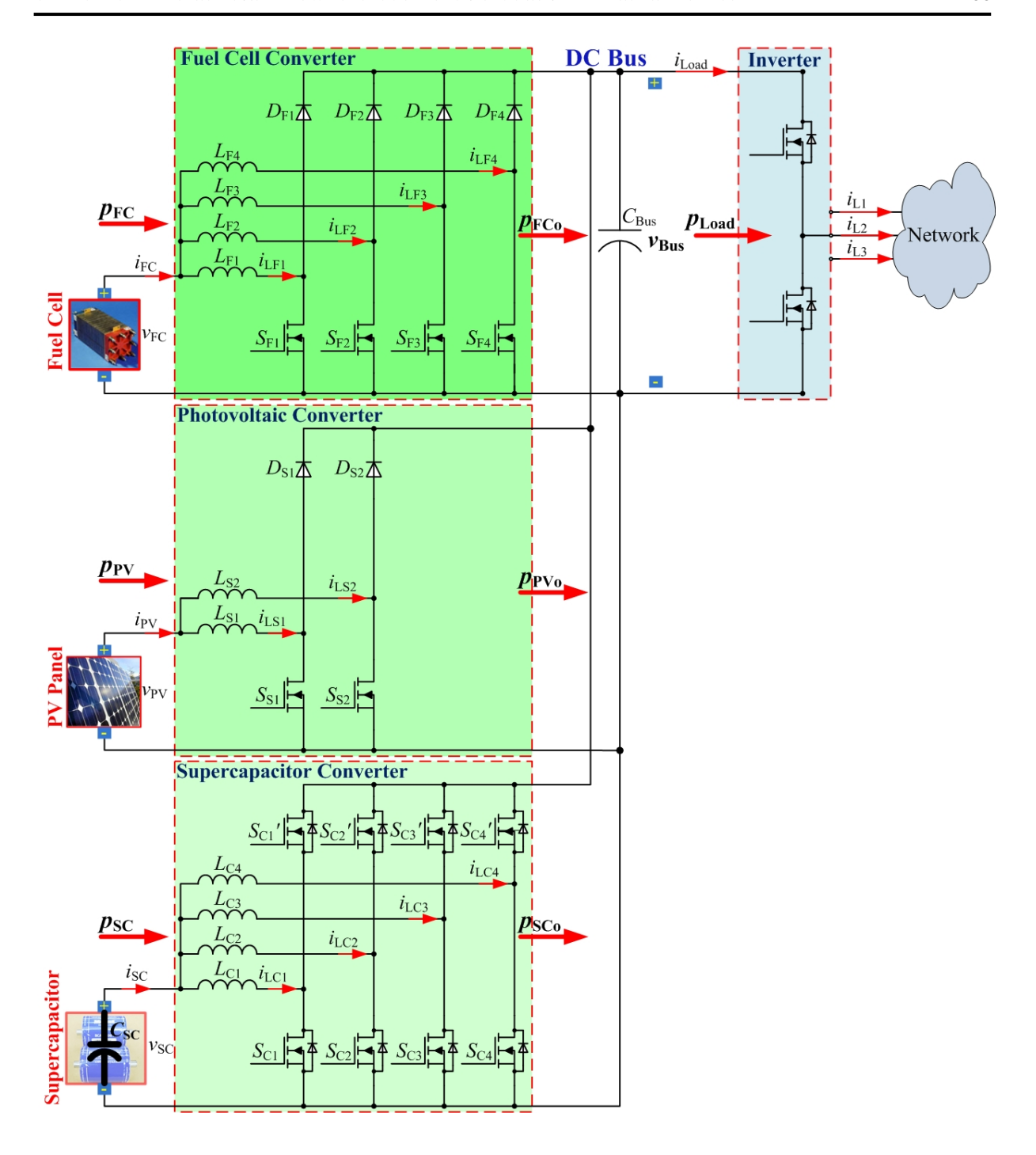
$$i_{\text{FC}} = i_{\text{FCREF}} = \frac{p_{\text{FC}}}{v_{\text{FC}}} = \frac{p_{\text{FCREF}}}{v_{\text{FC}}}$$
 (2-25)

$$i_{\text{PV}} = i_{\text{PVREF}} = \frac{p_{\text{PV}}}{v_{\text{PV}}} = \frac{p_{\text{PVREF}}}{v_{\text{PV}}}$$
 (2-26)

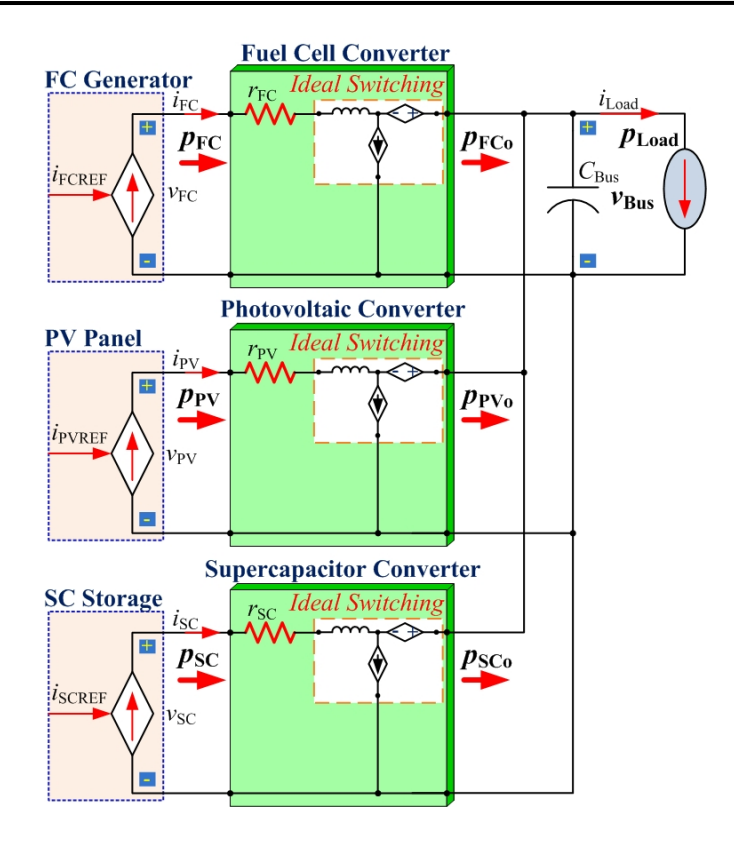
$$i_{\text{SC}} = i_{\text{SCREF}} = \frac{p_{\text{SC}}}{v_{\text{SC}}} = \frac{p_{\text{SCREF}}}{v_{\text{SC}}}$$
 (2-27)

เป็นผลทำให้เซลล์เชื้อเพลิง เซลล์แสงอาทิตย์และกระแสของซุปเปอร์คาปาซิเตอร์ทำงานเป็น แหล่งจ่ายกระแสที่ควบคุมได้ (Controlled current sources) แสดงได้ดังภาพที่ 2-25 เราพิจารณาให้มี ค่าสูญเสียในตัวแปลงไฟแต่ละตัวเป็นตัวต้านทานที่มีค่าสูญเสียคงที่คือ r_{FC} , r_{PV} และ r_{SC} ของตัวแปลงไฟ ของเซลล์เชื้อเพลิง ของตัวแปลงไฟของเซลล์แสงอาทิตย์และของตัวแปลงไฟของซุปเปอร์คาปาซิเตอร์ ตามลำดับ

พลังงานไฟฟ้าที่คาปาซิเตอร์ในบัสไฟตรง (E_{Bus}) และพลังงานไฟฟ้าที่ซุปเปอร์คาปาซิเตอร์ (E_{SC}) สามารถเขียนได้ดังนี้



ภาพที่ 2-24 ใดอะแกรมของระบบจ่ายไฟด้วยเซลล์เชื้อเพลิง เซลล์แสงอาทิตย์และซุปเปอร์คาปาซิเตอร์ ซึ่ง p_{Load} (= $v_{\text{Bus}} \times i_{\text{Load}}$), v_{Bus} , และ i_{Load} คือกำลังของโหลด แรงดันที่บัสไฟตรงและกระแสที่บัสไฟตรง ตามลำดับ p_{FC} (= $v_{\text{FC}} \times i_{\text{FC}}$), v_{FC} , และ i_{FC} คือกำลัง แรงดันและกระแสของเซลล์เชื้อเพลิง ตามลำดับ p_{FC} (= $v_{\text{PV}} \times i_{\text{PV}}$), v_{PV} , และ i_{PV} คือกำลัง แรงดันและกระแสของเซลล์แสงอาทิตย์ ตามลำดับ p_{FC} (= $v_{\text{SC}} \times i_{\text{SC}}$), v_{SC} , และ i_{SC} คือกำลัง แรงดันและกระแสของซุปเปอร์คาปาซิเตอร์ ตามลำดับ p_{FCo} , p_{PVo} และ p_{SCo} คือกำลังเอาต์พุตที่ส่งไปยังบัสไฟตรงของเซลล์เชื้อเพลิง เซลล์แสงอาทิตย์และซุปเปอร์คาปาซิเตอร์ ตามลำดับ



ภาพที่ 2-25 วงจรเทียบเคียงของแหล่งจ่ายไฟแบบผสมที่นำเสนอ

$$E_{\text{Bus}} = \frac{1}{2} C_{\text{Bus}} v_{\text{Bus}}^2 \tag{2-28}$$

$$E_{\rm SC} = \frac{1}{2} C_{\rm SC} v_{\rm SC}^2 \tag{2-29}$$

ขณะที่พลังงานสะสมรวม (E_{T}) ที่เก็บอยู่ในคาปาซิเตอร์ที่บัสไปตรง (C_{Bus}) และในซุปเปอร์คาปาซิเตอร์ (C_{SC}) สามารถเขียนได้ดังนี้

$$E_{\rm T} = \frac{1}{2} C_{\rm Bus} v_{\rm Bus}^2 + \frac{1}{2} C_{\rm SC} v_{\rm SC}^2$$
 (2-30)

ดังแสดงในภาพที่ 2-25 สามารถเขียนเป็นสมการอนุพันธ์ของพลังงานไฟฟ้าที่คาปาซิเตอร์ในบัส ไฟตรง ($E_{
m Bus}$) กับ $p_{
m FCo}$, $p_{
m PVo}$, $p_{
m SCo}$, และ $p_{
m Load}$ ได้ดังนี้

$$\dot{E}_{\rm Bus} = p_{\rm FCo} + p_{\rm PVo} + p_{\rm SCo} - p_{\rm Load} \tag{2-31}$$

ซึ่ง

$$p_{\text{FCo}} = p_{\text{FC}} - r_{\text{FC}} \left(\frac{p_{\text{FC}}}{v_{\text{FC}}}\right)^2$$
 (2-32)

$$p_{\text{PVo}} = p_{\text{PV}} - r_{\text{PV}} \left(\frac{p_{\text{PV}}}{v_{\text{PV}}}\right)^2$$
 (2-33)

$$p_{\text{SCo}} = p_{\text{SC}} - r_{\text{SC}} \left(\frac{p_{\text{SC}}}{v_{\text{SC}}}\right)^2$$
 (2-34)

$$p_{\text{Load}} = v_{\text{Bus}} \cdot i_{\text{Load}} = \sqrt{\frac{2E_{\text{Bus}}}{C_{\text{Bus}}}} \cdot i_{\text{Load}}$$
 (2-35)

$$p_{\text{SC}} = v_{\text{SC}} \cdot i_{\text{SC}} = \sqrt{\frac{2E_{\text{SC}}}{C_{\text{SC}}}} \cdot i_{\text{SC}}$$
 (2-36)

2.4.3 การควบคุมแบบไม่เชิงเส้นสำหรับแหล่งจ่ายไฟแบบผสม

2.4.3.1 พลังงานสมดุลย์

วัตถุประสงค์ของการควบคุมคือความมีเสถียรภาพ (stability) ความแข็งแรง (robustness) ประสิทธิภาพ (high overall efficiency) และการทำงานที่เหมาะสมที่สุด (optimization) เพื่อจ่าย พลังงานให้กับโหลดและชาร์จซุปเปอร์คาปาซิเตอร์ ระบบควบคุมแบบหลายตัวแปรนี้จึงต้องมีคำสั่งอ้างอิง ของแรงดันที่บัสไฟตรง (v_{BusREF}) (แทนพลังงานที่บัสไฟตรง (E_{Bus}) ที่เราเรียกว่า "การมีเสถียรภาพที่บัส ไฟตรง DC link stabilization") และคำสั่งอ้างอิงของแรงดันที่ซุปเปอร์คาปาซิเตอร์ (v_{SCREF}) (แทน พลังงานที่ซุปเปอร์คาปาซิเตอร์ (E_{SC}) ที่เราเรียกว่า "supercapacitor state-of-charge SOC")

จากแนวคิดงานวิจัยก่อนหน้านี้ [26], [27] เซลล์แสงอาทิตย์จะถูกควบคุมเป็นแหล่งจ่ายหลัก เซลล์เชื้อเพลิงทำงานเป็นแหล่งจ่ายจ่ายไฟเมื่อพลังงานในสภาวะอยู่ตัวไม่พอจากเซลล์แสงอาทิตย์ ขณะที่ซุปเปอร์คาปาซิเตอร์เป็นแหล่งพลังงานที่มีความเร็วสูงมากๆ จะช่วยจ่ายไฟช่วงไดนามิกส์สูงๆ ดังนั้นหลักการบริหารจัดการพลังงานในระบบคือให้ซุปเปอร์คาปาซิเตอร์จ่ายไฟเพื่อรักษาระดับแรงดันที่ บัสไฟตรง ส่วนเซลล์แสงอาทิตย์และเซลล์เชื้อเพลิง (เป็นเครื่องกำเนิดพลังงานที่ช้ากว่าซุปเปอร์คาปาซิเตอร์ ทำหน้าที่รักษาระดับแรงดันที่บัสไฟตรงและที่ซุปเปอร์คาปาซิเตอร์

2.4.3.2 พิสูจน์การมีคุณสมบัติแบบ flatness ของแหล่งจ่ายแบบผสม

เพื่อยืนยันการมีคุณสมบัติแบบ flatness ดังได้อธิบายไปแล้วในหัวข้อ 1.6 จะถูกพิสูจน์ดังต่อไปนี้ เพื่อรักษาระดับแรงดันไฟที่บัสไฟตรงและที่ซุปเปอร์คาปาซิเตอร์ บนพื้นฐานของทฤษฎีการควบคุมแบบ flatness ตัวแปรเอาต์พุต (y) ตัวแปรควบคุมอินพุต (u) และตัวแปรสเตท (x) ถูกกำหนดดังนี้

$$\mathbf{y} = \begin{bmatrix} y_1 \\ y_2 \end{bmatrix} = \begin{bmatrix} E_{\text{Bus}} \\ E_{\text{T}} \end{bmatrix} \tag{2-37}$$

$$\mathbf{u} = \begin{bmatrix} u_1 \\ u_2 \end{bmatrix} = \begin{bmatrix} p_{\text{SCREF}} \\ p_{\text{TREF}} \end{bmatrix}$$
 (2-38)

$$\mathbf{x} = \begin{bmatrix} x_1 \\ x_2 \end{bmatrix} = \begin{bmatrix} v_{\text{Bus}} \\ v_{\text{SC}} \end{bmatrix}$$
 (2-39)

ซึ่ง p_{TREF} คือกำลังไฟฟ้ารวมจากเซลล์แสงอาทิตย์และเซลล์เชื้อเพลิง จากสมการที่ (1-32) (1-33) และ (1-34) ตัวแปรสเตทสามารถเขียนได้ดังนี้

$$\mathbf{x} = \begin{bmatrix} x_1 \\ x_2 \end{bmatrix} = \begin{bmatrix} \sqrt{\frac{2y_1}{C_{\text{Bus}}}} \\ \sqrt{\frac{2(y_2 - y_1)}{C_{\text{SC}}}} \end{bmatrix} = \begin{bmatrix} \varphi_1(y_1) \\ \varphi_2(y_1, y_2) \end{bmatrix}$$
(2-40)

จากสมการที่ (2-31) ตัวแปรอินพุต (**u**) สามารถคำนวณได้จากตัวแปรเอาต์พุตตัว (**y**) และ อนุพันธ์เทียบกับเวลาคือ

$$u_{1} = 2p_{\text{SCLim}} \cdot \left[1 - \sqrt{1 - \left(\frac{\dot{y}_{1} + \sqrt{\frac{2y_{1}}{C_{\text{Bus}}}} \cdot i_{\text{Load}} - p_{\text{FCo}} - p_{\text{PVo}}}{p_{\text{SCLim}}}\right)}\right]$$

$$= \psi_{1}(y_{1}, \dot{y}_{1}) = p_{\text{SCREF}}$$
(2-41)

$$u_{2} = 2p_{\text{TMax}} \cdot \left[1 - \sqrt{1 - \left(\frac{\dot{y}_{2} + \sqrt{\frac{2y_{1}}{C_{\text{Bus}}}} \cdot i_{\text{Load}}}{p_{\text{TMax}}} \right)} \right]$$

$$= \psi_{2}(y_{1}, \dot{y}_{2}) = p_{\text{TREF}}$$
(2-42)

สึ่ง

$$p_{\text{SCLim}} = \frac{v_{\text{SC}}^2}{4r_{\text{SC}}}, \ p_{\text{TMax}} = \frac{v_{\text{T}}^2}{4r_{\text{T}}}$$
 (2-43)

ขณะที่ p_{SCLim} คือกำลังไฟฟ้าสูงสุดที่ถูกจำกัดจากตัวแปลงไฟของซุปเปอร์คาปาซิเตอร์ p_{TMax} คือ เทียบเคียงกำลังไฟฟ้าสูงสุดที่ถูกจำกัดจากตัวแปลงไฟของเซลล์แสงอาทิตย์และเซลล์เชื้อเพลิง v_T คือ แรงดันไฟฟ้าเทียบเคียงจากแหล่งจ่ายไฟจากเซลล์แสงอาทิตย์และเซลล์เชื้อเพลิงและ r_T คือค่าตัว ต้านทานเทียบเคียงในตัวแปลงไฟของเซลล์แสงอาทิตย์และเซลล์เชื้อเพลิง

อันที่จริงแล้ว

$$p_{\text{TMax}} = p_{\text{FCMax}} + p_{\text{PVMax}} \tag{2-44}$$

ซึ่ง p_{FCMax} คือกำลังไฟฟ้าสูงสุดจากเซลล์เชื้อเพลิงและ p_{PVMax} คือกำลังไฟฟ้าสูงสุดจากเซลล์แสงอาทิตย์

2.4.3.3 กฎการควบคุมและเสถียรภาพ (Control Law and Stability)

จากสมการที่ (1.35) กฎการควบคุมพลังงานแสดงได้ดังนี้ [28], [29]

$$v_1 = \dot{y}_1 = \dot{y}_{1REF} + K_{11} (y_{1REF} - y_1) + K_{12} \int_0^t (y_{1REF} - y_1) d\tau$$
 (2-45)

$$v_2 = \dot{y}_2 = \dot{y}_{2REF} + K_{21}(y_{2REF} - y_2)$$
 (2-46)

ซึ่ง y_{IREF} คือคำสั่งอ้างอิงของตัวแปรเอาต์พุตตัวที่ 1 (พลังงานที่คาปาซิเตอร์ที่บัสไฟตรง) และ y_{2REF} คือคำสั่งอ้างอิงของตัวแปรเอาต์พุตตัวที่ 2 (พลังงานรวามที่คาปาซิเตอร์ที่บัสไฟตรงกับที่ซุปเปอร์คาปาซิเตอร์)

จากสมการที่ (2-45) ถ้ากำหนดให้ $e_1=y_1-y_{1{
m REF}}$, $K_{11}=2\zeta\omega_n$ และ $K_{12}=\omega_n^2$ จะได้

$$\ddot{e}_1 + 2\zeta \omega_n \cdot \dot{e}_1 + \omega_n^2 \cdot e_1 = 0$$
 (2-47)

แทน $\dot{y}_{
m l}$ ลงในสมการที่ (2-41) จะได้สมการในเทอมของการควบคุมแบบป้อนกลับ เราอาจจะ เรียกว่า "inverse dynamics"

$$u_1 = 2p_{\text{SCLim}} \cdot \left[1 - \sqrt{1 - \left(\frac{equ.(2-45) + p_{\text{Load}} - p_{\text{FCo}} - p_{\text{PVo}}}{p_{\text{SCLim}}} \right)} \right]$$
 (2-48)

เพื่อการคำนวณที่ง่ายลง เราอาจจะประมาณว่า $r_{\rm SC}=0$ ทำให้ $p_{\rm SC}=P_{\rm SCo}$ โดยการกำหนดให้ $P_{\rm SCMax} \leq P_{\rm SCLim}$ เราอาจจะเขียนสมการ inverse dynamics ได้ง่ายขึ้นคือ

$$\frac{\dot{y}_1 = \dot{E}_{\text{Bus}}}{\dot{y}_{1\text{REF}} - 2\zeta\omega_n e_1 - \omega_n^2 \int_0^t e_1 d\tau} + p_{\text{Load}} - p_{\text{FCo}} - p_{\text{PVo}}$$

$$= p_{\text{SCREF}}$$
(2-49)

เช่นเดียวกันจากสมการที่ (2-46) ถ้ากำหนดให้ $e_2=y_2-y_{2{
m REF}}$, $K_{21}=1/ au_{
m S}$ จะได้

$$\tau_{\rm S} \cdot \dot{e}_{\rm l} + e_{\rm l} = 0 \tag{2-50}$$

แทน \dot{y}_2 ลงในสมการที่ (2-42) จะได้สมการในเทอมของการควบคุมแบบป้อนกลับ ที่เรียกว่า "inverse dynamics"

$$\dot{y}_2 = \dot{E}_T$$

$$u_2 = (\dot{y}_{2REF} - (1/\tau_S)e_2) + p_{Load}$$

$$= p_{TREF}$$

$$= p_{PVREF} + p_{FCREF}$$
(2-51)

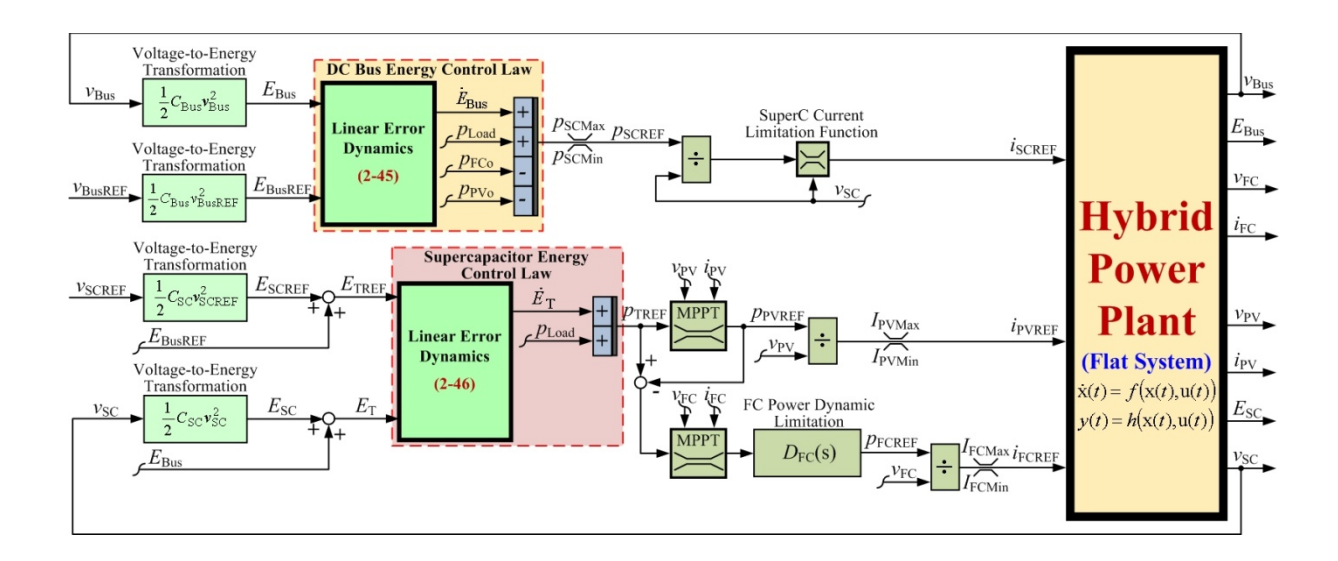
จากสมการที่ (2-49) และ (2-51) เห็นได้ชัดว่าระบบควบคุมจะมีเสถียรภาพแน่นอนสำหรับค่า K_{11} , $K_{12} > 0$ และ $K_{21} > 0$ อย่างไรก็ตาม บนพื้นฐานของระบบควบคุมเป็นชั้นๆ (cascade control structure) และความถี่ของการสวิชต์อิเล็กทรอนิกส์กำลัง ($\omega_{\rm S}$) วงควบคุมชั้นนอก (ในที่นี้คือการควบคุม พลังงานที่บัสไฟตรง) จะต้องทำงานที่ cut-off frequency $\omega_{\rm E} << \omega_{\rm C}$ ซึ่ง $\omega_{\rm C}$ คือ cut-off frequency ของระบบควบคุมของวงควบคุมกำลังจากซุปเปอร์คาปาซิเตอร์ซึ่งเป็นวงชั้นในนั้นเองและ $\omega_{\rm C} << \omega_{\rm S}$ เมื่อตัวแปรเอาต์พุตมีเสถียรภาพ ระบบควบคุมทั้งหมดก็จะมีเสถียรภาพไปด้วยเพราะตัวแปรทั้งหมด สามารถแสดงในเทอมของ differtial flatness

ภาพที่ 2-26 ได้อธิบายถึงแนวคิดระบบควบคุมที่ได้นำเสนอสำหรับแหล่งจ่ายไฟจากพลังงาน ทดแทนที่ได้อธิบายดังข้างบน กฎการควบคุมพลังงานที่บัสไฟตรงสร้างกำลังไฟฟ้าอ้างอิงสำหรับ ซุปเปอร์คาปาซิเตอร์ p_{SCREF} (อ้างอิงสมการที่ (2-41)) สัญญาณ p_{SCREF} นี้จะถูกหารด้วยแรงดันที่วัดมา จากซุปเปอร์คาปาซิเตอร์ v_{SC} และจะจำกัดแรงดันของซุปเปอร์คาปาซิเตอร์ให้อยู่ในช่วงต่ำสุดและสูงสุด [V_{SCMin} , V_{SCMax}] โดยการจำกัดกระแสซาร์จหรือกระแสคายประจุ (ไม่ได้อธิบายในเอกสารนี้ สามารถหา อ่านเพิ่มเติมได้จาก [19], [30]) ผลลัพธ์ก็คือได้กระแสอ้างอิงสำหรับซุปเปอร์คาปาซิเตอร์ i_{SCREF}

กฎการควบคุมพลังงานรวมหรือกฎการควบคุมพลังงานสำหรับซุปเปอร์คาปาซิเตอร์กำเนิด กำลังไฟฟ้าอ้างอิงรวม p_{TREF} (อ้างอิงสมการที่ (2-42)) อย่างแรก สัญญาณ p_{TREF} นี้จะถูกพิจารณาให้ เป็นกำลังอ้างอิงสำหรับโซล่าเซลล์ p_{PVREF} สัญญาณนี้จะถูกจำกัดไม่ให้เกินกำลังไฟฟ้าสูงสุด p_{PVMax} ด้วย ตัวติดตามกำลังไฟฟ้า (maximum power point tracking MPPT) ซึ่งไม่ได้อธิบายในงานวิจัยนี้ อย่างที่ สอง ความแตกต่างระหว่างกำลังไฟฟ้าอ้างอิงรวม p_{TREF} กับกำลังอ้างอิงสำหรับโซล่าเซลล์ p_{PVREF} คือ กำลังไฟฟ้าอ้างอิงสำหรับเซลล์เชื้อเพลิง p_{FCREF} สัญญาณนี้จะถูกจำกัดไม่ให้เกินกำลังไฟฟ้าสูงสุด p_{FCMax} และจะจำกัดไดนามิกส์ของเซลล์เชื้อเพลิง [31], [32] ในที่นี้ ตัวหน่วงลำดับที่ 2 (p_{FC}) ถูกเลือกสำหรับ การจำกัดไดนามิกส์ของเซลล์เชื้อเพลิง (p_{FC}) แต่งได้ดังนี้

$$D_{FC}(s) = \frac{1}{\left(\frac{s}{\omega_{n1}}\right)^2 + \frac{2\zeta_1}{\omega_{n1}}s + 1}$$
(2-52)

ซึ่ง $\omega_{\scriptscriptstyle{\mathsf{n}}^1}$ และ $\zeta_{\scriptscriptstyle{\mathsf{1}}}$ คือตัวแปรการควบคุม



ภาพที่ **2-26** ไดอะแกรมระบบควบคุมแหล่งจ่ายไฟแบบผสม

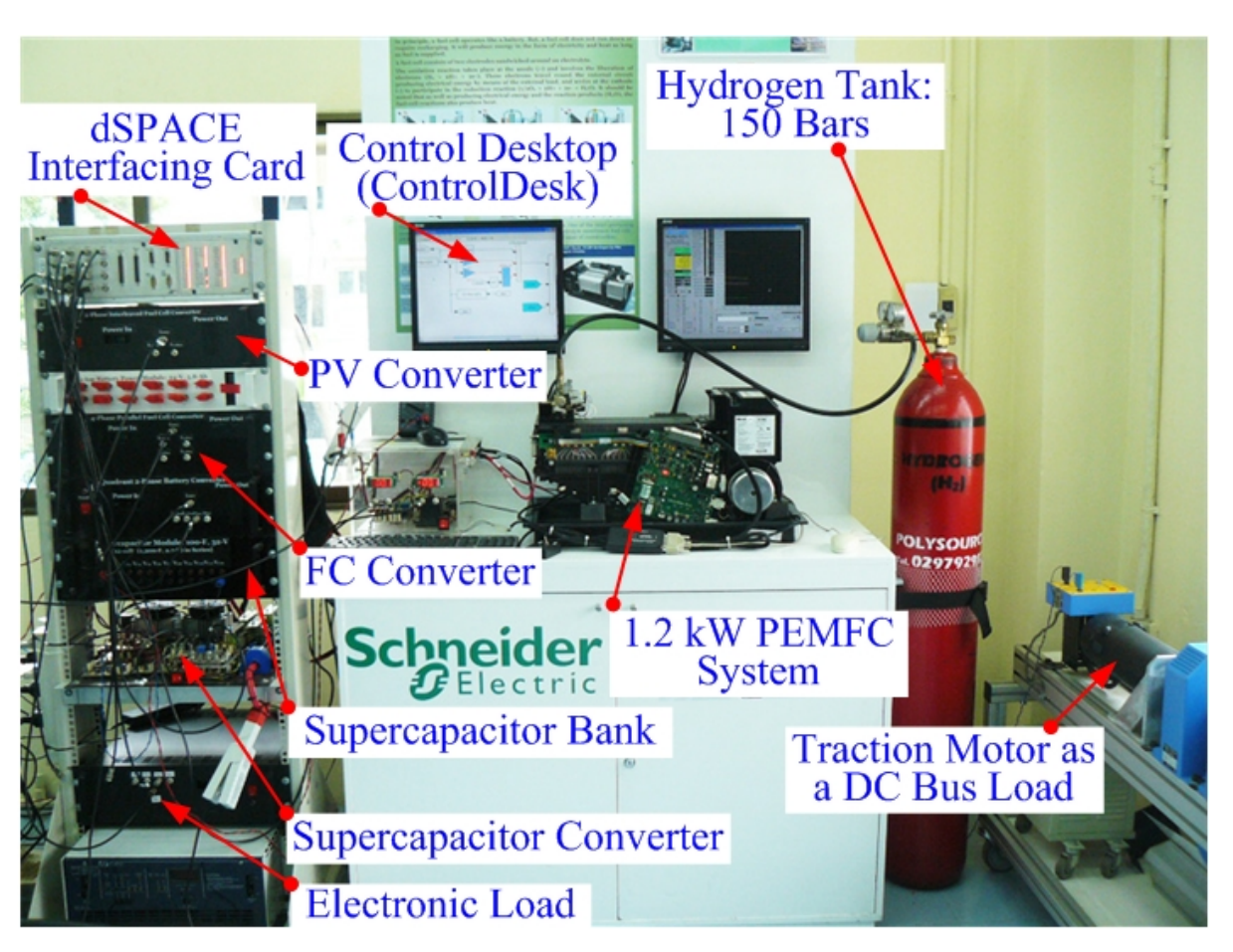
บทที่ 3

วิธีการทดลอง ผลการทดลองและวิจารณ์ผลการทดลอง

จากขั้นตอนการออกแบบและดำเนินงานตามที่ได้กล่าวไปแล้วในบทที่ 2 เมื่อนำวงจรต่าง ๆ มา ประกอบรวมกันเป็นชิ้นงานที่สมบูรณ์เรียบร้อยแล้ว ในบทนี้จะกล่าวถึงผลการดำเนินงานของวงจรที่ได้ ออกแบบไว้และผลการทดสอบการทำงานของวงจรต่างๆ ดังนี้

3.1 รายละเอียดชุดทดลอง

ชุดทดลองระบบจ่ายไฟแบบผสมต้นแบบขนาดเล็กแสดงดังภาพที่ 3-1 ระบบเซลล์เชื้อเพลิง (Ballard Nexa fuel cell system) แผงโซล่าเซลล์ (ติดตั้งบนดาดฟ้าสถาบันนวัตกรรมเทคโนโลยี ไทย-ฝรั่งเศส)และโมดูลซุปเปอร์คาปาซิเตอร์แสดงดังภาพที่ 3-1 ถึงภาพที่ 3-3 ตามลำดับ รายละเอียด แหล่งจ่ายแต่ละตัวแสดงในตารางที่ 3-1



ภาพที่ 3-1 ชุดทดลองระบบจ่ายไฟแบบผสมตันแบบขนาดเล็ก



ภาพที่ 3-2 แผงโซล่าเซลล์ (ติดตั้งบนดาดฟ้าสถาบันนวัตกรรมเทคโนโลยี ไทย-ฝรั่งเศส)

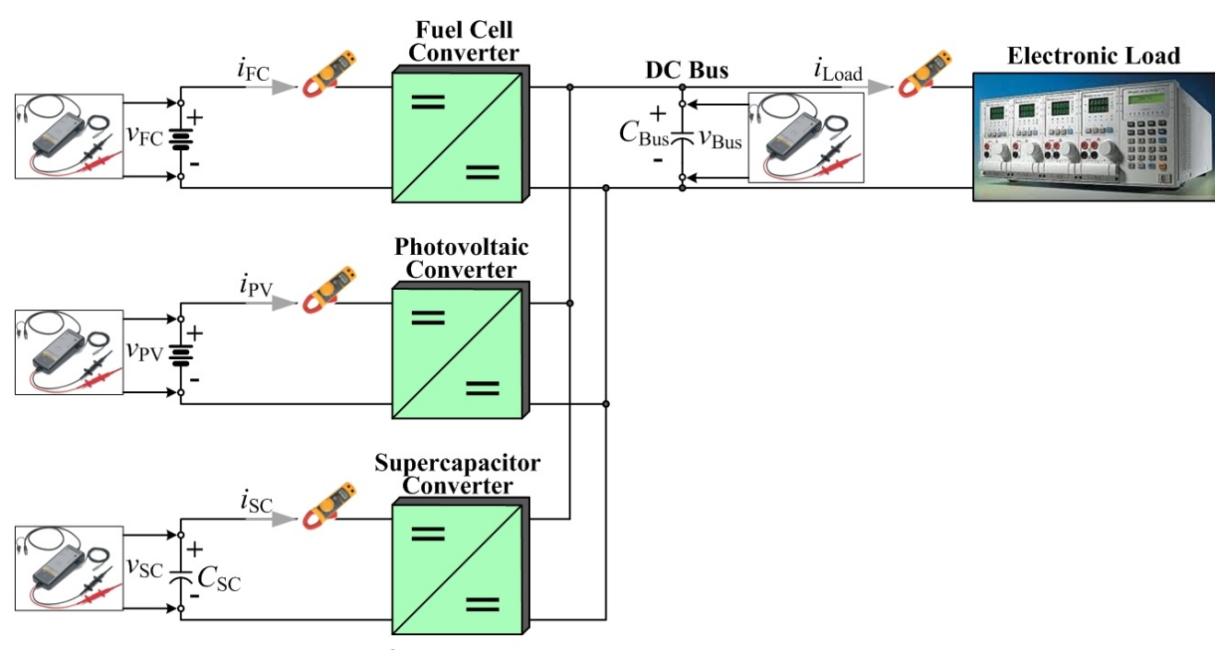


ภาพที่ 3-3 โมดูลซุปเปอร์คาปาซิเตอร์

ตารางที่ 3-1 รายละเอียดแหล่งจ่ายไฟแต่ละตัว

Fuel Cell System (by Ballard Power Sys	stems Inc)	:		
Rated Power	1,200	W		
Rated Current	46	A		
Rated Voltage	26	V		
Photovoltaic Array (by Ekarat Solar Company):				
Number of Panels in Parallel	4			
Panel Open Circuit Voltage	33.5	V		
Panel Rated Voltage	26	V		
Panel Rated Current	7.7	A		
Panel Rated Power	200	W		
Array Rated Power	800	W		
Supercapacitor Bank (by Maxwell Technologies Comp):				
(Cell Model: BCAP1200)				
Number of Cells in Series	12			
Cell Capacity	1,200	F		
Cell Maximum Voltage	2.7	V		
Bank Capacity (C_{SC})	100	F		
Bank Maximum Voltage	32	V		

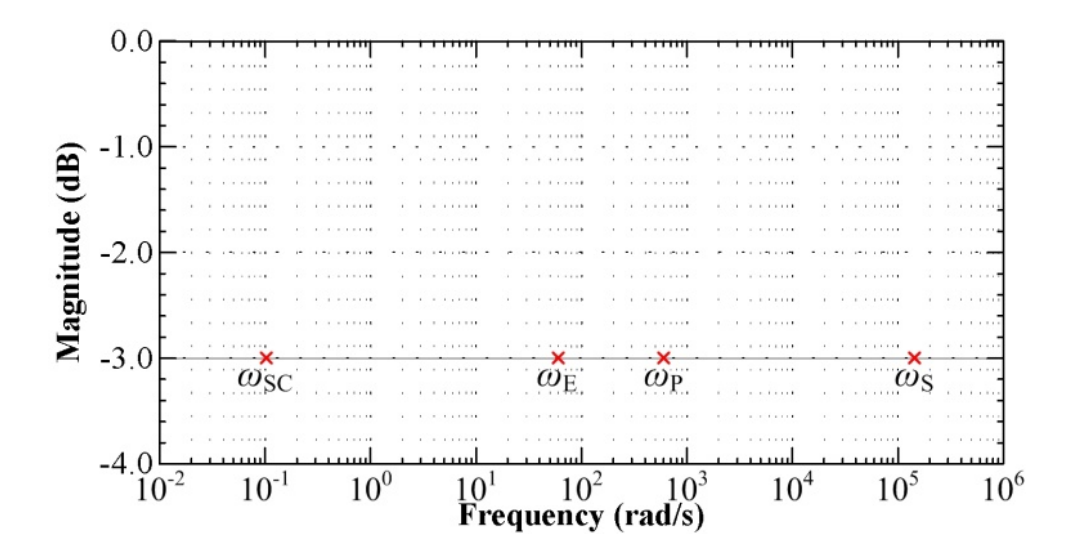
แรงดันที่บัสไฟตรงจะถูกควบคุมที่ 60 V และบัสไฟตรงจะถูกต่อเข้ากับโหลดอิเล็กทรอนิกส์เพื่อ จำลองสถานะต่างๆ ของบัสไฟตรง การวัดค่ากระแสของเซลล์เชื้อเพลิง (i_{FC}) กระแสของโซล่าเซลล์ (i_{PV}) กระแสของซุปเปอร์คาปาซิเตอร์ (i_{SC}) กระแสของโหลด (i_{Load}) แรงดันที่บัสไฟตรง (v_{Bus}) แรงดันของเซลล์ เชื้อเพลิง (v_{FC}) แรงดันของโซล่าเซลล์ (v_{PV}) และแรงดันของซุปเปอร์คาปาซิเตอร์ (v_{SC}) จะถูกวัดด้วย zero-flux Hall effect sensors ตำแหน่งจุดวัดต่างๆ แสดงดังภาพที่ 3-4 ระบบควบคุมพลังงานทั้งระบบ ถูกสร้างในตัวควบคุมแบบ real time ในการ์ด dSPACE DS1104 (ดังภาพที่ 3-1) ผ่านตัวคำนวณใน Matlab—Simulink ที่มีความถี่สุ่ม (sampling frequency) ที่ 25 kHz



ภาพที่ 3-4 จุดวัดแรงดันและกระแสของชุดทดลอง

3.2 รายละเอียดระบบควบคุม

อัตราขยายของตัวควบคุม $K_{11}=450~{
m rad\cdot s}^1~{
m las}$ $K_{12}=22{,}500~{
m rad}^2\cdot {
m s}^2$ เพื่อให้ระบบมีอัตราหน่วง (damping ratio) เท่ากับ 1.5 และมีความถี่ธรรมชาติ (natural frequency) เท่ากับ 150 rad·s $^{-1}$ ซึ่ง จะทำให้ cutoff frequency ($\omega_{
m E}$) ของวงปิดของระบบควบคุมพลังงานที่บัสไฟตรงมีค่าเท่ากับ 60 rad·s $^{-1}$ ซึ่งมีค่าต่ำกว่า cutoff frequency ($\omega_{
m P}$) ของวงปิดของระบบควบคุมกำลังของซุปเปอร์คาปาซิเตอร์จะถูกประมาณเป็นตัว หน่วงลำดับที่ 1 มีค่าคงที่ของเวลา (time constant) เท่ากับ 2.2 ms ที่ได้จากการทดลอง identification) ดังนั้นระบบควบคุมมีเสถียรภาพ อัตราขยายของตัวควบคุมของวงปิดระบบควบคุมพลังงานรวม (หรือ พลังงานของซุปเปอร์คาปาซิเตอร์) $K_{21}=0.1~{
m W\cdot J}^1~{
m ทำให้}$ cutoff frequency ($\omega_{
m SC}$) ของวงปิดระบบควบคุมพลังงานรวมเท่ากับ 0.1 rad·s $^{-1}$ ที่ซึ่ง $\omega_{
m SC}<<\omega_{
m E}$ เพื่อเป็นการการันตีสำหรับการมีเสถียรภาพ ของทั้งระบบควบคุม ดังนั้น cutoff frequency ของทุกวงปิดแสดงได้ดังภาพที่ 3-5 ดังนั้นพารามิเตอร์ ของระบบควบคุมทั้งสองวงแสดงดังตารางที่ 3-2 และ 3-3



ภาพที่ 3-5 การกำหนดค่าของตัวควบคุมโดยเลือกกำหนดค่า cutoff frequency ที่ซึ่ง $\omega_{\rm S}$ คือความถึ่ สวิตช์ของตัวแปลงไฟของซุปเปอร์คาปาซิเตอร์ที่ 25 kHz (157,080 rad·s⁻¹) $\omega_{\rm P}$ คือ cutoff frequency ของวงปิดของระบบควบคุมกำลังของซุปเปอร์คาปาซิเตอร์มีค่าเท่ากับ 600 rad·s⁻¹ $\omega_{\rm E}$ คือ cutoff frequency ของวงปิดของระบบควบคุมพลังงานที่บัสไฟตรงมีค่าเท่ากับ 60 rad·s⁻¹ $\omega_{\rm SC}$ และ คือ cutoff frequency ของวงปิดของระบบควบคุมพลังงานรวม (หรือพลังงานของซุปเปอร์คาปาซิเตอร์)

ตารางที่ 3-2 พารามิเตอร์ของระบบควบคุมพลังงานที่บัสไฟตรง

$v_{ m BusREF}$	60	V
$C_{ m Bus}$	12200	$\mu \mathrm{F}$
K_{11}	450	rad·s ⁻¹
K_{12}	22,500	rad ² ·s ⁻²
r_{FC}	0.13	Ω
r_{SO}	0.10	Ω
$r_{ m SC}$	0.08	Ω
$V_{ m SCMax}$	32	V
$V_{ m SCMin}$	15	V
$I_{ m SCRated}$	150	A

ตารางที่ 3-3 พารามิเตอร์ของระบบควบคุมพลังงานรวม (หรือพลังงานของซุปเปอร์คาปาซิเตอร์)

$v_{ m SCREF}$	25	V	
$C_{ m SC}$	100	F	
K_{21}	0.1	$W \cdot J^{-1}$	
p_{FCMin}	0	W	
I_{FCMax} (Rated)	46	A	
$I_{ m FCMin}$	0	A	
ζ_1	1		
$\omega_{\mathrm{n}1}$	0.4	rad·s ⁻¹	

3.3 ผลการทดลอง

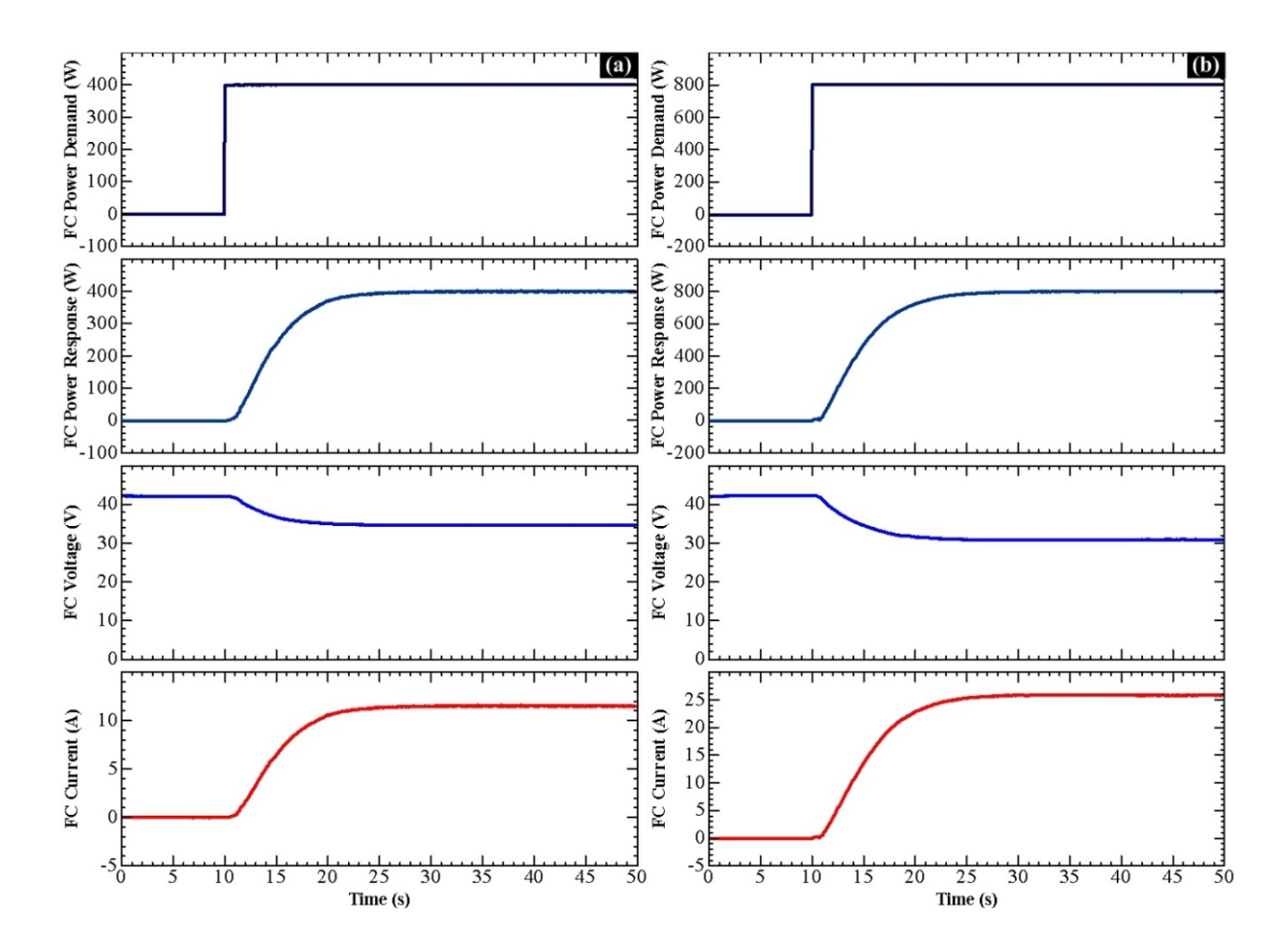
3.3.1 ไดนามิกส์ของระบบควบคุมกำลังของแต่ละแหล่งจ่าย (Power Loop Identification)

เพื่อเป็นการยืนยันถึงใดนามิกส์ของระบบควบคุมกำลัง (หรือกระแส) ของแหล่งจ่ายแต่ละตัว ภาพ ที่ 3-6 ถึงภาพที่ 3-8 แสดงผลการทดลองที่ทดสอบความเร็วในการตอบสนองต่อสัญญาณคำสั่งของกำลัง ของแต่ละแหล่งจ่าย ภาพที่ 3-6 แสดงการตอบสนองต่อสัญญาณคำสั่งของกำลังของเซลล์์เชื้อเพลิง ใน ภาพนำเสนอคำสั่งอ้างอิงของกำลังของเซลล์เชื้อเพลิง (FC Power Demand) กำลังของเซลล์เชื้อเพลิง (FC Power Response) แรงดันของเซลล์เชื้อเพลิง (FC Voltage) และกระแสของเซลล์เชื้อเพลิง (FC ชัดเชนที่การตอบสนองของกำลังของเซลล์เชื้อเพลิงเป็นตัวหน่วงลำดับที่ 2 (second order characteristics) เป็นไปตามสมการที่ (2-52) และเห็นได้ชัดที่ไม่มีปรากฏการกระหายเชื้อเพลิง (fuel starvation phenomenon) เกิดขึ้นในเซลล์ เนื่องจากระบบมีการหน่วงการทำงานของกำลังจากเซลล์ เชื้อเพลิงไม่ให้ทำงานเร็วเกินไปนั้นเอง ส่วนในภาพที่ 3-7 แสดงการตอบสนองต่อสัญญาณคำสั่งของ กำลังของโซล่าเซลล์ ในภาพนำเสนอคำสั่งอ้างอิงของกำลังของโซล่าเซลล์ (PV Power Demand) กำลัง ของโซล่าเซลล์ (PV Power Response) แรงดันของโซล่าเซลล์ (PV Voltage) และกระแสของโซล่าเซลล์ แสดงการตอบสนองต่อสัญญาณคำสั่งของกำลังของ สุดท้ายภาพที่ 3-8 ซุปเปอร์คาปาซิเตอร์ ในภาพนำเสนอคำสั่งอ้างอิงของกำลังของซุปเปอร์คาปาซิเตอร์ (PV Power Demand) กำลังของซุปเปอร์คาปาซิเตอร์ (PV Power Response) แรงดันของซุปเปอร์คาปาซิเตอร์ (PV Voltage) และกระแสของซุปเปอร์คาปาซิเตอร์ (PV Current) เห็นได้ชัดว่าการตอบสนองของกำลัง จากซุปเปอร์คาปาซิเตอร์เป็นไปอย่างรวดเร็วมาก มันสามารถจ่ายกำลังไปสู่บัสไฟตรงจาก 0 W ถึง 400 W ใช้เวลาแค่ประมาณ 50 ms เท่านั้น ซึ่งนี้คือจุดเด่นของแบตเตอร์รี่ชนิดซุปเปอร์คาปาซิเตอร์ที่ เหนือกว่าแบตเตอร์รี่ชนิดอื่นๆ ในด้านไดนามิกส์และ Power Densities

3.3.2 ไดนามิกส์ของการควบคุมบัสไฟตรง

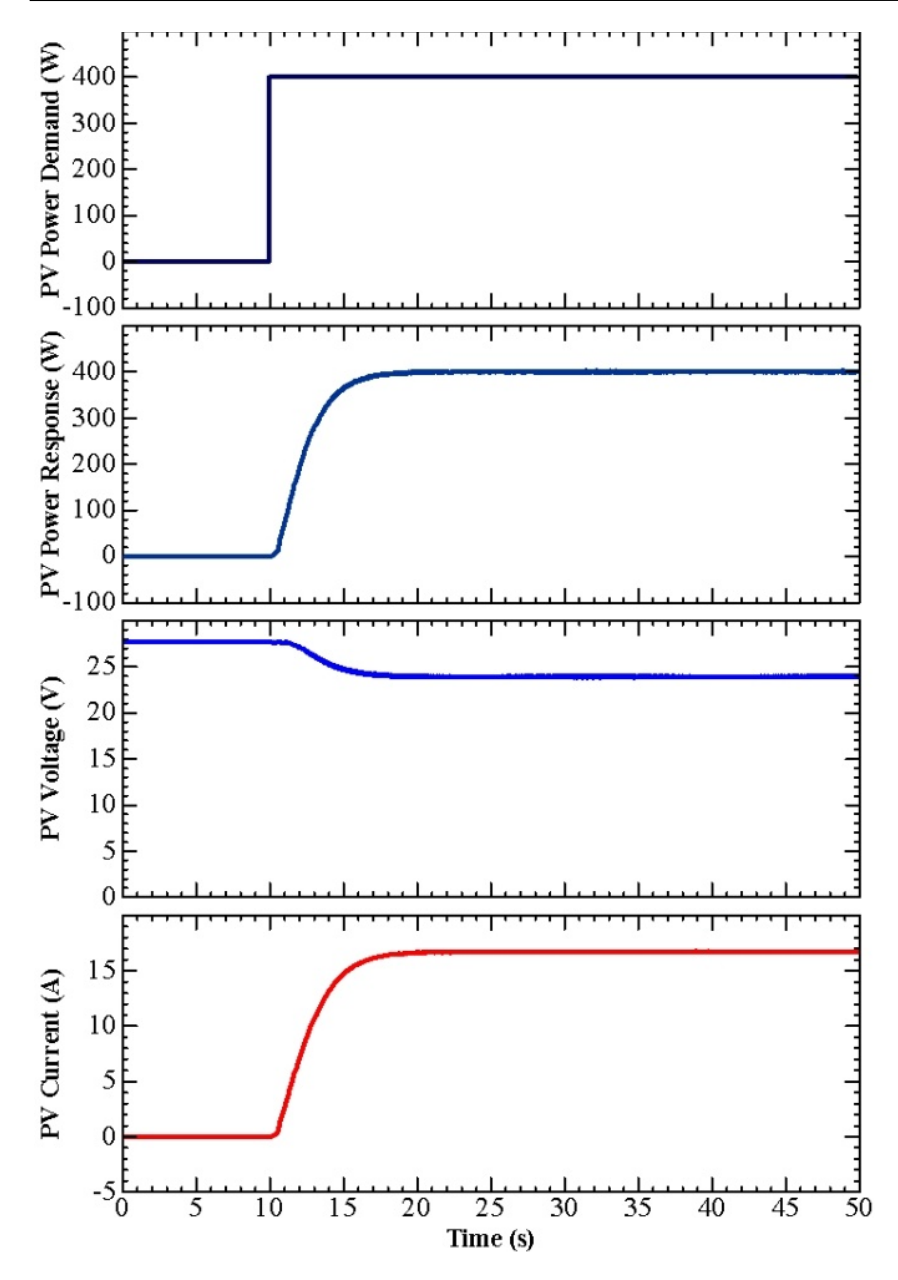
ภาพที่ 3-9 แสดงสัญญาณขณะมีการสเตปโหลดขนาดใหญ่ แสดงแรงดันบัสไฟตรง (dc bus voltage) (ซึ่งคือตัวแปรสเตท x_1 นำเสนอแทนตัวแปรเอาต์พุท y_1) โหลด (load power) (หรือก็คือ สัญญาณรบกวน) กำลังของซุปเปอร์คาปาซิเตอร์ (supercapacitor power) (ซึ่งคือตัวแปรควบคุมที่เป็น อินพุตตัวที่ 1 u_1) และกำลังของโซล่าเซลล์ (PV power) เริ่มต้นขณะที่ไม่มีโหลด ซุปเปอร์คาปาซิเตอร์ ถูกชาร์จเต็มแล้ว (นั้นคือ $v_{\text{SCREF}} = 25 \text{ V}$) และบัสไฟตรงถูกควบคุมให้คงที่ที่ 60 V ($v_{\text{BusREF}} = 60 \text{ V}$) เป็นผลทำให้กำลังของเซลล์เชื้อเพลิง โซล่าเซลล์และซุปเปอร์คาปาซิเตอร์มีค่าเท่ากับศูนย์ ขณะทดลอง กำลังสูงสุดจากโซล่าเซลล์ถูกจำกัดอยู่ที่ประมาณ 400 W โดยตัวติดตามกำลังสูงสุด (MPPT) ผลการ ทดลองแสดงให้เห็นการตอบสนองทางไดนามิกส์ต่อการสเตปโหลดขนาดใหญ่เป็นไปตามสมการที่ (2-47) ซึ่งเป็นไปตามลักษณะสมบัติของสมการหน่วงลำดับที่ 2 การแกว่งเล็กน้อยของบัสไฟตรงเพราะว่า อัตราขยาย K_{12} มีค่าสูงและโหลดมีค่าสูงมาก ค่าอัตราขยาย K_{12} สามารถลดลงได้เพื่อลดการแกว่ง อย่างไรก็ตาม มันจะทำให้การตอบสนองซ้าลง กฎการควบคุม (control law) แสดงให้เห็นว่าระบบมี เสถียรภาพและมีการตอบสนองที่ดีที่สุดเพื่อควบคุมแรงดันที่บัสไฟตรงที่ 60 V ถึงแม้ว่าไดนามิกส์ของ ระบบควบคุมสามารถทำให้ดีขึ้นได้แต่ระบบอาจจะเข้าไปใกล้ขอบของการไม่มีเสถียรภาพได้ (reduced

stability margin) ข้อสังเกต ในทางปฏิบัติการสร้างโหลดที่เป็นสเตปจะทำได้ยากดังแสดงในภาพ และ เนื่องจากกำลังของเซลล์เชื้อเพลิงถูกจำกัดด้านไดนามิกส์ ดังนั้นไดนามิกส์ของโหลดจะจ่ายโดยซุปเปอร์ คาปาซิเตอร์และโซล่าเซลล์

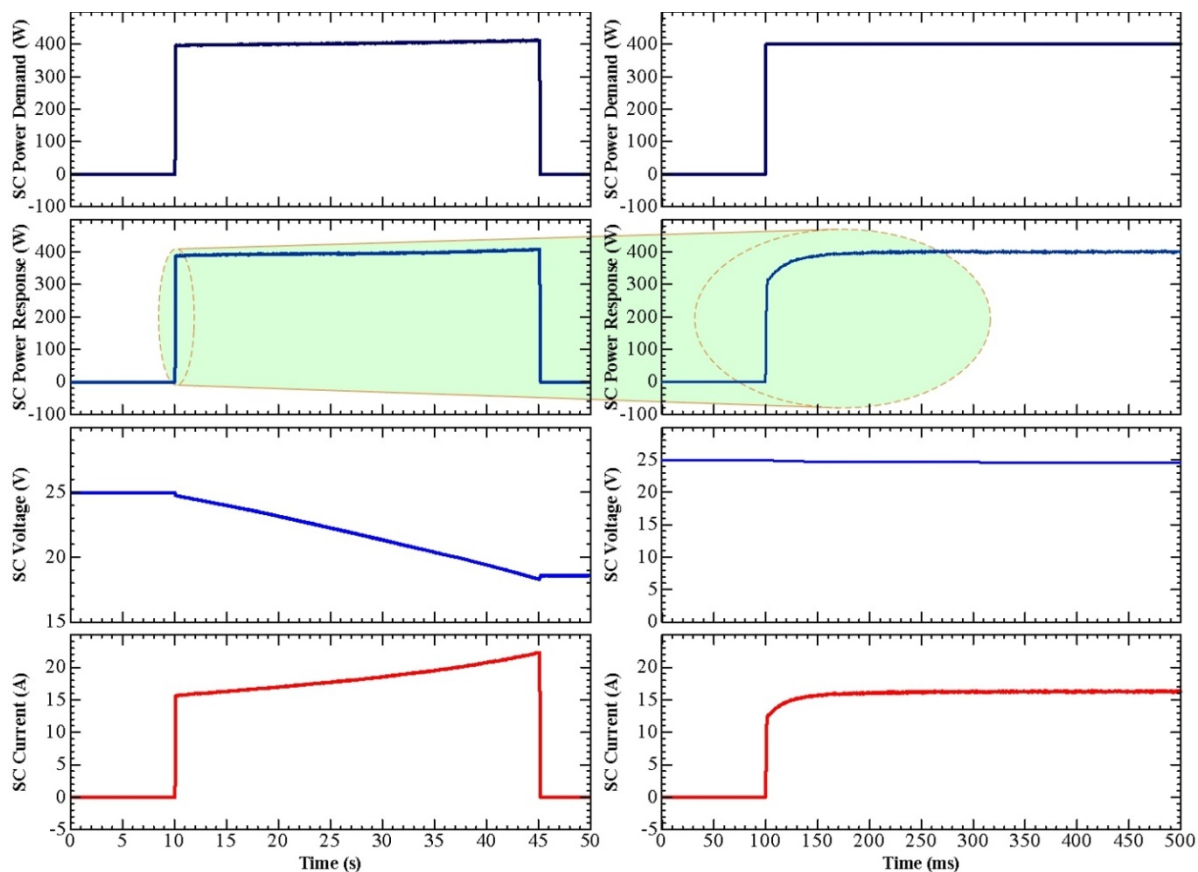


ภาพที่ 3-6 ใดนามิกส์ของระบบควบคุมกำลังของเซลล์เชื้อเพลิง นำเสนอคำสั่งอ้างอิงของกำลังของ เซลล์เชื้อเพลิง (FC Power Demand) กำลังของเซลล์เชื้อเพลิง (FC Power Response) แรงดันของ เซลล์เชื้อเพลิง (FC Voltage) และกระแสของเซลล์เชื้อเพลิง (FC Current)

- a). คำสั่งอ้างอิงของกำลังของเซลล์เชื้อเพลิงสเตปจาก 0 W ไปยัง 400 W ที่เวลา 10 s
- b). คำสั่งอ้างอิงของกำลังของเซลล์เชื้อเพลิงสเตปจาก 0 W ไปยัง 800 W ที่เวลา 10 s

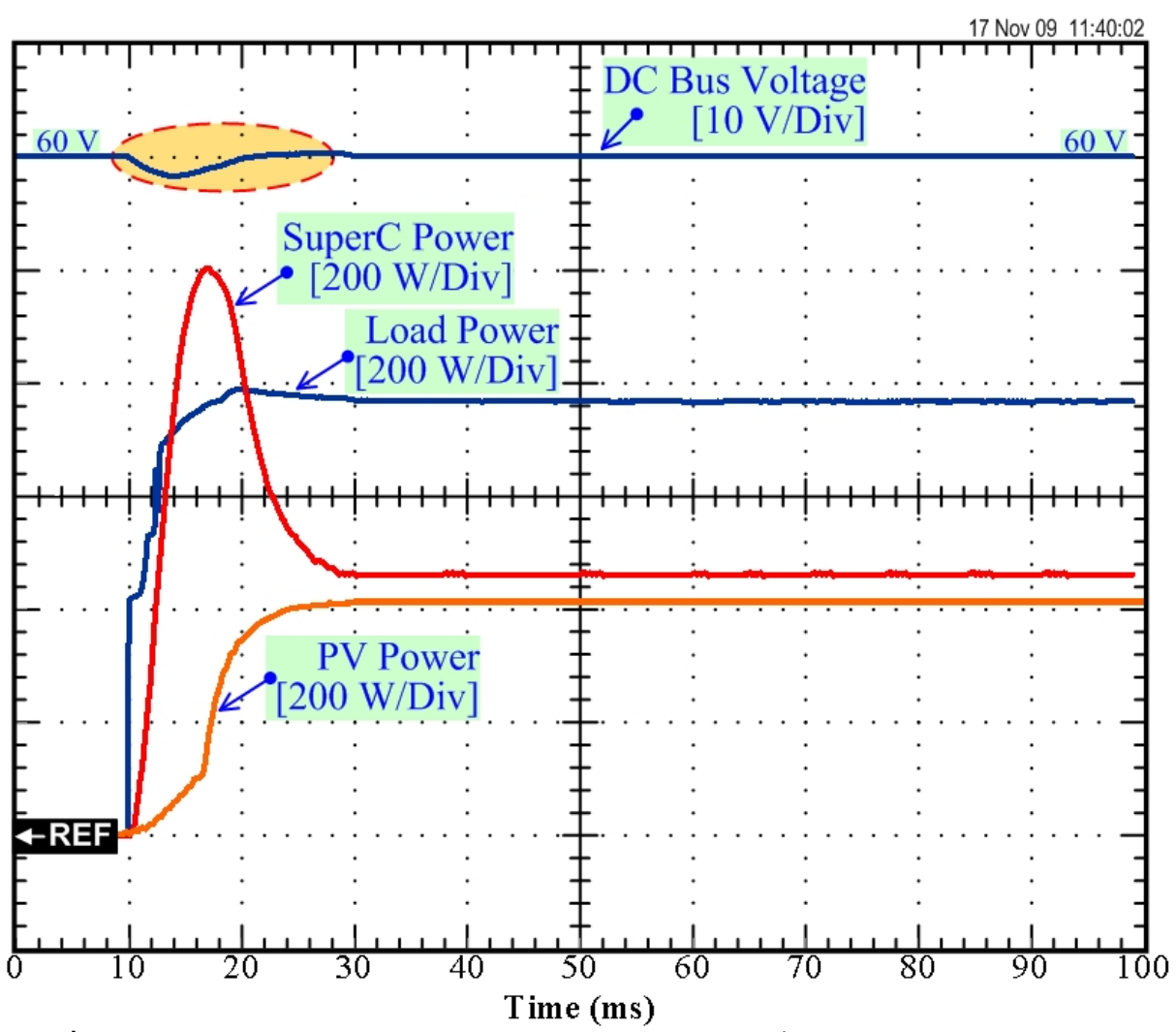


ภาพที่ 3-7 ใดนามิกส์ของระบบควบคุมกำลังของโซล่าเซลล์ นำเสนอคำสั่งอ้างอิงของกำลังของโซล่า เซลล์ (PV Power Demand) กำลังของโซล่าเซลล์ (PV Power Response) แรงดันของโซล่าเซลล์ (PV Voltage) และกระแสของโซล่าเซลล์ (PV Current)

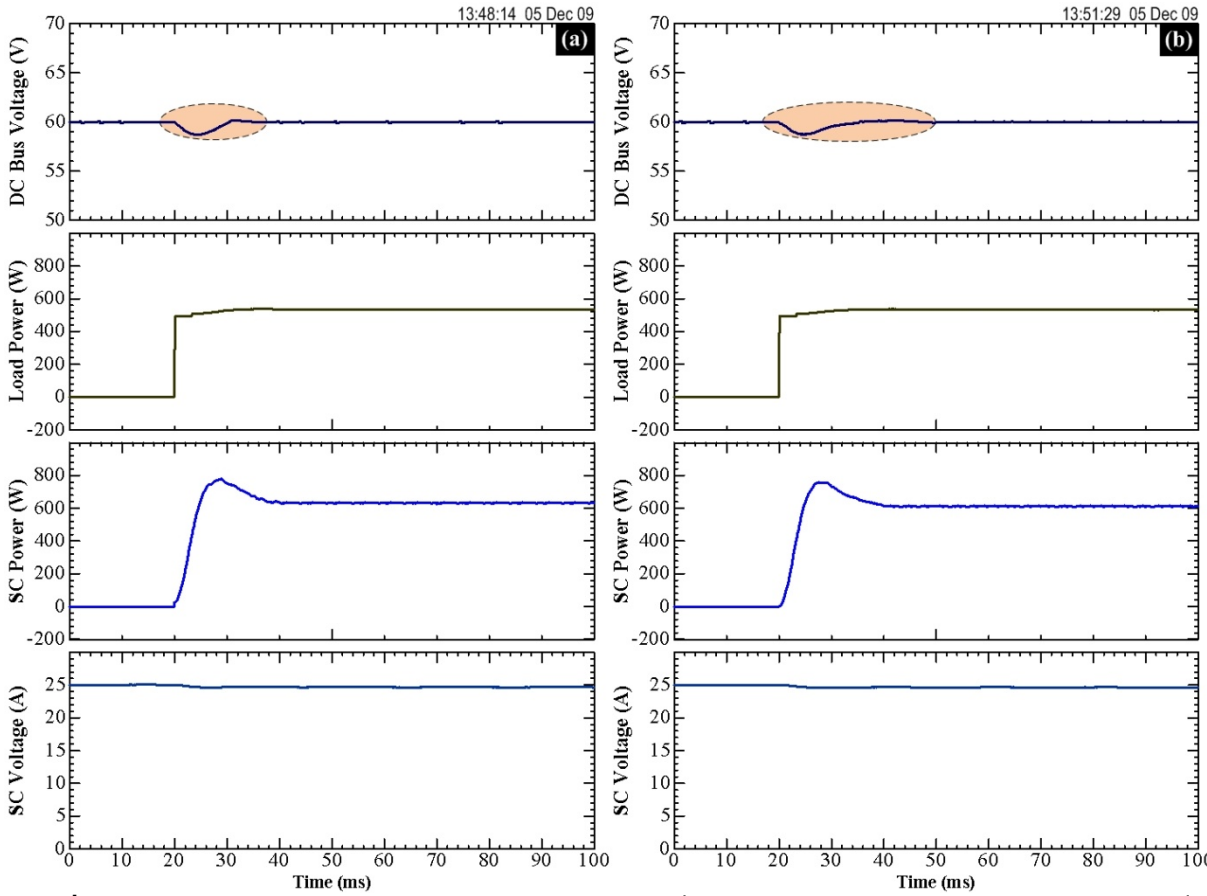


ภาพที่ 3-8 ใดนามิกส์ของระบบควบคุมกำลังของซุปเปอร์คาปาซิเตอร์ นำเสนอคำสั่งอ้างอิงของกำลัง ของซุปเปอร์คาปาซิเตอร์ (SC Power Demand) กำลังของซุปเปอร์คาปาซิเตอร์ (SC Power Response) แรงดันของซุปเปอร์คาปาซิเตอร์ (SC Voltage) และกระแสของซุปเปอร์คาปาซิเตอร์ (SC Current)

เนื่องจากระบบควบคุมโดยวิธีการคำนวณแบบ flatness จะต้องมีพารามิเตอร์ของระบบเข้ามา คำนวณด้วย ซึ่งระบบอาจจะมีผลกระทบต่อการเปลี่ยนแปลงของพารามิเตอร์เหล่านี้ เพื่อยืนยันว่า วิธีการควบคุมแบบนี้มีไม่มีผลกระทบต่อการเปลี่ยนแปลงพารามิเตอร์ในระบบ (robustness) ระบบ ควบคุมถูกทดลองเปรียบเทียบดังนี้คือพารามิเตอร์ของระบบถูกต้อง ($r_{\rm FC}$ = 0.14 Ω , $r_{\rm PV}$ = 0.12 Ω , $r_{\rm SC}$ = 0.10 Ω) และพารามิเตอร์คลาดเคลื่อน ($r_{\rm FC}$ = 0 Ω , $r_{\rm PV}$ = 0 Ω , $r_{\rm SC}$ = 0 Ω) ผลการทดลองเพื่อ เปรียบเทียบโมเดลถูกต้องและโมเดลคลาดเคลื่อนแสดงดังภาพที่ 3-10 เป็นการทดลองขณะที่มี การสเตปของโหลดขนาดใหญ่จาก 0 W ถึง 500 W แสดงสัญญาณแรงดันที่บัสไฟตรง (DC bus voltage) กำลังของโหลด (Load power) กำลังของซุปเปอร์คาปาซิเตอร์ (SC power) และแรงดันของ ซุปเปอร์คาปาซิเตอร์ (SC voltage) เพราะว่ากำลังจากเซลล์เชื้อเพลิงและโซล่าเซลล์ซ้ากว่ากำลังจาก ซุปเปอร์คาปาซิเตอร์ (SC voltage) เพราะว่ากำลังจากเซลล์เชื้อเพลิงและโซล่าเซลล์ซ้ากว่ากำลังจาก เห็นได้ชัดว่าสัญญาณในภาพที่ 3-10(a) และ (b) จะไม่แตกต่างกันมากนัก แรงดันที่บัสไฟตรงจะมี ผลกระทบมาจากการสเตปของโหลดขนาดใหญ่ แต่ระบบควบคุมไม่มีผลกระทบมากนักจากที่ พารามิเตอร์ในโมเดลคลาดเคลื่อน ดังนั้นทำให้สรุปได้ว่าระบบควบคุมแบบ flatness มีความทนทานต่อ การเปลี่ยนแปลงพารามิเตอร์ (robustness)



ภาพที่ 3-9 การตอบสนองต่อการสเตปโหลดจาก 0 W ถึง 760 W ที่เวลา t = 10 ms หมายเหตุ p_{Load} $\approx p_{\mathsf{SC}} + p_{\mathsf{PV}} (p_{\mathsf{FC}} \approx 0 ช่วงไดนามิกส์)$



ภาพที่ 3-10 เปรียบเทียบไดนามิกส์การควบคุมแรงดันที่บัสไฟตรงของแหล่งจา๋ยใฟแบบผสมขณะที่มีการสเตปของโหลดค่าสูง

- a). โมเดลถูกต้อง ($r_{\rm FC}$ = 0.14 Ω , $r_{\rm PV}$ = 0.12 Ω , $r_{\rm SC}$ = 0.10 Ω)
- b). โมเดลคลาดเคลื่อน ($r_{\rm FC}$ = 0 Ω , $r_{\rm PV}$ = 0 Ω , $r_{\rm SC}$ = 0 Ω)

3.3.3 รอบของโหลด (Load Cycle)

ภาพที่ 3-11 แสดงสัญญาณขณะจ่ายไฟให้กับโหลดรอบเดี่ยว แสดงแรงดันที่บัสไฟตรง (dc bus voltage) (ซึ่งคือตัวแปรสเตทตัวที่ 1 x_1 , นำเสนอแทนตัวแปรเอาต์พุต y_1) แรงดันของเซลล์เชื้อเพลิง (FC voltage) แรงดันของโซล่าเซลล์ (PV voltage) กำลังของโหลด (load power) กำลังของซุปเปอร์คาปาซิ เตอร์ (supercapacitor power) (หรือตัวแปรอินพุต u_1) กำลังของเซลล์เชื้อเพลิง (FC power) กำลังของโซล่าเซลล์ (PV power) กระแสของซุปเปอร์คาปาซิเตอร์ (supercapacitor current) กระแสของเซลล์ เชื้อเพลิง (FC current) กระแสของโซล่าเซลล์ (PV current) และแรงดันของซุปเปอร์คาปาซิเตอร์ (supercapacitor voltage) (ซึ่งคือตัวแปรสเตทตัวที่ 2 x_2 หรือนำเสนอสถานะการซาร์จของซุปเปอร์คาปาซิเตอร์ (supercapacitor state-of-charge)) สถานะเริ่มต้นอยู่ในสถานะที่ไม่มีโหลดและซุปเปอร์คาปาซิเตอร์ถูกซาร์จเต็มแล้ว ($v_{SC}=25$ V) เป็นผลให้กำลังของเซลล์เชื้อเพลิง โซล่าเซลล์และซุปเปอร์คาปาซิเตอร์เท่ากับศูนย์ ที่เวลา t=20 s โหลดขนาดใหญ่สเตปจาก 0 W ไปยัง 840 W ขณะทำการทดลอง กำลังสูงสุดของโซล่าเซลล์ (ซึ่งขึ้นอยู่กับมุมรับแสง สภาวะอากาศและอุณหภูมิ) มีค่าเท่ากับประมาณ 200 W ถูกคำนวณโดยตัว MPPT และกำลังสูงสุดของเซลล์เชื้อเพลิงถูกจำกัดใว้ที่ 360 W ดังนั้น กำลังของ

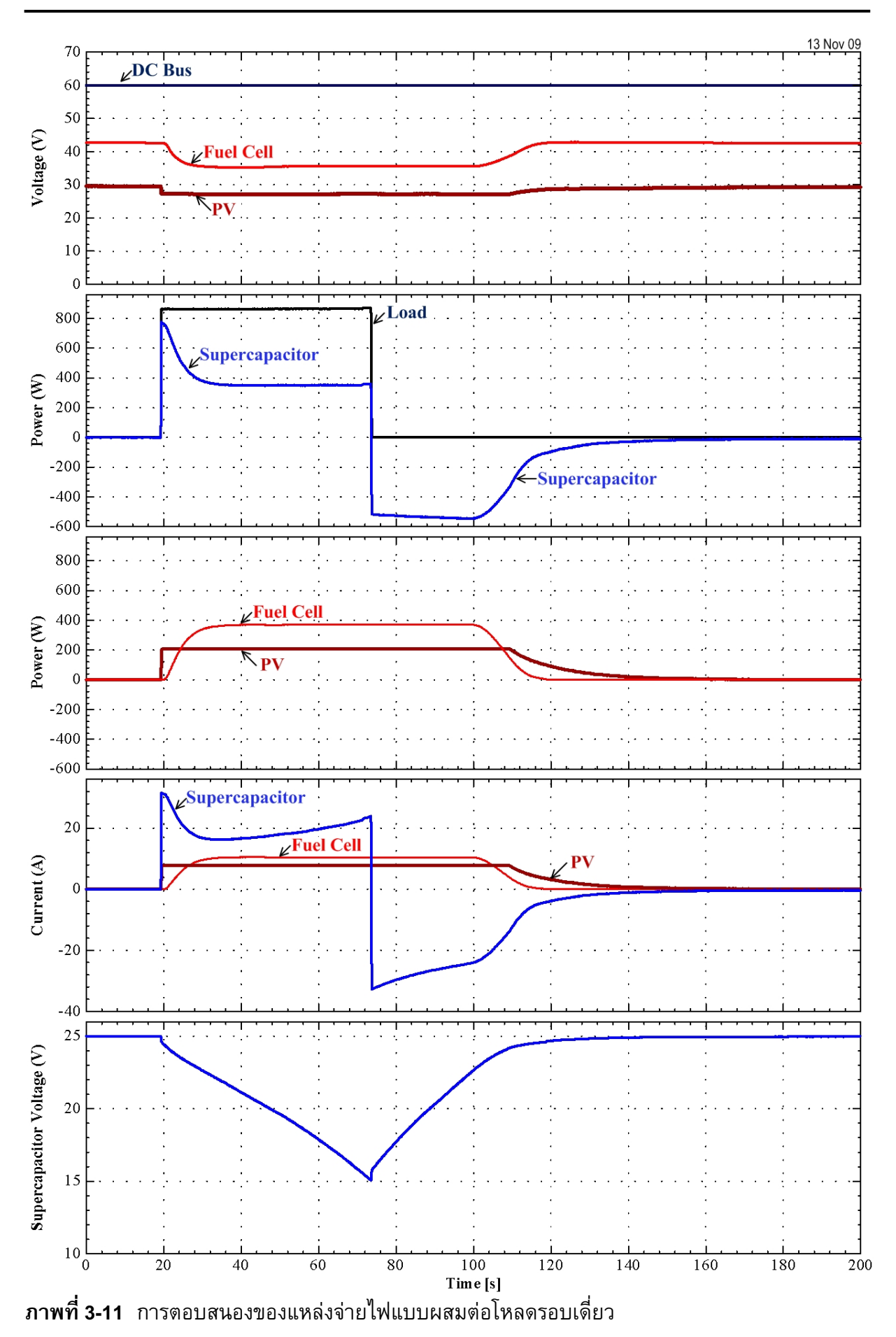
เซลล์เชื้อเพลิงใหลเพิ่มขึ้นพร้อมๆ กับการจำกัดความชั้นในลักษณะของตัวหนวงลำดับที่ 2 (second order dynamics) ไปจนถึงกำลังสูงสุดที่จำกัดที่ 360 W ซุปเปอร์คาปาซิเตอร์และโซล่าเซลล์จ่ายไฟ ทั้งหมดช่วงไดนามิกส์ขณะโหลดกระชาก ซุปเปอร์คาปาซิเตอร์ยังคงอยู่ในสถานะคายประจุหลังจาก โหลดสเตปเพราะโหลดที่สภาวะอยู่ตัว (840 W) มีค่าสูงกว่ากำลังสูงสุดรวมกันจากเซลล์เชื้อเพลิงและโซล่าเซลล์

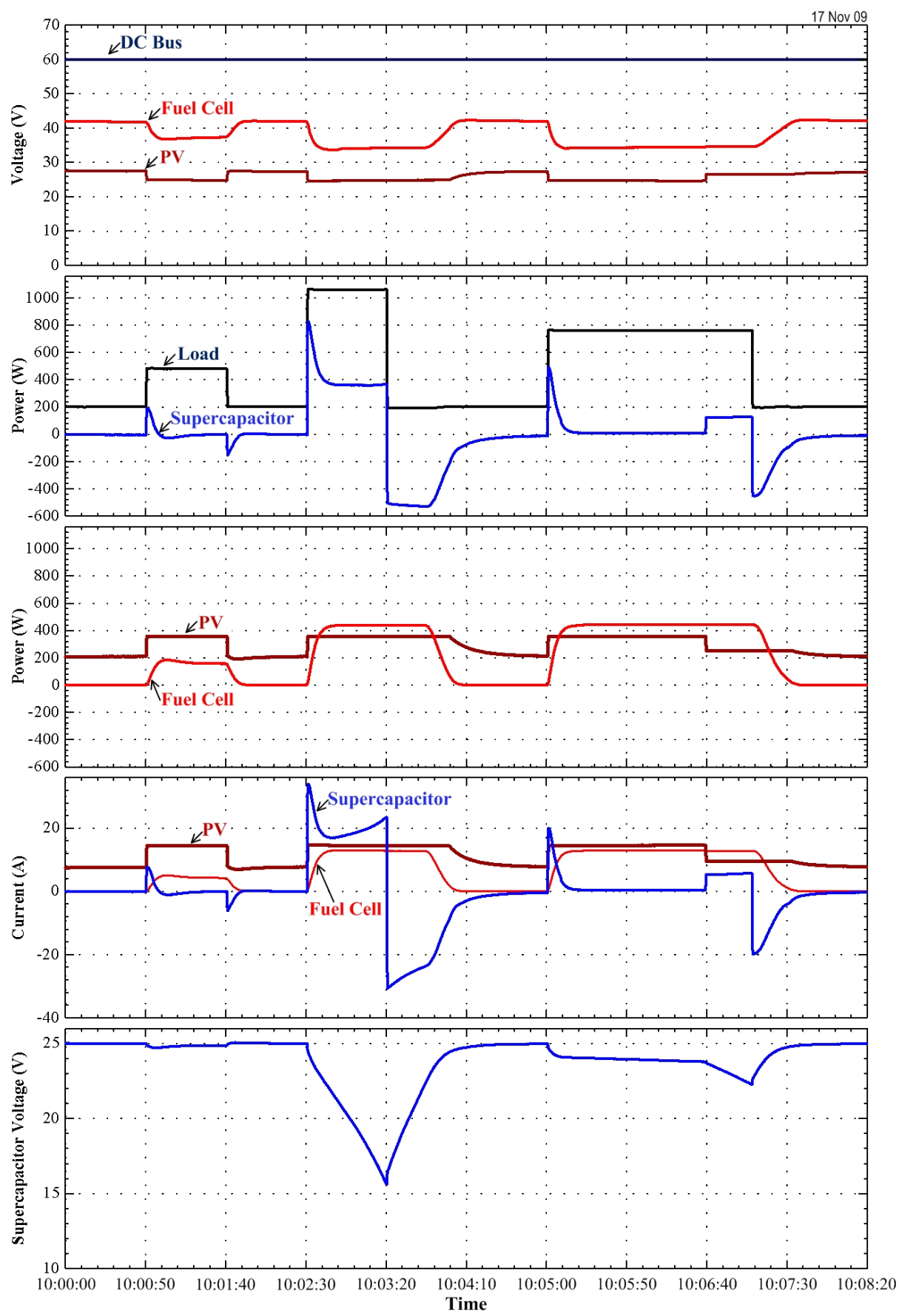
หลังจากนั้นที่เวลา $t=72~\mathrm{s}$ โหลดสเตปจาก 840 W ไปยัง 0 เป็นผลให้ซุปเปอร์คาปาซิเตอร์ เปลี่ยนสถานะจากคายประจุเป็นชาร์จประจุ มีปรากฏการณ์ 4 อย่างเกิดขึ้น

- ปรากฏการณ์แรก เซลล์เชื้อเพลิงและโซล่าเซลล์ยังคงจ่ายไฟที่กำลังสูงสุด เพื่อขับ
 โหลดและชาร์จซุปเปอร์คาปาซิเตอร์
- ปรากฏการณ์ที่สอง ที่เวลา $t = 100 \text{ s} (v_{\text{SC}} = 23 \text{ V})$ ซุปเปอร์คาปาซิเตอร์ถูกชาร์จ เก็บประจุเกือบเต็ม ทำให้ซุปเปอร์คาปาซิเตอร์ลดกำลังในการชาร์จประจุลง เป็นผล ให้กำลังจากเซลล์เชื้อเพลิงลดลง
- ปรากฏการณ์ที่สาม ที่เวลา $t = 108 \text{ s} (v_{SC} = 24.5 \text{ V})$ ซุปเปอร์คาปาซิเตอร์ถูก ชาร์จเก็บประจุเกือบเต็มที่แล้ว เป็นผลให้กำลังจากเซลล์เชื้อเพลิงและโซล่าเซลล์ ลดลง
- ปรากฏการณ์ที่สี่ ที่เวลา t = 160 s ซุปเปอร์คาปาซิเตอร์ถูกชาร์จเต็ม เป็นผลให้ กำลังของเซลล์เชื้อเพลิง โซล่าเซลล์และซุปเปอร์คาปาซิเตอร์มีค่าเท่ากับศูนย์

เห็นได้ชัดว่าสัญญาณแรงดันที่บัสไฟตรงมีเสถียรภาพตลอดรอบของโหลดขนาดใหญ่ ซึ่งเป็น จุดเด่นที่สำคัญที่มีซุปเปอร์คาปาซิเตอร์ช่วยทำให้สมรรถนะด้านไดนามิกส์ของทั้งระบบดีขึ้น

สุดท้าย ภาพที่ 3-12 แสดงสัญญาณขณะทดลองมีรอบของโหลดหลายรอบ สัญญาณก็จะคล้าย ๆ กับภาพที่ 3-11 ขณะทำการทดลอง กำลังสูงสุดจากเซลล์เชื้อเพลิงถูกจำกัดที่ 440 W และกำลังจากโซ ล่าเซลล์ถูกจำกัดโดย MPPT ตัวอย่างเช่นที่เวลา 10:00:50 กำลังสูงสุดจากโซล่าเซลล์มีค่าประมาณ 360 W ที่เวลา 10:03:20 กำลังสูงสุดจากโซล่าเซลล์มีค่าประมาณ 360 W ที่เวลา 10:05:50 กำลังสูงสุดจากโซล่าเซลล์มีค่าประมาณ 360 W ที่เวลา 10:06:40 กำลังสูงสุดจากโซล่าเซลล์มีค่าลดลงจาก 360 W ไป ยัง 240 W ชัดเจนมากที่แหล่งจ่ายไฟแบบผสมนี้มีการทำงานที่สมดุลย์ตลอดเวลา ($p_{\text{Load}}(t) \approx p_{\text{FC}}(t) + p_{\text{PV}}(t) + p_{\text{SC}}(t)$) ด้วยวิธีการควบคุมที่นำเสนอ





ภาพที่ 3-12 การตอบสนองของแหล่งจ่ายไฟแบบผสมต่อโหลดหลายรอบ

จุดเด่นหลักของงานวิจัยนี้คือนำเสนอการหาโมเดลและการควบคุมโรงไฟฟ้าแบบผสมที่จ่ายไฟโดย เซลล์เชื้อเพลิง โซล่าเซลล์และแบตเตอร์รี่ชนิดซุปเปอร์คาปาซิเตอร์ โรงไฟฟ้าต้นแบบที่ทำการศึกษา ประกอบด้วยระบบเซลล์เชื้อเพลิงชนิด PEMFC (ขนาด 1200 W เรียกว่า Nexa Ballard FC power system) แผงโซล่าเซลล์ (ขนาด 800 W ของบริษัท เอกรัฐโซล่า จำกัด) และโมดูลของซุปเปอร์คาปาซิเตอร์ (100 F, 32 V ของบริษัท Maxwell Technologies) วงจรแปลงไฟแบบทบแรงดันขนานกันสี่ตัวสำหรับเซลล์เชื้อเพลิง วงจรแปลงไฟแบบทบแรงดันขนานกันสองตัวสำหรับโซล่าเซลล์และวงจรแปลงไฟ แบบสองทิศทางขนานกันสี่ตัวสำหรับซุปเปอร์คาปาซิเตอร์ ซึ่งเป็นต้นแบบสำหรับงานกำลังสูง หลักการ ทำงาน การวิเคราะห์และการออกแบบแต่ละขั้นตอนได้ถูกนำเสนอ

โซล่าเซลล์จะทำงานเป็นแหล่งจ่ายไฟหลัก ขณะที่เซลล์เชื้อเพลิงจะช่วยจ่ายไฟเพื่อชดเชยบาง สถานการณ์ที่โซล่าเซลล์ไม่สามารถจ่ายไฟได้ในสถาวะอยู่ตัว ซุปเปอร์คาปาซิเตอร์ทำหน้าที่เป็นแหล่ง พลังงานสำรองหรือแหล่งจ่ายไฟสำรอง ช่วยจ่ายไฟเมื่อเซลล์เชื้อเพลิงและโซล่าเซลล์ไม่สามารถจ่ายไฟ ทั้งในสภาวะอยู่ตัวและไดนามิกส์

ด้วยวิธีการควบคุมแบบไม่เชิงเส้นแบบ flatness งานวิจัยนี้นำเสนอวิธีการแก้ปัญหาอย่างง่าย สำหรับปัญหาด้านไดนามิกส์ เสถียรภาพและความทนทานต่อการเปลี่ยนแปลงของพารามิเตอร์ในระบบ อิเล็กทรอนิกส์กำลังซึ่งเป็นระบบไม่เป็นเชิงเส้น ซึ่งเป็นแนวคิดต้นแบบสำหรับการประยุกต์ใช้งานใน ลักษณะนี้

ชุดทดลองด้านฮาร์ดแวร์ได้ถูกออกแบบและสร้างขึ้นจริงในห้องทดลอง เพื่อพิสูจน์ยืนยันวิธีการ ควบคุมและกฎการควบคุม ผลการทดลองพิสูจน์ให้เห็นว่าระบบทำงานได้เป็นอย่างดี

อย่างไรก็ตาม กฎการควบคุมที่นำเสนอมีความจำเป็นต้องวัดกระแสของโหลด เพื่อคำนวณกำลัง ของโหลด งานในอนาคต ระบบจะต้องมีตัวสังเกตการณ์ของโหลด (load observer) เพื่อหลีกเลี่ยงการ วัดกระแสของโหลดนี้

- [1] P. Thounthong, B. Davat, and S. Raël, "Drive friendly," *IEEE Power Energy Mag.*, vol. 6, no. 1, pp. 69–76, Jan./Feb. 2008.
- [2] M. W. Ellis, M. R. Von Spakovsky, and D. J. Nelson, "Fuel cell systems: Efficient, flexible energy conversion for the 21st century," *Proc. IEEE*, vol. 89, no. 12, pp. 1808–1818, Dec. 2001.
- [3] W. Friede, S. Raël, and B. Davat, "Mathematical model and characterization of the transient behavior of a PEM fuel cell," *IEEE Trans. Power Electron.*, vol. 19, no. 5, pp. 1234–1241, Sept. 2004.
- [4] P. Thounthong, B. Davat, S. Raël, and P. Sethakul, "Fuel cell high power applications," *IEEE Ind. Electron. Mag.*, vol. 3, no. 1, pp. 32–46, Mar. 2009.
- [5] M. Hinaje, I. Sadli, J.-P. Martin, P. Thounthong, S. Raël, and B. Davat, "Online humidification diagnosis of a PEMFC using a static dc-dc converter," *Int. J. Hydrogen Energy*, vol. 34, no. 6, pp. 2718–2723, Mar. 2009.
- [6] I. Sadli, P. Thounthong, J.-P. Martin, S. Raël, and B. Davat, "Behaviour of a PEMFC supplying a low voltage static converter," *J. Power Sources*, vol. 156, no. 1, pp. 119–125, May 2006.
- [7] The IEA Photovoltaic Power Systems Programme, "Trends in photovoltaic applications," Survey report 2008.
- [8] R. M. Nelms, D. R. Cahela, and B. J. Tatarchuk, "Modeling double-layer capacitor behavior using ladder circuits," *IEEE Trans. Aerosp. Electron. Syst.*, vol. 39, no. 2, pp. 430–438, Apr. 2003.
- [9] P. Thounthong and S. Raël, "The Benefits of hybridization," *IEEE Ind. Electron. Mag.*, vol. 3, no. 3, pp. 25–37, Sept. 2009.
- [10] P. Thounthong, S. Raël, and B. Davat, "Analysis of supercapacitor as second source based on fuel cell power generation," *IEEE Trans. Energy Convers.*, vol. 24, no. 1, pp. 247–255, Mar. 2009.
- [11] J. R. Miller and D. A. Evans, "Performance characteristics of high reliability double layer capacitor components," in *Proc. 35th IEEE Int. Power Sources Symp.*, Cherry Hill, NJ, Jan. 22–25, 1992, pp. 302–305.
- [12] Rajashekara, J. Grieve, and D. Daggett, "Hybrid fuel cell power in aircraft," *IEEE Ind. Appl. Mag.*, vol. 14, no. 4, pp. 54–60, July-Aug. 2008.
- [13] D. Maksimovic, A. M. Stankovic, V. J. Thsottuvelil, and G. C. Verghese, "Modeling and simulation of power electronic converters," *Proc. IEEE*, vol. 89, no. 6, pp. 898–942, Jun. 2001.
- [14] E. V. Dijk, H. J. N. Spruijt, D. M. O'Sullivan, and J. B. Klaassens, "PWM-switch modeling of DC–DC converters," *IEEE Trans. Power Electron.*, vol. 10, no. 6, pp. 659–665, Nov. 1995.
- [15] D. J. Perreault and J. G. Kassakian, "Distributed Interleaving of Paralleled Power Converters," *IEEE Trans. Circuits Syst. I, Fundam. Theory Appl.*, vol. 44, no. 8, pp. 728–734, Aug. 1997.

- [16] M. Veerachary, T. Senjyu, and K.Uezato, "Signal flow graph nonlinear modelling of interleaved Converters," *IEE Proc. Electr. Power Appl.*, vol. 148, no. 5, pp. 410–418, Sep. 2001.
- [17] H. B. Shin, J. G. Park, S. K. Chung, H. W. Lee, and T.A. Lipo, "Generalised steady-state analysis of multiphase interleaved boost converter with coupled inductors," *IEE Proc. Electr. Power Appl.*, vol. 152, no. 3, pp. 584–594, May 2005.
- [18] M. Baumann, and J. W. Kolar, "Parallel connection of two three-phase three-switch buck-type unity-power-factor rectifier systems with DC-link current balancing," *IEEE Trans. Ind. Electron.*, vol. 54, no. 6, pp. 3042–3053, Dec. 2007.
- [19] P. Thounthong, S. Raël, and B. Davat, "Control strategy of fuel cell/supercapacitors hybrid power sources for electric vehicle," *J. Power Sources*, vol. 158, no. 1, pp. 806–814, Jul. 2006.
- [20] M. Fliess, J. Lévine, Ph. Martin, and P. Rouchon, "Flatness and defect of nonlinear systems: Introductory theory and examples," *Int. J. Contr.*, vol. 61, no. 6, pp. 1327–1361, 1995.
- [21] M. Fliess, J. Lévine, P.Martin, and P. Rouchon, "A lie-bäcklund approach to equivalence and flatness of nonlinear systems," *IEEE Trans. Autom. Control*, vol. 44, no. 5, pp. 922–937, May 1999.
- [22] V. Morio, F. Cazaurang, and P. Vernis, "Flatness-based hypersonic reentry guidance of a lifting-body vehicle," *Control Engineering Practice*, vol. 17, no. 5, pp. 588–596, May 2009.
- [23] P. Thounthong and B. Davat, "Study of a multiphase interleaved step-up converter for fuel cell high power applications," *Energy Convers. Manage.*, vol. 51, no. 1, pp. 826–832, April 2010.
- [24] P. Thounthong, V. Chunkag, P. Sethakul, S. Sikkabut, S. Pierfederici, and B. Davat, "Energy management of fuel cell/solar cell/supercapacitor hybrid power source," *J. Power Sources*, 2010 (in press).
- [25] C. P. Mudannayake and M. F. Rahman, "Future automotive 42-V powernet application," *IEEE Ind. Appl. Mag.*, vol. 15, no. 4, pp. 14–25, July-Aug. 2009.
- [26] P. Thounthong, S. Raël, and B. Davat, "Control strategy of fuel cell and supercapacitors association for a distributed generation system," *IEEE Trans. Ind. Electron.*, vol. 54, no. 6, pp. 3225–3233, Dec. 2007.
- [27] P. Thounthong, S. Raël, and B. Davat, "Energy management of fuel cell/battery/supercapacitor hybrid power source for vehicle applications," *J. Power Sources*, no. 193, no. 1, pp. 376–385, August 2009.
- [28] E. Song, A. F. Lynch, and V. Dinavahi. "Experimental validation of nonlinear control for a voltage source converter," *IEEE Trans. Control System Technology*, vol. 17, no. 5, pp. 1135–1144, Sept. 2009.
- [29] A. Gensior, H. Sira-Ramirez, J. Rudolph, H. Guldner, "On some nonlinear current controllers for three-phase boost rectifiers," *IEEE Trans. Ind. Electron.*, vol. 56, no. 2, pp. 360–370, Feb. 2009.
- [30] P. Thounthong, V. Chunkag, P. Sethakul, B. Davat, and M. Hinaje, "Comparative study of fuel-cell vehicle hybridization with battery or supercapacitor storage device," *IEEE Trans. Veh. Technol.*, vol. 58, no. 8, pp. 3892–3904, Oct. 2009.

- [31] P. Thounthong, B. Davat, S. Raël, and P. Sethakul, "Fuel starvation: Analysis of a PEM fuel cell system," *IEEE Ind. Appl. Mag.*, vol. 15, no. 4, pp. 52–59, Jul./Aug. 2009.
- [32] P. Thounthong, S. Raël, and B. Davat, "Control algorithm of fuel cell and batteries for distributed generation system," *IEEE Trans. Energy Convers.*, vol. 23, no. 1, pp. 148–155, Jan. 2008.

Output จากโครงการวิจัยที่ได้รับทุนจาก สกว.

- 1). ผลงานตีพิมพ์ในวารสารวิชาการนานาชาติ (The Thailand Research Fund (TRF) under Grant MRG5180348)
 - 1.1 **P. Thounthong**, V. Chunkag, P. Sethakul, B. Davat, and M. Hinaje, "Comparative study of fuelcell vehicle hybridization with battery or supercapacitor storage device," *IEEE Trans. Veh. Technol.*, vol. 58, no. 8, pp. 3892–3904, Oct. 2009. (2009 Impact Factor: 1.488) (ดูเอกสารแนบ)
 - 1.2 **P. Thounthong**, V. Chunkag, P. Sethakul, S. Sikkabut, S. Pierfederici, and B. Davat, "Energy management of fuel cell/solar cell/supercapacitor hybrid power source," *J. Power Sources*, 2010 (in press). (2009 Impact Factor: 3.792) (ดูเอกสารแนบ)
 - 1.3 **P. Thounthong**, B. Davat, S. Raël, and P. Sethakul, "Fuel cell high power applications," *IEEE Ind. Electron. Mag.*, vol. 3, no. 1, pp. 32–46, Mar. 2009. (2009 Impact Factor: 1.750) (ดูเอกสาร แนบ)
 - 1.4 **P. Thounthong**, B. Davat, S. Raël, and P. Sethakul, "Fuel starvation: Analysis of a PEM fuel cell system," *IEEE Ind. Appl. Mag.*, vol. 15, no. 4, pp. 52–59, Jul./Aug. 2009. (2009 Impact Factor: **0.727**) (ดูเอกสารแนบ)
 - 1.5 **P. Thounthong**, S. Raël, and B. Davat, "Energy management of fuel cell/battery/supercapacitor hybrid power source for vehicle applications," *J. Power Sources*, no. 193, no. 1, pp. 376–385, August 2009. (2009 Impact Factor: 3.792) (ดูเอกสารแนบ)
 - 1.6 **P. Thounthong** and S. Raël, "The Benefits of hybridization," *IEEE Ind. Electron. Mag.*, vol. 3, no. 3, pp. 25–37, Sept. 2009. (2009 Impact Factor: 1.750) (ดูเอกสารแนบ)
 - 1.7 **P. Thounthong** and B. Davat, "Study of a multiphase interleaved step-up converter for fuel cell high power applications," *Energy Convers. Manage.*, vol. 51, no. 1, pp. 826–832, April 2010. (2009 Impact Factor: 1.944) (ดูเอกสารแนบ)
 - 1.8 **P. Thounthong**, S. Pierfederici, J.-P. Martin, M. Hinaje, and B. Davat, "Modeling and control of fuel cell/supercapacitor hybrid source based on differential flatness control," *IEEE Trans. Veh. Technol.*, vol. 59, no. 9, pp. 2700–2710, July 2010. (2009 Impact Factor: 1.488) (ดูเอกสารแนบ)
 - 1.9 **P. Thounthong**, S. Pierfederici, and B. Davat, "Analysis of differential flatness-based control for a fuel cell hybrid power source," *IEEE Trans. Energy Convers.*, 2010 (in press). (2009 Impact Factor: 2.635) (ดูเอกสารแนบ)

2). การนำผลงานวิจัยไปใช้ประโยชน์

- เชิงวิชาการ (มีการพัฒนาการเรียนการสอน/สร้างนักวิจัยใหม่)

<u>พัฒนาการเรียนการสอน</u> ชุดทดลองในงานวิจัยนี้ ใช้ประกอบการเรียนการสอน
ระดับ ปริญญาตรี วิชาอิเล็กทรอนิกส์กำลัง (Power Electronics) รหัสวิชา: 223304
ภาควิชาครุศาสตร์ไฟฟ้า คณะครุศาสตร์อุตสาหกรรม
มหาวิทยาลัยเทคโนโลยีพระจอมเกล้าพระนครเหนือ

<u>สร้างนักวิจัยใหม่</u> 2 คนคือนายสุวัจน์ สิกบุตรและนายพงษ์ศิริ มุ่งพร ตำแหน่งวิศวกรไฟฟ้า สถาบันเทคโนโลยีไทย-ฝรั่งเศส มหาวิทยาลัยเทคโนโลยีพระจอมเกล้าพระนครเหนือ

3). การเสนอผลงานในที่ประชุมวิชาการระดับนานาชาติ

- 3.1 **P. Thounthong**, V. Chunkag, P. Sethakul, S. Pierfederici, and B. Davat, "Energy Management of Fuel Cell/Solar Cell/Battery/Supercapacitor Hybrid Power Source for Distributed Generation System," *in Proceeding of the Eleventh Grove Fuel Cell Symposium*, Queen Elizabeth II Conference Centre, Westminster, London, United Kingdom, 22-24 September 2009. Organized by Elsevier Publisher.
- 3.2 **P. Thounthong**, V. Chunkag, P. Sethakul, and B. Davat, "High-gain high-power converter for fuel cell applications," *in Proceeding of the Eleventh Grove Fuel Cell Symposium*, Queen Elizabeth II Conference Centre, Westminster, London, United Kingdom, 22-24 September 2009. Organized by Elsevier Publisher.
- 3.3 **P. Thounthong**, P. Sethakul, S. Raël, and B. Davat, "Performance Evaluation of Fuel Cell/Battery/Supercapacitor Hybrid Power Source for Vehicle Applications," *in Proceeding of the 2009 IEEE Industry Applications Society Annual Meeting (IAS-2009)*, Houston, Texas, USA, 4-8 October 2009. pp. 1-8 (CD-ROM).
- 3.4 **P. Thounthong**, N. Poonnoi, P. Sethakul, and B. Davat, "Performance Evaluation of Modified 4-phase Interleaved Fuel Cell Converter for High-Gain High-Power Applications," *in Proceeding of the 2009 IEEE Industry Applications Society Annual Meeting (IAS-2009)*, Houston, Texas, USA, 4-8 October 2009. pp. 1-8 (CD-ROM).
- 3.5 **P. Thounthong**, P. Sethakul, S. Raël, and B. Davat, "Fuel Cell Current Ripple Mitigation by Interleaved Technique for High Power Applications," *in Proceeding of the 2009 IEEE Industry Applications Society Annual Meeting (IAS-2009)*, Houston, Texas, USA, 4-8 October 2009. pp. 1-8 (CD-ROM).
- P. Thounthong, S. Sikkabut, P. Sethakul, and B. Davat, "Control Algorithm of Renewable Energy Power Plant Supplied by Fuel Cell/Solar Cell/Supercapacitor Power Source," in Proceeding of the 2010 International Power Electronics Conference (IPEC-Sapporo, ECCE ASIA), Sapporo, Hokkaido, Japan, USA, 21-24 June 2010, pp. 1155-1162, Organized by The Industry Applications Society of the Institute of Electrical Engineers of Japan (IEEJ) and IEEE.
- 3.7 **P. Thounthong**, S. Sikkabut, P. Sethakul, S. Pierfederici, and B. Davat, "Fuel Cell Power Regulation Based-on Differential Flatness Theory for High-Power Converter Applications," *in Proceeding of the 2010 IEEE-XIX International Conference on Electrical Machines* (ICEM2010), Rome, Italy, 6-10 September 2010.
- 3.8 **P. Thounthong**, S. Pierfederici, and B. Davat, "Performance Evaluation of Differential Flatness Based-Control of Fuel Cell/Supercapacitor Hybrid Power Source," *in Proceeding of the 2010 IEEE-XIX International Conference on Electrical Machines* (ICEM2010), Rome, Italy, 6-10 September 2010.
- 3.9 **P. Thounthong**, P. Mungporn, and B. Davat, "A Nonlinear Control Approach to the Energy Management of Solar Power Plant with Supercapacitor for Grid-Independent Applications," *in Proceeding of the 2010 IEEE-XIX International Conference on Electrical Machines* (ICEM2010), Rome, Italy, 6-10 September 2010.

4). นักวิจัยที่สำเร็จการศึกษาระดับปริญญาโทจำนวน 3 คน

- 4.1 นายณิชมน พูนน้อย หัวข้อวิทยานิพนธ์เรื่อง "High Voltage Gain Non-Isolated Converter for Fuel Cell Distributed Generation"
 - ภาควิชาวิศวกรรมไฟฟ้า มหาวิทยาลัยเทคโนโลยีพระจอมเกล้าพระนครเหนือ
- 4.2 นายสิทธิกร ธนาวุฒิ หัวข้อวิทยานิพนธ์เรื่อง "Hybrid DC Source by Fuel Cell and Lithium-ion Battery" ภาควิชาวิศวกรรมไฟฟ้า มหาวิทยาลัยเทคโนโลยีพระจอมเกล้าพระนครเหนือ
- 4.3 นายประเสริฐ สารการ
 หัวข้อวิทยานิพนธ์เรื่อง "The Investigation in Hybrid DC Energy Control of Fuel Cell and Battery"
 ภาควิชาวิศวกรรมไฟฟ้า มหาวิทยาลัยเทคโนโลยีราชมงคลธัญบุรี

TRF: MRG5180348

IEEE TRANSACTIONS ON

VEHICULAR TECHNOLOGY

A PUBLICATION OF THE IEEE VEHICULAR TECHNOLOGY SOCIETY

OCTOBER 2009 VOLUME 58 NUMBER 8 ITVTAB (ISSN 0018-9545)

SPECIAL SECTION ON VEHICULAR ENERGY-STORAGE SYSTEMS				
GUEST EDITORIAL				
Special Section on Vehicular Energy-Storage Systems	3879			
SPECIAL SECTION PAPERS				
Influence of Battery/Ultracapacitor Energy-Storage Sizing on Battery Lifetime in a Fuel Cell Hybrid Electric Vehicle	3882			
Comparative Study of Fuel-Cell Vehicle Hybridization with Battery or Supercapacitor Storage Device	3892			
New Battery Model and State-of-Health Determination Through Subspace Parameter Estimation and State-Observer Techniques	3905			
Imped of Calcindar Effe and Cycling Agents of Supercapacitor Ferformance	3917			
Feasibility Analysis of a Novel Cell Equalizer Topology for Plug-In Hybrid Electric Vehicle Energy-Storage Systems	3930			
Sizing and Energy Management of a Hybrid Locomotive Based on Flywheel and Accumulators	3938			
	3947			
Advanced Integrated Bidirectional AC/DC and DC/DC Converter for Plug-In Hybrid Electric Vehicles	3959			
YJ. Lee, A. Khaligh, and A. Emadi	3970			
Dynamic Voltage Equalization for Series-Connected Ultracapacitors in EV/HEV Applications A. Xu, S. Xie, and X. Liu	3981			
REGULAR SECTION PAPERS				
Channel Models				
Unified Laguerre Polynomial-Series-Based Distribution of Small-Scale Fading Envelopes C. C. Chai and T. T. Tjhung Ricean K-Factors in Narrow-Band Fixed Wireless Channels: Theory, Experiments, and Statistical Models	3988			
L. J. Greenstein, S. S. Ghassemzadeh, V. Erceg, and D. G. Michelson	4000			

(Contents Continued on Page 3877)



IEEE VEHICULAR TECHNOLOGY SOCIETY

The Vehicular Technology Society is an organization, within the framework of the IEEE are eligible for members with principal professional interest in vehicular communications. All members of the IEEE are eligible for membership in the Society and will receive this TRANSACTIONS upon payment of the annual Society membership fee of \$18.00 plus an annual subscription fee of \$22.00. For information on joining, write to the IEEE at the address below. *Member copies of Transactions/Journals are for personal use only.*

IEEE TRANSACTIONS ON VEHICULAR TECHNOLOGY

WEIHUA ZHUANG

Department of Electrical and Computer Engineering, University of Waterloo Waterloo, ON N2L 3G1, Canada Phone: +1 519 888 4567 x35354 Fax: +1 519 746 3077 wzhuang@uwaterloo.ca wzhuang@uwaterloo.ca

Associate Editors

M. SHAHGIR AHMED Daimler Chrysler Corp. Auburn Hills, MI 48326-2757 USA

OZGUR AKAN Middle East Technical Univ. Ankara, Turkey

SOHEL ANWAR

Purdue School of Engineering and Technology Indianapolis, IN 46202 USA

NALLANATHAN ARUMUGAM King's College London London, WC2R 2LS, U.K. GERHARD BAUCH

Universität der Bundeswehr München D-85577 Neubiberg, Germany

MOHAMED E. BENBOUZID Univ. of Western Brittany Brest Cedex 3, France

ERNST BONEK Vienna Univ. of Technology A-1040 Vienna, Austria AZZEDINE BOUKERCHE

Univ. of Ottawa Ottawa, ON K1N 6N5, Canada

LIN CAL Univ. of Victoria Victoria, BC V8W 3P6, Canada

GUOHONG CAO Pennsylvania State Univ. Univ. Park, PA 16801 USA

SUJEET CHAUDHURI Univ. of Waterloo Waterloo, ON N2L 3G1, Canada

SONG CI Univ. of Nebraska Omaha, NE 68182 USA

HSIAO-HWA CHEN National Cheng Kung Univ. Tainan, Taiwan, R.O.C.

JOHN R. VIG, President PEDRO A. RAY, President-Elect

PEDRO A. RAT, Trestaent-lect BARRY L. SHOOP, Secretary PETER W. STAECKER, Treasurer LEWIS M. TERMAN, Past President TEOFILO RAMOS, Vice President, Educational Activities

LIQUN CHEN Hewlett-Packard Laboratories Bristol BS34 8QZ, U.K.

YU CHENG

Illinois Institute of Technology Chicago, IL 60616-3793 USA

JOOHWAN CHUN KAIST Daejon City, Korea

CARMELA COZZO ViaSat Inc. El Cajon, CA 92020 USA

JING DENG

Univ. of North Carolina at Greensboro Greensboro, 27402-6170 USA

DEMBA DIALLO

Univ. Paris-Sud, P11, IUT of Cachan 91192 Gif-Sur-Yvette, France

MISCHA DOHLER France Telecom R&D 38243 Meylan Cedex, France

KAZUHIKO FUKAWA Tokyo Institute of Technology Tokyo, Japan

YANG GAO Univ. of Calgary Calgary, AB T2N 1N4, Canada

ALL GHRAYER Concordia Univ

Montreal, QC H3G 1M8, Canada HOSSAM S. HASSANEIN

Oueen's Univ. Kingston, ON K7L 3N6, Canada

EKRAM HOSSAIN

Univ. of Manitoba Winnipeg, MB R3T 5V6, Canada

JIN HUR Univ. of Ulsan Ulsan, 680-749, Korea

HUAPING LIU Helsinki Univ. of Technology

FI-02015 TKK, Finland HAI JIANG

RIKU JÄNTTI

Univ. of Alberta Edmonton, AB T6G 2V4, Canada ALIREZA KHALIGH

Illinois Institute of Technology Chicago, IL 60616-3793 USA WITOLD KRZYMIEN

Univ. of Alberta Edmonton, AB T6G 2V4, Canada

THOMAS KÜRNER Braunschweig Technical Univ. Braunschweig, Germany SHU HUNG LEUNG

City Univ. of Hong Kong Kowloon, Hong Kong JIE LI

Univ. of Tsukuba Tsukuba, Japan YING CHANG LIANG

Inst. for Infocomm Res., A*STAR Singapore 119613 CHUANG LIN Tsinghua Univ. Beijing, China

HAI LIN Osaka Prefecture Univ. Osaka, Japan JIA-CHIN LIN

National Central Univ. Taoyuan, Taiwan, R.O.C. PHONE LIN

National Taiwan Univ. Taipei, Taiwan, R.O.C. YI-BING (JASON) LIN

National Chiao Tung Univ. Hsinchu, Taiwan, R.O.C. CONG LING

Imperial College London London, SW7 2AZ, U.K.

Oregon State Univ Corvallis, OR 97331 USA

HSIAO-FENG LU National Chiao Tung Univ. Hsinchu, Taiwan

Iowa State Univ. Ames, IA 50011 USA

DAVID MATOLAK Ohio Univ. Athens, OH 45701 USA

CHRIS (CHUNTING) MI Univ. of Michigan—Dearborn Dearborn, MI 48128 USA

JELENA MISIC Univ. of Manitoba Winnipeg, BC R3T 2N2, Canada

HA H. NGUYEN Univ. of Saskatchewar Saskatoon, SK S7N 5A9, Canada

CLAUDE OESTGES Université catholique de Louvain Louvain-la-Neuve, B-1348 Belgium

ROBERT OIU Tennessee Technological Univ. Cookeville, TN 38505 USA

YU TED SU National Chiao Tung Univ. Hsinchu, Taiwan

TOMOHIKO TANIGUCHI Fujitsu Laboratories Limited Kanagawa, 239-0847, Japan

Andrea M. Tonello Universita di Udine Udine, 33100, Italy

UFUK TURELI

WVU Institute of Technology Montgomery, WV25136 USA

XIANBIN WANG Univ. of Western Ontario London, ON N6A 3K7, Canada

SHUANGOING WEI Louisiana State Univ Baton Rouge, LA 70803 USA

KAINAM T. WONG Hong Kong Polytechnic Univ. Kowloon, Hong Kong

VINCENT WONG Univ. of British Columbia Vancouver, BC V6T 1Z4, Canada HSIAO-CHUN WU

Louisiana State Univ Baton Rouge, LA 70803 USA

JINGXIAN WU Univ. of Arkansas Fayetteville, AR 72701 USA

Univ. of Alabama Tuscaloosa, AL 35487-0290 USA

CHAU YUEN Institute for Infocomm Research Singapore 119613

ZHENGOING YUN Univ. of Hawaii at Manoa Honolulu, HI 96822 USA

KAMBIZ ZANGI Ericsson Research

Research Triangle Park, NC 27709 USA

XI ZHANG Texas A&M Univ. College Station, TX 77843 USA

YANCHAO ZHANG

New Jersey Institute of Technology Newark, NJ 07102 USA

DONGMEI ZHAO McMaster Univ

Hamilton, ON L8S 4K1, Canada

IEEE Officers

JON G. ROKNE, Vice President, Publication Services and Products JOSEPH V. LILLIE, Vice President, Membership and Geographic Activities
W. CHARLTON (CHUCK) ADAMS, President, IEEE Standards Association
HAROLD L. FLESCHER, Vice President, Technical Activities GORDON W. DAY, President, IEEE-USA

FREDERICK C. MINTZER, Director, Division IX-Signals and Applications

IEEE Executive Staff

DR. E. JAMES PRENDERGAST, Executive Director & Chief Operating Officer

BETSY DAVIS, SPHR, Human Resources ANTHONY DURNIAK, Publications Activities JUDITH GORMAN, Standards Activities CECELIA JANKOWSKI, Member and Geographic Activities
DOUGLAS GORHAM, Educational Activities MATTHEW LOEB, Corporate Strategy & Communications RICHARD D. SCHWARTZ, Business Administration CHRIS BRANTLEY, IEEE-USA MARY WARD-CALLAN, Technical Activities

IEEE Periodicals Transactions/Journals Department

Staff Director: Fran Zappulla Editorial Director: Dawn Melley Production Director: Peter M. Tuohy Senior Managing Editor: William A. Colacchio Senior Editor: Christopher Perry

IEEE TRANSACTIONS ON VEHICULAR TECHNOLOGY (ISSN 0018-9545) is published nine times a year in January, February, March, May, June, July, September, October, and November by The Institute of Electrical and Electronics Engineers, Inc. Responsibility for the contents rests upon the authors and not upon the IEEE, the Society/Council, or its members. IEEE Corporate Office: 3 Park Avenue, 17th Floor, New York, NY 10016-5997. IEEE Operations Center: 445 Hoes Lane, Piscataway, NJ 08854-4141. NJ Telephone: +1 732 981 0060. Price/Publication Information: Individual copies: IEEE Members \$20.00 (first copy only), nonmembers \$84.00 per copy. (Note: Postage and handling charge not included.) Member and nonmember subscription prices available upon request. Available in microfiche and microfilm. Copyright and Reprint Permissions: Abstracting is permitted with credit to the source. Libraries are permitted to photocopy for private use of patrons, provided the per-copy fee indicated in the code at the bottom of the first page is paid through the Copyright Clearance Center, 222 Rosewood Drive, Danvers, MA 01923. For all other copying, reprint, or republication permission, write to Copyrights and Permissions Department, IEEE Publications Administration, 445 Hoes Lane, Piscataway, NJ 08854-4141. Copyright © 2009 by The Institute of Electrical and Electronics Engineers, Inc. All rights reserved. Periodicals Postage Paid at New York, NY and at additional mailing offices. Postmaster: Send address changes to IEEE TRANSACTIONS ON VEHICULAR TECHNOLOGY, IEEE, 445 Hoes Lane, Piscataway, NJ 08854-4141. GST Registration No. 125634188. CPC Sales Agreement #40013087. Return undeliverable Canada addresses to: Pitney Bowes IMEX, P.O. Box 4332, Stanton Rd., Toronto, ON M5W 3J4, Canada. Printed in U.S.A.

Digital Object Identifier 10.1109/TVT.2009.2033653

Comparative Study of Fuel-Cell Vehicle Hybridization with Battery or Supercapacitor Storage Device

Phatiphat Thounthong, *Member, IEEE*, Viboon Chunkag, Panarit Sethakul, Bernard Davat, *Member, IEEE*, and Melika Hinaje

Abstract—This paper studies the impact of fuel-cell (FC) performance and control strategies on the benefits of hybridization. One of the main weak points of the FC is slow dynamics dominated by a temperature and fuel-delivery system (pumps, valves, and, in some cases, a hydrogen reformer). As a result, fast load demand will cause a high voltage drop in a short time, which is recognized as a fuel-starvation phenomenon. Therefore, to employ an FC in vehicle applications, the electrical system must have at least an auxiliary power source to improve system performance when electrical loads demand high energy in a short time. The possibilities of using a supercapacitor or a battery bank as an auxiliary source with an FC main source are presented in detail. The studies of two hybrid power systems for vehicle applications, i.e., FC/battery and FC/supercapacitor hybrid power sources, are explained. Experimental results with small-scale devices (a polymer electrolyte membrane FC of 500 W, 40 A, and 13 V; a lead-acid battery module of 33 Ah and 48 V; and a supercapacitor module of 292 F, 500 A, and 30 V) in a laboratory authenticate that energy-storage devices can assist the FC to meet the vehicle power demand and help achieve better performance, as well as to substantiate the excellent control schemes during motor-drive cycles.

Index Terms—Battery, converters, current control, electric vehicles, fuel cells (FCs), power supplies, supercapacitor, voltage regulation.

I. Introduction

F UEL CELLS (FCs) are able to generate electrical power with high efficiency, low operation noise, and no emissions

Manuscript received October 27, 2008; revised May 10, 2009 and July 6, 2009. First published July 31, 2009; current version published October 2, 2009. This work was supported in part by a research program in cooperation with the Thai-French Innovation Institute, King Mongkut's University of Technology North Bangkok, with the Institut National Polytechnique de Lorraine under the "Franco-Thai on Higher Education and Research Joint Project," and in part by the French National Center for Scientific Research, the Nancy Research Group in Electrical Engineering (GREEN: UMR 7037), and the Thailand Research Fund under Grant MRG5180348. The review of this paper was coordinated by Dr. A. Khaligh.

- P. Thounthong and P. Sethakul are with the Department of Teacher Training in Electrical Engineering, King Mongkut's University of Technology North Bangkok, Bangkok 10800, Thailand (e-mail: phtt@kmutnb.ac.th; pnrit@kmutnb.ac.th).
- V. Chunkag is with the Department of Electrical Engineering, King Mongkut's University of Technology North Bangkok, Bangkok 10800, Thailand (e-mail: vck@kmutnb.ac.th).
- B. Davat and M. Hinaje are with the Groupe de Recherche en Electrotechnique et Electronique de Nancy, Institut National Polytechnique de Lorraine, Nancy Université, 54510 Nancy, France (e-mail: Bernard.Davat@ensem.inpl-nancy.fr; Melika.Hinaje@ensem.inpl-nancy.fr).

Color versions of one or more of the figures in this paper are available online at http://ieeexplore.ieee.org.

Digital Object Identifier 10.1109/TVT.2009.2028571

from hydrogen gaze and air. Byproducts are exhaust gases, water, and waste heat. The supplied electrical power can be used in vehicles for propulsion as well as for the operation of electrically powered accessories. Polymer electrolyte membrane (or proton exchange membrane) FCs (PEMFCs) utilize a solid polymer electrolyte membrane, operate at lower temperature, and are considered by many to be the most suitable for vehicle applications (such as cars, buses, tramways, trains, or aircraft) [1], [2].

Although recent literature portrays FCs as a newly emerging energy source, the technology was actually invented in the 19th century. In 1839, Sir William Grove, a Welsh judge and scientist, assembled the first FC. Since then, FCs have been primarily used in research settings. The National Aeronautics and Space Administration selected PEMFCs for the space program in the 1960s, rejecting both nuclear power, which had a higher safety risk, and solar power, which had a higher cost [1]. FCs provided power for the Gemini and Apollo missions and, at present, provide water and electricity to the space shuttle. Despite their high-profile use in the space program, the commercialization of FC technology was not explored until the early 1980s.

Many factors have limited the marketable development of FCs, including manufacturing cost, fuel generation and distribution, and system complexity. The high manufacturing cost is caused by a number of factors: expensive raw materials used as catalysts, expensive membrane materials, and expensive fabrication processes for collector plates.

In addition to manufacturing cost, fuel generation and distribution have also prevented widespread commercialization. Most FCs consume pure hydrogen or hydrogen-rich gas as the primary fuel. So far, experimental results and real-world applications of PEMFCs revealed that they perform best on pure hydrogen (H₂) as anode input gas. However, for many applications, particularly mobile, due to a lack of availability of refueling infrastructure and impractical storage techniques, pure hydrogen is not yet a viable option. Pure hydrogen as an anode gas source for PEMFCs, at this time, has a number of formidable limitations. One of the major limitations is onboard hydrogen storage. As a viable alternative for carrying pure hydrogen, onboard hydrogen generation by reforming hydrocarbons such as natural gas, gasoline, or alcohol fuels would be an obvious choice. However, gas produced from a reformer contains about 70%-75% hydrogen, 20%-25% carbon dioxide (CO₂ poisoning), and 10-100 ppm carbon monoxide

0018-9545/\$26.00 © 2009 IEEE

(CO poisoning) [3]; furthermore, these reformers are large and expensive, and they operate at high temperatures.

Since most advanced vehicles like FC electric vehicles have one energy storage (buffer) device as part of the propulsion system, it is possible and necessary to apply advanced control technologies to significantly optimize the vehicle's fuel economy, emissions, and/or drivability [4], [5].

Nonetheless, the recent studies of Corrêa et al. [6], who worked with a 0.5-kW PEMFC (BCS Technology Company) and a 0.5-kW PEMFC (Avista Company), Thounthong et al. [5], [7], who worked with a 0.5-kW PEMFC [Zentrum für Sonnenenergie und Wasserstoff-Forschung (ZSW) Company, Germany] and a 1.2-kW Nexa PEMFC (Ballard Power System Company, Canada), Adzakpa et al. [8], who worked with a 0.6-kW PEMFC (H Power Company), Wang et al. [9], who worked with a 0.5-kW PEMFC (Avista Company), and Gaynor et al. [10], who worked with a 350-kW Solid Oxide FC, have demonstrated the fact that the FC time constants are dominated by a temperature and fuel-delivery system (pumps, valves, and, in some cases, a hydrogen reformer). As a result, fast energy demand will cause a high voltage drop in a short time, which is recognized as a fuel-starvation phenomenon [11].

When starved from fuel or oxygen, the FC performance degrades, and the cell voltage drops. This condition of operation is evidently hazardous for the FC stack [11], [12]. Fuel starvation can result in generation of hydrogen in the cathode or oxygen in the anode. For instance, in the event of hydrogen starvation, the cell current cannot be maintained, causing a high anode potential. Therefore, the water, which is present at the anode, may split into hydrogen and oxygen, producing oxygen in the anode. In the same way, during oxygen starvation, the reaction at the cathode will produce hydrogen. The presence of oxygen at the anode and hydrogen at the cathode will lead to the reversal of the cell potential, which is a negative potential difference between the anode and the cathode. Cell reversal accelerates the corrosion of carbon components such as backing layers with ensuing electrocatalyst corrosion and eventually leads to damaged components. During hydrogen starvation, oxygen at the anode can react with the carbon present in the gas diffusion and backing layers to form carbon dioxide (CO₂) poisoning).

Thus, to utilize an FC in dynamic applications, its current or power slope must be limited to circumvent the fuel-starvation problem, e.g., $4 \text{ A} \cdot \text{s}^{-1}$ for a 0.5-kW 12.5-V PEMFC [13] and 5, 10, and 50 $\text{A} \cdot \text{s}^{-1}$ for a 20-kW 48-V PEMFC [14]. As a result, the vehicle electrical system must have at least an auxiliary power source (an energy storage device), such as a battery, supercapacitor, or flywheel, to improve the system performance when electrical loads at a dc bus demand high power in a short time (e.g., vehicle acceleration and deceleration) [15], [16]. Therefore, an FC vehicle can benefit from being hybridized with an energy-storage device [17]–[19], which assumes some of the roles that the FC would normally handle.

This paper deals with the conception and the achievement of a hybrid power source that is supplied by a PEMFC as the main energy source and a battery or a supercapacitor as an auxiliary power source, particularly for future vehicle applications. Its interest is focused on control algorithms. It enables the management of transient power demand, power peaks, and regenerative braking with regard to FC, battery, and supercapacitor constraints. The general structures of the studied systems, the control principles of the hybrid sources, the realization of the experimental bench, and the experimental validation will be presented in the following sections.

II. BATTERY VERSUS SUPERCAPACITOR AS AN ENERGY-STORAGE DEVICE

Currently, the battery is still the most extensive energy-storage device for providing and deliver electricity. There are many kinds of battery technology, such as lead-acid, NiCd, NiMH, or Li-ion. For a lead-acid cell, the terminal voltage of battery V_b and the internal resistance R_b are strong functions of the state of charge (SOC). The battery actual voltage curve is not constant. This is because the internal resistance is almost linear during the discharge, but the losses are substantially below 25% SOC due to the increase in the internal resistance. Therefore, the battery SOC estimation is defined here again as [20], [21]

$$SOC(t) = \frac{1}{Q_{\text{Bat}}} \int_{t_0}^{t} i_{\text{Bat}}(t) \cdot dt + SOC_0(t_0)$$
 (1)

where SOC_0 is the known battery SOC (in percentage) at time t_0 , $Q_{\rm Bat}$ is the rated capacity (in ampere-hours), and $i_{\rm Bat}(t)$ is the charging battery current (in amperes).

Supercapacitors (or ultracapacitors) are an emerging technology in the field of energy storage systems. Current breakthroughs in material design and fabrication methods that are aimed at maximizing rated capacitance have provided tremendous increases in the energy-storage capabilities of supercapacitors [22], [23]. The terminal voltage of supercapacitors is limited, however, due to the dissociation of the electrolyte. This limits the maximum voltage to 2.5–3 V.

When comparing the power characteristics of supercapacitors and batteries, the comparisons should be made for the same charge/discharge efficiency. The relative performance of supercapacitors and power batteries can be directly assessed from the pulse power tests since both types of devices are capable of high-power pulses, although batteries are not intended to be charged/discharged for long periods at these high power levels. The pulse testing of a battery is usually done at a specified partial SOC, as only a small fraction of the energy stored in the battery is used in the cycle tests. Of particular interest in the pulse tests is the round-trip efficiency of the devices. This is determined from the ratio of the energy out of the devices to the energy into the devices during the test cycle. This efficiency primarily depends on the internal equivalent series resistance (ESR) of the device. For supercapacitors, their charge/discharge efficiency is high, and the energy lost to heat during each cycle is relatively small and readily removed. The energy lost to heat in batteries is a much larger amount, making heat removal more crucial and its extraction costs much higher. This is to say that the cycle efficiency of batteries is around 80%, and the cycle efficiency of supercapacitors is around 95% [24], [25]. For a

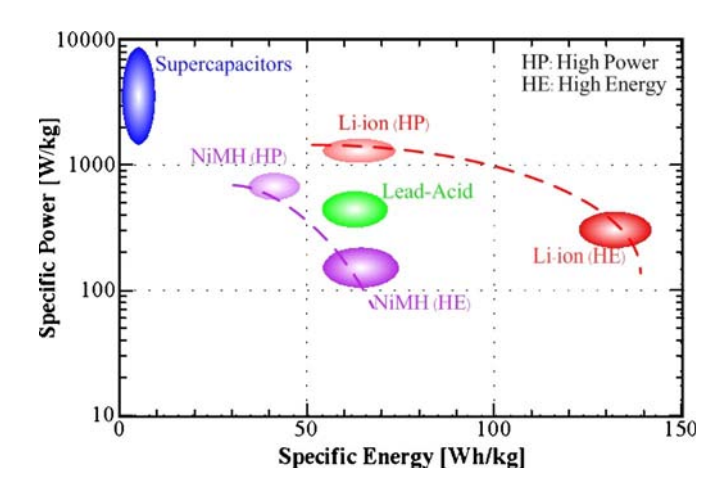


Fig. 1. Specific power versus specific energy of modern storage devices: supercapacitor, lead-acid, NiMH, and Li-ion battery technology. Note that the supercapacitors, NiMH, and Li-ion batteries are based on SAFT Company (France) technology.

corresponding high-efficiency discharge, batteries would have a much lower power capability.

Furthermore, the main drawback of batteries is a slow charging time, limited by a charging current [25], [26]; in contrast, supercapacitors may be charged over a short time, depending on a high charging current (power) that is available from the main source. Capacitor voltage $v_{\rm C}$ can then be found using the following classical equation:

$$v_C(t) = \frac{1}{C} \int_{t_0}^{t} i_C(t) \cdot dt + v_C(t_0)$$
 (2)

where $i_C(t)$ is the charging capacitor current.

Moreover, Fig. 1 compares the advanced technologies of batteries and supercapacitors in terms of specific power and energy. Although it is true that a battery has the largest energy density (i.e., more energy is stored per weight than other technologies), it is important to consider the availability of that energy. This is the traditional advantage of capacitors. With a time constant of less than 0.1 s, energy can be taken from a capacitor at a very high rate [27], [28]. On the contrary, a battery of the same size will not be able to supply the necessary energy in the same time period. Unlike batteries, more advantageous for the case of supercapacitors is the fact that they can withstand a very large number of charge/discharge cycles without degradation (or virtually infinite cycles) [24], [25].

III. FC/BATTERY AND FC/SUPERCAPACITOR HYBRID POWER SOURCES

A. Structure of the Hybrid Power Sources

Different power converter topologies can be used for the power electronic interface between the FC and the utility dc bus. For the dc link voltage level, it depends on its applications. Basically, low-voltage high-current structures are needed because of FC electrical characteristics. A classical boost converter is often selected as an "FC converter" [29]–[31] because it can be operated in the current control mode in a continuous

condition mode. Then, one does not need a blocking diode and a passive filter between an FC and a converter. Based on the load conditions, the boost converter can be commanded to draw a specific amount of current from the FC with a ripple that is well defined by the frequency, the size of the inductor, and the duty ratio. However, a classical boost converter will be limited when the power increases or for higher step-up ratios.

In many applications, the use of an isolation transformer can provide an increased output/input voltage conversion ratio, as required, and full-bridge topologies can be used [7]. However, there are applications where transformer-less energy converter systems could potentially offer significant advantages, including simplicity, cost, and converter size reduction, particularly in high-power applications. That way, the use of paralleling power converters with an interleaved technique may offer some better performances [7].

One may summarize here again that the constraints to operate an FC are as follows.

- 1) The FC power or current must be kept within an interval (a rated value, a minimum value, or zero).
- 2) The FC current must be controlled as a unidirectional current
- 3) The FC current slope must be limited to the maximum absolute value (e.g., $4 \text{ A} \cdot \text{s}^{-1}$ [13], [32]) to prevent an FC stack from the fuel starvation phenomenon.
- 4) The switching frequency of the FC current must be greater than 1.25 kHz and the FC ripple current must be lower than around 5% of the rated value to ensure minor impact to the FC conditions [7].

Proposed hybrid power sources are depicted in Figs. 2 and 3. The battery actual voltage curve is not constant. It is linear over most of its operating range. The battery voltage variation is at least 25%. Nonetheless, at the end of discharge, the battery voltage decreases very rapidly toward zero. This is because the internal resistance of a lead-acid battery is almost linear during discharge, but the losses are largely below 25% SOC due to the increase in the internal resistance of the battery. As depicted in Fig. 2, we propose the FC/battery hybrid source by directly connecting the battery module to a dc bus [33], [34]. For this reason, there is no battery converter in this structure to improve system efficiency and converter cost. Then, this system will be operated based on unregulated dc bus voltage, in which the dc bus voltage is equal to the battery voltage.

For the FC/supercapacitor hybrid source (see Fig. 3), a supercapacitor module is frequently connected to the dc bus by means of a classical two-quadrant (bidirectional) dc/dc converter [35]–[38]. Supercapacitor current $i_{\rm SuperC}$, which flows across the storage device, can be positive or negative, allowing energy to be transferred in both directions.

B. Energy Management of the Hybrid Power Sources

When an FC operates, its fuel (hydrogen and oxygen) flows are controlled by an "FC controller," which receives current demand. This current demand is the FC current reference $i_{\rm FCREF}$ coming from the hybrid control algorithms detailed hereafter. The fuel flows must be adjusted to match the reactant delivery

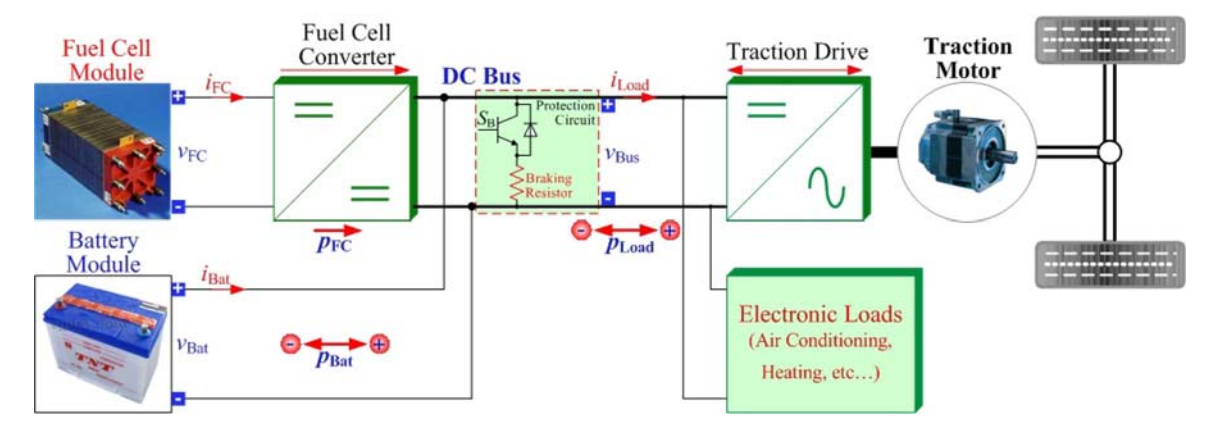


Fig. 2. Proposed structure of the FC/battery hybrid power source, where $p_{\rm FC}$ (= $v_{\rm FC}$ × $i_{\rm FC}$), $v_{\rm FC}$, and $i_{\rm FC}$ are the FC power, voltage, and current, respectively. $p_{\rm Bat}$ (= $v_{\rm Bat}$ × $i_{\rm Bat}$), $v_{\rm Bat}$, and $i_{\rm Bat}$ are the battery power, voltage, and current, respectively. $p_{\rm Load}$ (= $v_{\rm Bus}$ × $i_{\rm Load}$), $v_{\rm Bus}$, and $i_{\rm Load}$ are the load power, the dc bus voltage, and the load current, respectively. Note that it has been assumed that there are no losses in the FC converter, and here, $v_{\rm Bus}$ is $v_{\rm Bat}$.

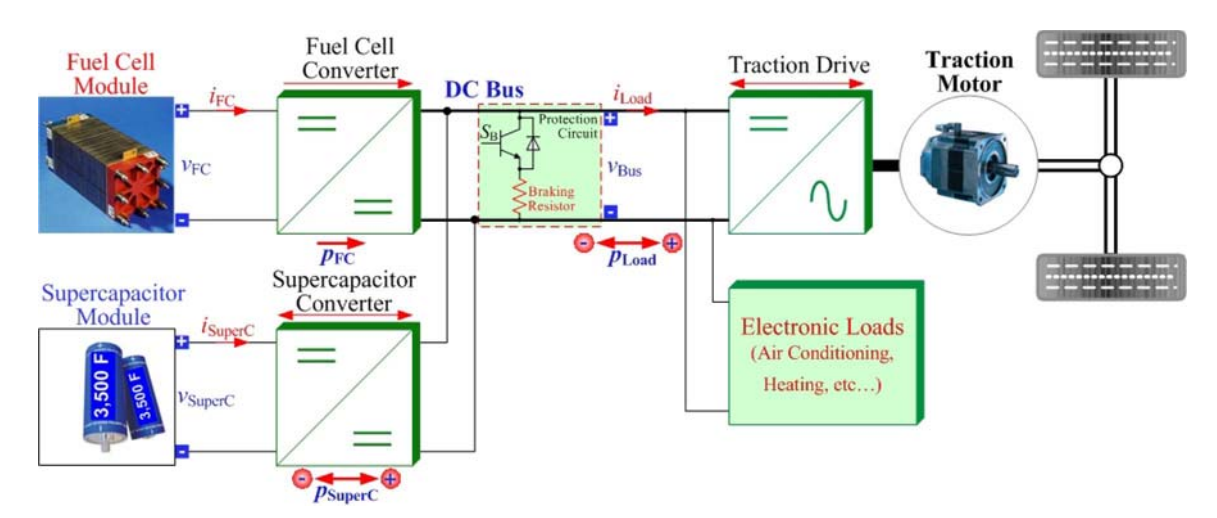


Fig. 3. Proposed structure of the FC/supercapacitor hybrid power source, where $p_{\rm FC}$ (= $v_{\rm FC} \times i_{\rm FC}$), $v_{\rm FC}$, and $i_{\rm FC}$ are the FC power, voltage, and current, respectively. $p_{\rm SuperC} = v_{\rm SuperC} \times i_{\rm SuperC}$, $v_{\rm SuperC} = v_{\rm SuperC} \times i_{\rm Edd}$, and $i_{\rm Edd} = v_{\rm SuperC} \times i_{\rm Edd}$, $v_{\rm Bus} \times i_{\rm Load}$), $v_{\rm Bus}$, and $i_{\rm Load}$ are the load power, the dc bus voltage, and the load current, respectively. Note that it has been assumed that there are no losses in the FC and supercapacitor converters.

rate to the usage rate by the FC controller [39]. For this reason, the inner FC current control loop is obligatory, and the hybrid control algorithms demand energy from the FC to the dc link by generating $i_{\rm FCREF}$ [1], which is synchronously sent to the FC system. One can take advantage of the safety and high dynamic characteristics of this loop as well. Note that the definitions of current direction are also illustrated in Figs. 2 and 3, and the dynamics of the current regulation loops are also supposed to be much faster than those of the outer control loops, which are detailed hereafter.

The energy management of hybrid power sources has already been studied recently, for example, by Jiang and Dougal [40], who worked on an unregulated voltage FC/battery hybrid source; by Ayad *et al.* [41], who studied the control of an unregulated voltage battery/supercapacitor hybrid source; and by Thounthong *et al.* [42], whose work concerned a regulated voltage FC/supercapacitor hybrid source. The problem of such a control strategy is well known: The definition of system states (state-machine-used) implies control algorithm permutations that may lead to a phenomenon of chattering when the system is operating near a border between two states. Of course, solutions

exist to avoid such a phenomenon—hard filtering, hysteretic transition, and transition defined by a continuous function.

The control algorithm presented here is not based on the state definition; therefore, naturally, it does not present the problem of chattering near state borders. Its basic principle lies in using the storage device, which is the fastest energy source of the system, to supply the energy that is required to the load, as if this device were a standard power supply. Therefore, the FC, although obviously the main energy source of the system, functions as the source that supplies energy to storage devices to keep them charged.

1) FC/Battery Hybrid Power Source: One takes advantage of a battery bank, which is directly connected to a dc bus to supply transient energy demand and peak loads that are required during traction motor acceleration and deceleration, as if this device is a standard power supply [43]–[45]. The proposed control strategy is a cascade control structure composed of three loops, as portrayed in Fig. 4. The outer loop is the battery SOC control that links the battery SOC to the battery charging current reference $i_{\rm BatREF}$. The middle loop controls the battery-charging current and links $i_{\rm BatREF}$ to the FC current

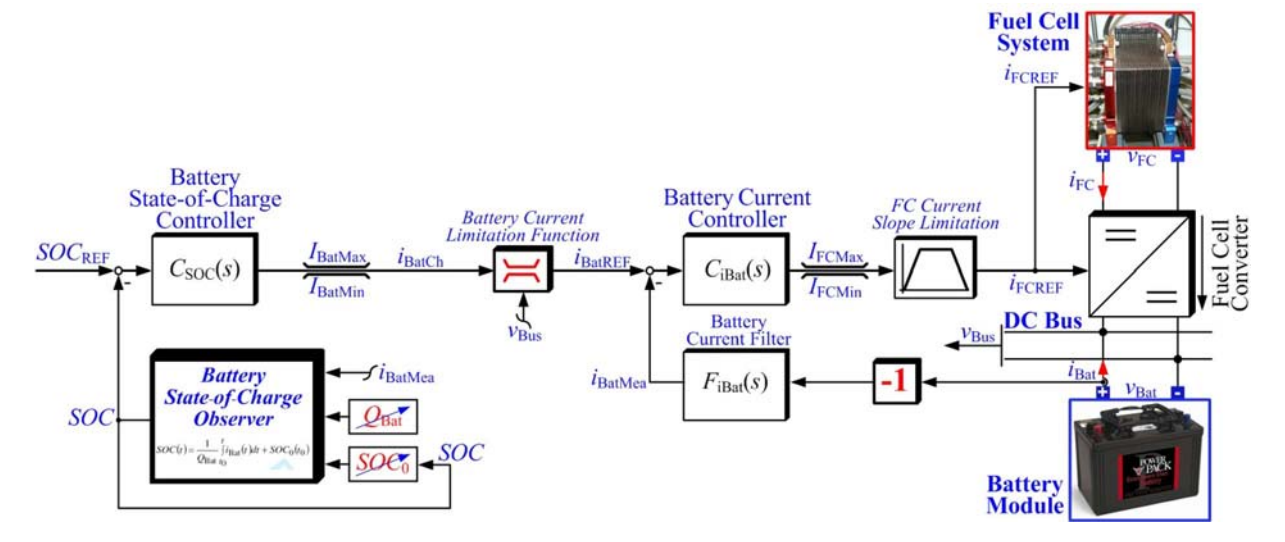


Fig. 4. Proposed energy management of the FC/battery hybrid power source.

reference $i_{\rm FCREF}$. The inner loop is the FC current control, which is not presented in Fig. 4.

A simple method to charge the battery is with constant current (maximum charging current $I_{\rm BatMax}$ is set around $Q_{\rm Bat}/10$; for a modern Li-ion battery, it can be set at $I_{\rm BatMax}=Q_{\rm Bat}$) when the SOC is far from the SOC reference ${\rm SOC_{REF}}$, with reduced current when the SOC is near ${\rm SOC_{REF}}$, or with no current when the SOC is equal to ${\rm SOC_{REF}}$. For the battery SOC, it is estimated from (1), as depicted in "Battery State-of-Charge Observer" in Fig. 4.

More importantly, in vehicle applications, to replace aged batteries, battery monitoring is compulsory. In particular, the potential capacity $Q_{\rm Bat}$ is dependent on the depth of the discharge, the discharge rate, the cell temperature, the charging regime, the dwell time at low and high SOCs, battery maintenance procedures, the current ripple, and the amount and frequency of overcharge [21].

It is beyond the scope of this paper to observe the potential capacity of the battery. It is assumed that $Q_{\rm Bat}$ is constant. Additionally, in a real system of applications, ${\rm SOC}_0$ can be retained in a storage device.

According to this SOC control algorithm, the "Battery State-of-Charge Controller" generates a battery-charging current i_{BatCh} for the battery current control loop. The battery current command i_{BatCh} must be limited within an interval [maximum charging current I_{BatMax} , maximum discharging current I_{BatMin}].

To avoid overvoltage at the dc bus in case of an erroneous SOC estimation or high regenerative braking, the dc bus voltage (the battery voltage) must be monitored to limit the charging current. The "Battery Current Limitation Function" consists of limiting the battery current reference $i_{\rm BatREF}$ versus the dc bus voltage as

$$i_{\mathrm{BatREF}}(t) = i_{\mathrm{BatCh}}(t) \cdot \min\left(1, \frac{V_{\mathrm{BusMax}} - v_{\mathrm{Bus}}(t)}{\Delta v_{\mathrm{Bus}}}\right)$$
 (3)

where $V_{
m BusMax}$ is the defined maximum dc bus voltage, and $\Delta v_{
m Bus}$ is the defined voltage band.

The battery-current control loop receives $i_{\rm BatREF}$ from an SOC regulation loop. The measured battery current must be reversed because the definition of the battery current is negative for the charging current. The battery current controller generates the FC current reference $i_{\rm FCREF}$. It must be limited in level, within the interval maximum $I_{\rm FCMax}$ (corresponding to a rated current of the FC) and minimum $I_{\rm FCMin}$ (set to 0 A) and limited in slope to the maximum absolute value (in amperes per second), which enables the safe operation of the FC with respect to the constraints that are associated with the FC.

One may summarize that the control principle of the whole system is based on the battery SOC, whatever the load power is.

- If the SOC is lower than SOC_{REF}, the battery-charging current reference is a negative value, and an FC current is necessary to charge the battery.
- If the SOC is higher than SOC_{REF}, the battery-charging current reference is a positive value or equal to zero, and the FC current reference is reduced to zero.

As a consequence, a transient in the load modifies the FC current when the battery SOC becomes lower than $SOC_{\rm REF}$. In any case, if the SOC is higher than $SOC_{\rm REF}$, the FC current reference is equal to zero. For transient conditions, as FC current dynamics have been intentionally reduced, the battery supplies all load variations.

It must be noted here that, in this system, the PEMFC is the main source, and the battery module is the secondary source. The battery functions to compensate the FC dynamic performance to avoid the FC starvation problem, supply the overenergy demand, and absorb the regenerative braking energy. There are two possibilities to connect a battery module with a dc bus. First, a battery bank is directly connected to the dc bus as proposed in our system. Second, a battery bank may be connected to the dc bus by a bidirectional converter, but it will increase system losses and cost. Nevertheless, the battery will be cycled whenever there is a load. Because, as mentioned earlier, the battery lifetime is usually limited by the number of cycles, its longevity might suffer. There are no solutions to improve the battery lifetime in the FC/battery hybrid source,

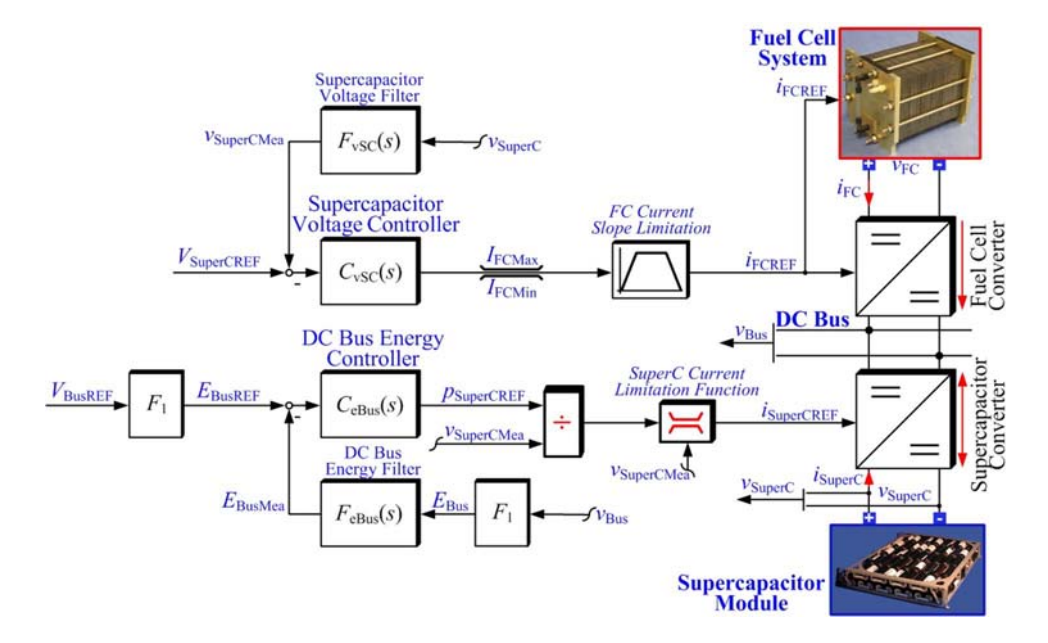


Fig. 5. Proposed energy management of the FC/supercapacitor hybrid power source.

even if a battery bank is directly connected to the dc bus or to the dc bus by a bidirectional converter. The battery will be always cycled whenever there is a load because the FC power dynamics are compensated by the battery power. To improve the battery lifetime, an FC/battery/supercapacitor hybrid source is proposed. We want the supercapacitor to supply or to absorb the load transient power and not the battery. Nonetheless, this system is under study [18].

2) FC/Supercapacitor Hybrid Power Source: To manage energy change in the system, its basic principle lies in using the supercapacitor, which is the fastest energy source of the system, to supply the energy that is required to achieve the dc bus voltage regulation, as if this device were a standard power supply. Therefore, the FC, although obviously the main energy source of the system, is equivalent to a load working only in regenerative braking and may be seen as a device that supplies energy to supercapacitors to keep them charged [44].

Consequently, the supercapacitor converter is driven to realize a classical dc bus voltage regulation, and the FC converter is driven to maintain the supercapacitor module at a given SOC. Therefore, the dynamics of the current regulation loops are also supposed to be much faster than those of the outer control loops. Thus, the currents $i_{\mathrm{SuperCREF}}$ and i_{FCREF} , respectively follow their references $i_{\mathrm{SuperCREF}}$ and i_{FCREF} , respectively. The supercapacitor and FC current control loops are supplied by two reference signals, i.e., $i_{\mathrm{SuperCREF}}$ and i_{FCREF} , which are generated by the dc bus voltage regulation loop and the supercapacitor voltage regulation loop, as shown in Fig. 5.

For the dc bus voltage control loop, it uses the dc bus capacitive energy $E_{\rm Bus}$ as the state variable and the supercapacitor delivered power $p_{\rm SuperCREF}$ as the command variable to obtain a natural linear transfer function for the system. If the losses in both the FC and supercapacitor converters are neglected, the dc link capacitive energy $E_{\rm Bus}$ is given versus supercapacitor

power p_{SuperC} , FC power p_{FC} , and load power p_{Load} by the following differential equation:

$$\frac{dE_{\text{Bus}}(t)}{dt} = p_{\text{SuperC}}(t) + p_{\text{FC}}(t) - p_{\text{Load}}(t). \tag{4}$$

Function " F_1 " presented in Fig. 5 is a voltage-to-energy transformation, which is proportional for the total dc bus capacitance C_{Bus} to the square function

$$E_{\text{Bus}}(t) = \frac{1}{2} \cdot C_{\text{Bus}} \cdot v_{\text{Bus}}^2(t). \tag{5}$$

It enables the generation of both dc bus energy reference $E_{\rm BusREF}$ and dc bus energy measurement $E_{\rm BusMea}$ through dc bus voltage reference $V_{\rm BusREF}$ and dc bus voltage measurement $v_{\rm Bus}$, respectively. The "DC Bus Energy Controller" generates a supercapacitor power reference $p_{\rm SuperCREF}$. This signal is then divided by the measured supercapacitor voltage $v_{\rm SuperCMea}$ and limited to maintain the supercapacitor voltage within an interval $[V_{\rm SuperCMin}, V_{\rm SuperCMax}]$. The upper value of this interval corresponds to the rated voltage of the storage device, and the lower value, which is traditionally equal to $V_{\rm SuperCMax}/2$, corresponds to a level under which the supercapacitor discharge becomes ineffective. This results in supercapacitor current reference $i_{\rm SuperCREF}$.

The "SuperC Current Limitation Function" consists of limiting reference $i_{\mathrm{SuperCREF}}$ to the interval $[I_{\mathrm{SuperCMin}}, I_{\mathrm{SuperCMax}}]$, which is defined, versus measured supercapacitor voltage $v_{\mathrm{SuperCMea}}$, as follows:

$$I_{\text{SuperCMin}} = -I_{\text{SuperCRated}} \times \min\left(1, \frac{V_{\text{SuperCMax}} - v_{\text{SuperCMea}}(t)}{\Delta v_{\text{SuperC}}}\right) \\ I_{\text{SuperCMax}} = +I_{\text{SuperCRated}} \times \min\left(1, \frac{v_{\text{SuperCMea}}(t) - V_{\text{SuperCMin}}}{\Delta v_{\text{SuperC}}}\right) \right\}. \quad (6)$$

 $I_{\mathrm{SuperCRated}}$ and $\Delta v_{\mathrm{SuperC}}$ are the regulation parameters.

For the supercapacitor voltage regulation loop, the "Supercapacitor Voltage Controller" generates an FC current reference $i_{\rm FCREF}$ limited in level and slope with respect to the constraints associated with the FC. The $i_{\rm FCREF}$ that drives the FC converter through the FC current loop is then kept within an interval $[I_{\rm FCMin}, I_{\rm FCMax}]$. The upper value of this interval corresponds to the rated current of the FC, and the lower value should be zero. Slope limitation to the maximum absolute value of some amperes per second enables safe operation of the FC, even during the transient power demand.

One may summarize that, using this form of control principle, the state of the supercapacitor module is naturally defined, through the dc bus voltage regulation, by the load power level, and by its SOC. In narrow steady-state conditions, we have the following.

- 1) If load power is negative, the dc link voltage regulation generates a negative supercapacitor current reference $i_{\mathrm{SuperCREF}}$.
- 2) If load power is greater than the approximate FC rated power, the dc bus voltage regulation generates a positive supercapacitor current reference $i_{\mathrm{SuperCREF}}$.
- 3) Otherwise, the state of the supercapacitor module depends on its SOC: the supercapacitor current will, therefore, be positive if $v_{\rm SuperCREF} > V_{\rm SuperCREF}$ and negative if $v_{\rm SuperC} < V_{\rm SuperCREF}$.

In all cases, the FC state depends only on the supercapacitor voltage; the FC current will be strictly positive and less than $I_{\rm FCRated}$ if $v_{\rm SuperC} < V_{\rm SuperCREF}.$ Otherwise, it will be zero. In transient conditions, as FC current dynamics have been intentionally reduced, the supercapacitor supplies load variations. In effect, the dc bus voltage regulation transforms a sudden increase in load power into a sudden increase in the supercapacitor current and, on the contrary, a sudden decrease in load power into a sudden decrease in the supercapacitor current.

3) Conclusion of Proposed Energy-Management Algorithms: The main important point in hybrid systems presented here is to balance the energy between the FC main source, the auxiliary source, and the load. The FC power (or current) dynamics have been intentionally reduced; the auxiliary source supplies all load variations.

Finally, Figs. 6 and 7 present simulation results during a high constant stepped load power. They show the load, auxiliary, and FC powers in per unit [p.u.]. In simulations, the FC minimum and maximum powers are set at 0 p.u. (corresponding to the FC minimum current) and 1.0 p.u. (corresponding to the FC maximum current), respectively. The power dynamics of the FC are set at 0.6 p.u. \cdot s⁻¹. As illustrated in Fig. 6, initially, the storage device is full of charge, and the load power is 0.2 p.u. As a result, the storage device power is zero, and the FC supplies 0.2 p.u. for the constant load power. At t=1 s, the constant load power steps to 3.0 p.u. One can observe the following.

- The auxiliary source supplies most of the transient power required.
- The FC power increases to the limited power 1.0 p.u. with a slope of 0.6 p.u. \cdot s⁻¹.

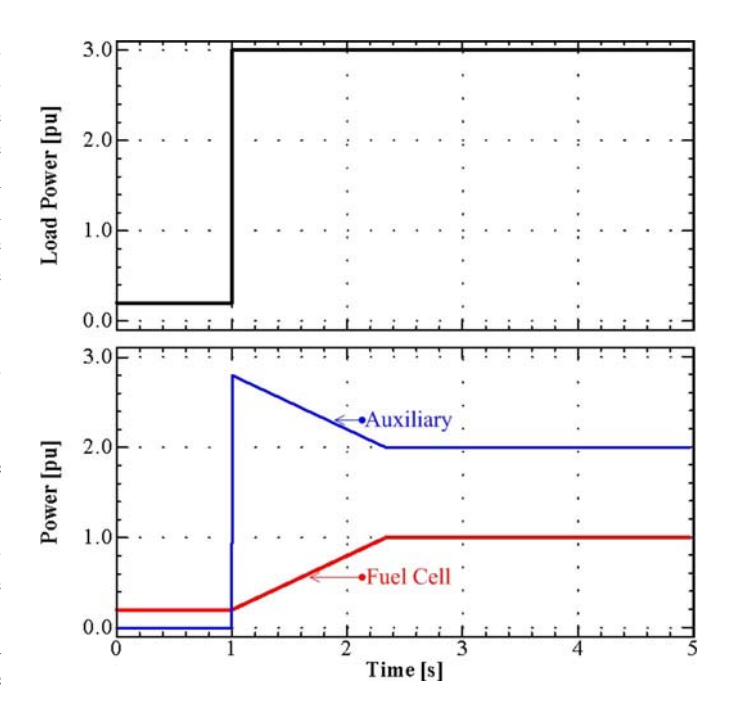


Fig. 6. Simulation result: hybrid source response during a high positive load step. Note that the power unit is per unit (p.u.).

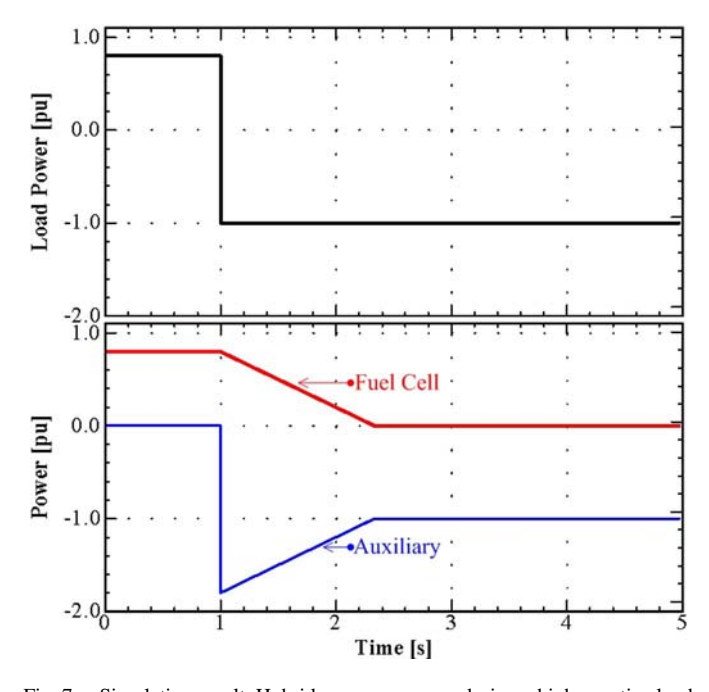


Fig. 7. Simulation result. Hybrid source response during a high negative load step (imitated regenerative braking).

 Synchronously, the auxiliary power, after a sharp increase (discharging), slowly decreases to a constant discharge of 2.0 p.u.

At a steady state, the constant load power of 3.0 p.u. is entirely supplied by the FC of 1.0 p.u. and the storage device of 2.0 p.u. (the discharging state).

As a final simulation illustrated in Fig. 7, initially, the auxiliary energy source is full of charge, and the load power is 0.8 p.u. As a result, the storage device power is zero, and the FC supplies 0.8 p.u. for the constant load power. At $t=1\,\mathrm{s}$, the

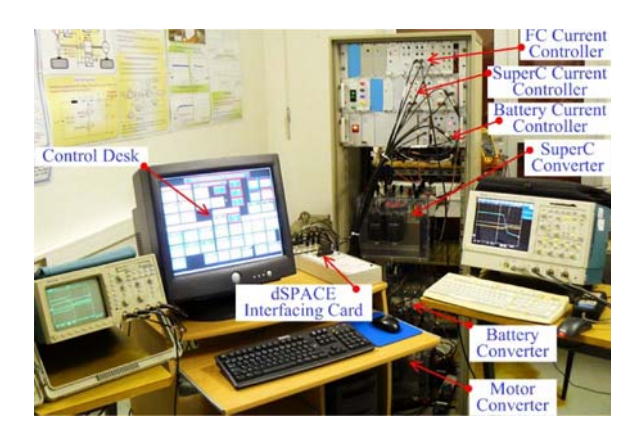


Fig. 8. Hybrid source test bench.



Fig. 9. PEMFC stack and storage devices.

constant load power steps to -1.0 p.u. (imitated regenerative braking). One can see, again, the following.

- The auxiliary source absorbs most of the transient negative power.
- The FC power reduces to zero with a slope of 0.6 p.u. · s⁻¹ because the FC power source is a unidirectional power flow.
- Simultaneously, the auxiliary source, after a sharp decrease (charging), slowly increases to a constant charge at -1.0 p.u.

IV. EXPERIMENTAL VERIFICATION

A. Test Bench Explanation

The small-scale test bench of the hybrid systems in our laboratory is presented in Fig. 8. As illustrated in Fig. 9, the PEMFC system (500 W, 40 A, 13 V) was achieved by the ZSW Company. It is composed of 23 cells of 100 cm² in series. It is supplied using pure hydrogen from bottles under pressure and with clean and dry air from a compressor. The battery module is obtained by means of four aged lead-acid batteries [7.78 Ah (33 Ah at the nameplate), 12 V] connected in series. The supercapacitor module is obtained by means of 12 SAFT supercapacitors SC3500 (capacitance: 3500 F; rated voltage: 2.5 V; rated current: 500 A; low-frequency ESR: 0.8 m Ω) connected in series.

The FC converter is a classical boost converter and is selected to adapt the low dc voltage delivered by the FC, which is approximately 12.5 V at rated power, to the 42-V dc bus. Thus, the FC converter is composed of a high-frequency input inductor (72 μ H), an output filtering capacitor (Panasonic aluminum electrolytic capacitors: 30 000 μ F), a diode (Schottky diode STPS80H100TV: 100 V, 40 A), and a main power switch (power metal–oxide–semiconductor field-effect

transistor STE180NE10: 100 V, 180 A). The frequency of the pulsewidth modulation that drives the FC converter is 25 kHz.

The supercapacitor converter is a classical two-quadrant dc/dc converter (a bidirectional converter). Thus, the supercapacitor converter is composed of a high-frequency input inductor (54 $\mu\rm H$), an output filtering capacitor (Panasonic aluminum electrolytic capacitors: 330 mF), and two power switches (power insulated-gate bipolar transistors SKM200GB123D: 1200 V, 200 A). The supercapacitor current, which flows across the storage device, can either be positive or negative, allowing energy to be transferred in both directions. The converter is driven by means of complementary pulses, which are generated by a hysteresis comparator, and applied on the gates of the power switches.

In the case of the FC/battery hybrid power source test bench, the total dc bus capacitance is 360 mF (30 mF of the output capacitance of the FC converter and 330 mF of the output capacitance of the load converter). In the case of the FC/supercapacitor hybrid power source test bench, the total dc bus capacitance is 690 mF (30 mF of the output capacitance of the FC converter, 330 mF of the output capacitance of the load converter, and 330 mF of the output capacitance of the supercapacitor converter).

The dc bus is connected to only a traction motor drive (10 kW) coupled with a small-inertia flywheel. The supercapacitor and FC current control loops, on the other hand, have been realized by analog circuits to function at a high bandwidth. The proposed energy-control algorithms have been implemented in the real-time card dSPACE DS1104 through the mathematical environment of MATLAB–Simulink, with a sampling frequency of 25 kHz. The ControlDesk software enables changes in the parameters of the control loops. Two digital oscilloscopes (Tektronix Com.), as shown in Fig. 8, are used as data acquisition to store signal waveforms, which are presented hereafter.

The control parameters of the PEMFC are set as follows.

- $I_{\rm FCMax} = 40$ A (rated FC current, corresponding to the rated FC power).
- $I_{\rm FCMin}=0$ A (minimum FC current, corresponding to the minimum FC power).
- The FC current absolute slope limitation is set to $4~{\rm A\cdot s^{-1}}$ (corresponding to the FC power slope of around 50 W · ${\rm s^{-1}}$). This value has been experimentally determined as the highest current slope of our FC system, where no fuel starvation occurs [13].

B. Test Results of the FC/Battery Hybrid Power Source

The controlled parameters of this system are set as follows:

- $SOC_{REF} = 100\%$ (equal to 7.78 Ah);
- $I_{\mathrm{BatMax}} = +6 \,\mathrm{A}$ (the maximum battery charging current);
- $I_{\mathrm{BatMin}} = -50$ A (the maximum battery discharging current);
- $V_{\text{BusMax}} = 61 \text{ V};$
- $\Delta v_{\text{Bus}} = 2 \text{ V}.$

Figs. 10 and 11 present waveforms that are obtained during the motor-drive cycle. They show the dc bus voltage (the battery voltage), the FC voltage, the load power, the battery power, the

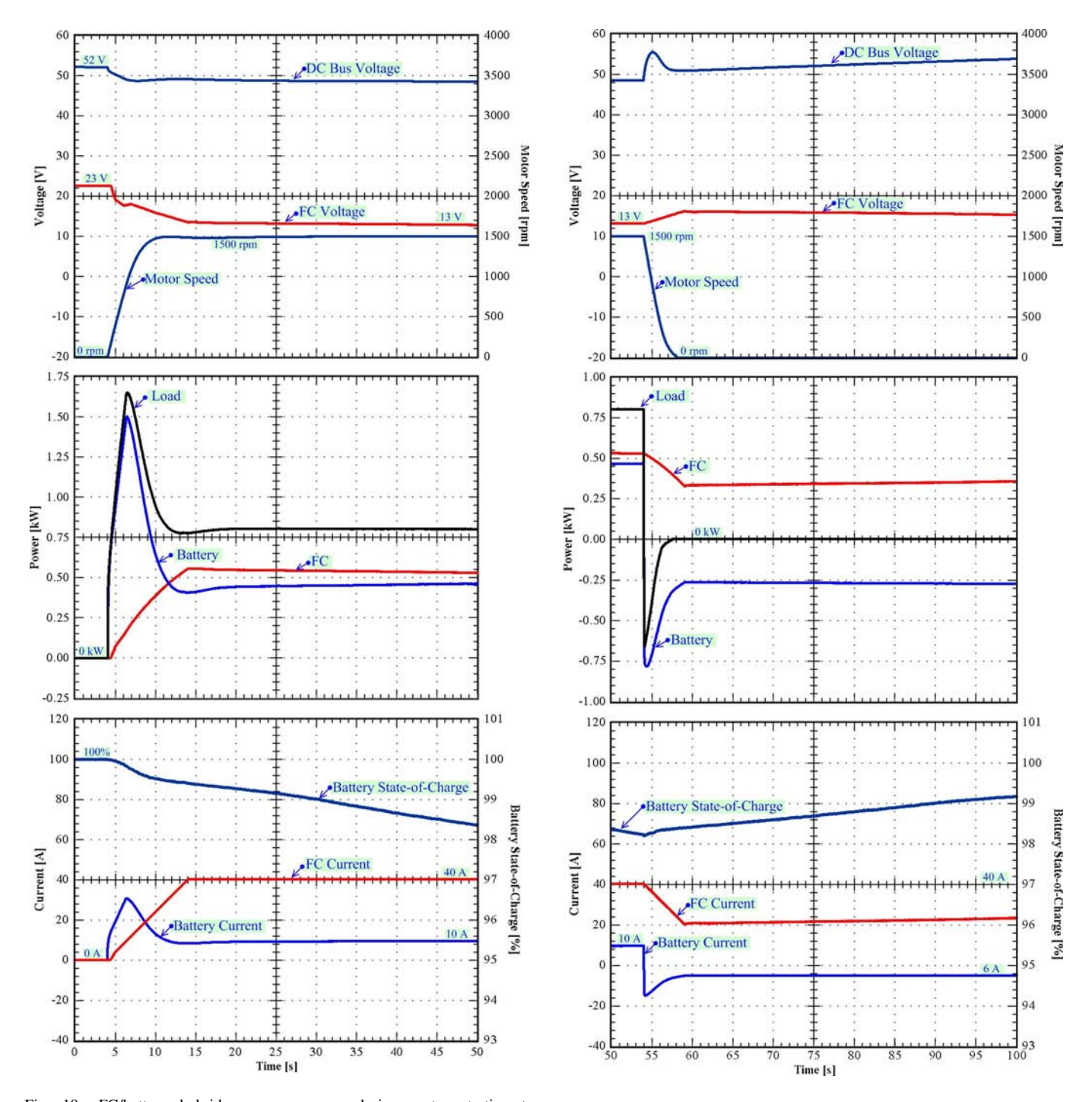


Fig. 10. FC/battery hybrid source response during motor starting to 1500 r/min.

FC power, the motor speed, the battery current, the FC current, and the battery SOC. The battery SOC is calculated from (1) by MATLAB–Simulink and is then sent through a digital-to-analog-converter card of dSPACE to an oscilloscope.

The initial state is zero for both the FC and battery powers and 100% for the battery SOC. At $t=4~\rm s$, the motor reaches the final speed of 1500 r/min such that the final FC current is $I_{\rm FCRated}$. One can observe the following.

• The battery supplies most of the power of 1600 W that is required during motor acceleration.

Fig. 11. FC/battery hybrid source response during motor braking from 1500 r/min.

- The FC power increases with a limited slope up to a level of the rated power of 500 W.
- Concurrently, the battery power, after a sharp increase during motor acceleration, slowly decreases to a constant discharging power of 400 W.
- The steady-state load power at the constant speed of 1500 r/min is about 800 W, which is entirely supplied by the FC and the battery.

Therefore, this characteristic can be comparable with the simulation results in Figs. 6 and 7. After that, at $t=54~\rm s$, the motor reduces speed and then stops. It can be scrutinized that

there are three phases. First, the battery recovers the power that is supplied to the dc link by the FC and the motor (known as the regenerative braking energy). Second, the battery recovers the reduced power that is supplied to the dc bus by only the FC. Third, the battery is charged at a constant current of 6 A by the FC. During the first and second phases, the FC power reduces from a rated power of 500 W with a constant slope of $50~W\cdot s^{-1}$. In the third phase, the FC power is nearly constant at around 300 W to charge the battery. After that, both the FC and the battery power will reduce to zero when the SOC reaches $SOC_{\rm REF}$.

C. Test Results of the FC/Supercapacitor Hybrid Power Source

The control parameters of this system are set as follows:

- $V_{\rm BusREF} = 42$ V (a new standard dc bus voltage in the automotive electrical system called "PowerNet" [17]);
- $V_{\text{SuperCREF}} = 25 \text{ V};$
- $V_{\text{SuperCMax}} = 30 \text{ V};$
- $V_{\text{SuperCMin}} = 15 \text{ V};$
- $I_{\text{SuperCRated}} = 200 \text{ A};$
- $\Delta v_{\text{SuperC}} = 0.5 \text{ V}.$

Figs. 12 and 13 present waveforms that are obtained during the motor-drive cycle. They show the dc bus voltage, the FC voltage, the load power, the supercapacitor power, the FC power, the motor speed, the supercapacitor current, the FC current, and the supercapacitor voltage (or the supercapacitor SOC).

The initial state is in no-load power, and the storage device is full of charge, i.e., $V_{\rm SuperC}=25$ V; as a result, both the FC and supercapacitor powers are zero. At t=20 s, the motor speed accelerates to the final speed of 1000 r/min; synchronously, the final FC power increases with a limited slope of $50~{\rm W}\cdot{\rm s}^{-1}$ to a rated power of $500~{\rm W}$. Thus, the supercapacitor, which supplies most of the power that is required during motor acceleration, remains in a discharge state after the motor start because the steady-state load power (approximately $600~{\rm W}$) is greater than the FC rated power ($500~{\rm W}$), and the peak load power is about $1000~{\rm W}$, which is about two times that of the FC rated power.

After that, at $t=50.5~\rm s$, the motor speed decelerates and stops with a peak load power of about $-500~\rm W$. The supercapacitor is deeply charged, demonstrating the three phases. First, the supercapacitor recovers the energy that is supplied to the dc bus by the FC (500 W) and the traction motor. Second, the supercapacitor is charged only by the FC. Third, the supercapacitor is nearly fully charged, which then reduces the charging current. After that, both the FC and supercapacitor powers reduce to zero when $V_{\rm SuperC}$ reaches $V_{\rm SuperCREF}$ of 25 V.

Only small perturbations on the dc bus voltage waveform can be seen, which is of major importance when using supercapacitors to improve the dynamic performance of the whole system. These characteristics can be, again, comparable with the simulation results in Figs. 6 and 7.

The proposed energy-management algorithms of FC/battery and FC/supercapacitor hybrid sources are used to balance powers in the system with respect to dynamic constraints. During motor acceleration or deceleration (a high stepped load), as can

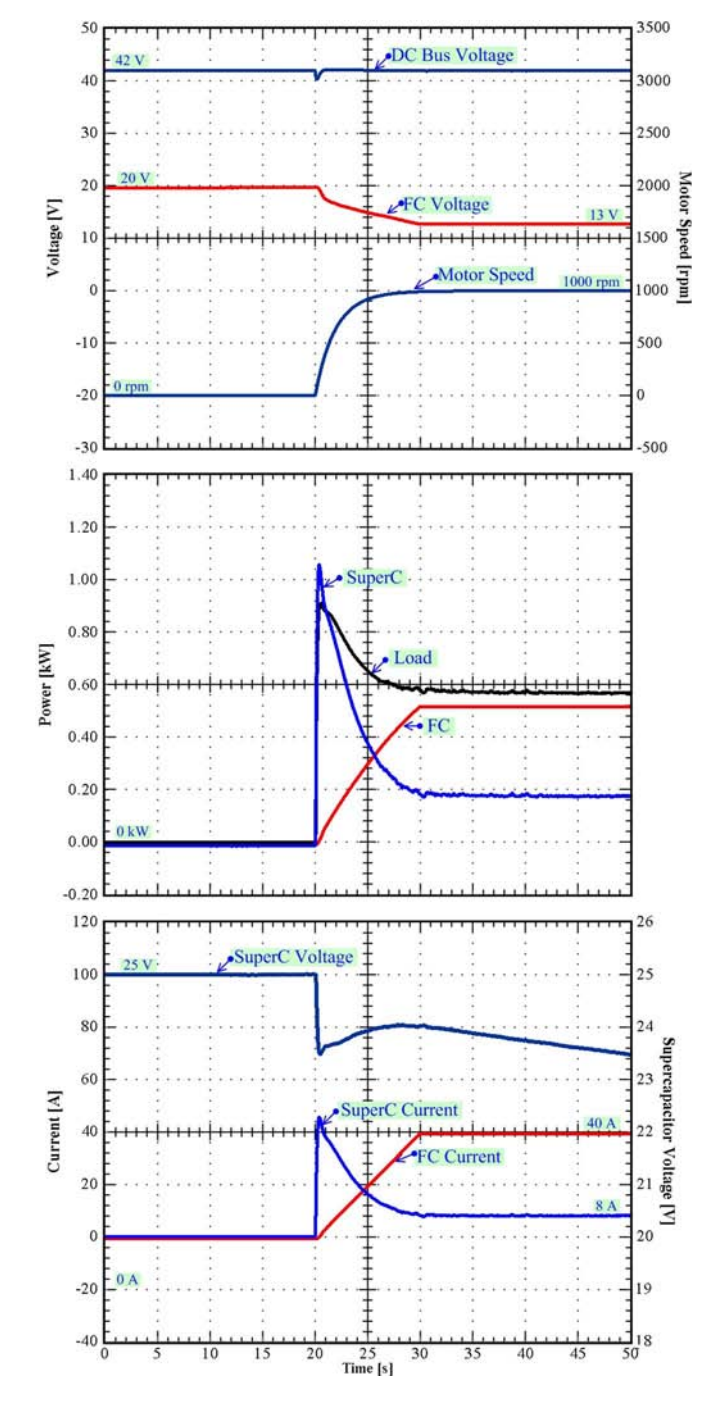


Fig. 12. FC/supercapacitor hybrid source response during motor startup to 1000 r/min.

be seen in Figs. 6 and 7 in simulation results (in per unit) and in Figs. 10–13 in experimental results, the powers are always balanced during dynamic and transient states. Importantly, the high dynamics during load steps are compensated by storage devices. For the FC/battery hybrid source, the stepped energy is naturally supplied or absorbed by the battery because the battery bank is directly connected to the dc bus based on the control algorithm of the unregulated dc bus voltage. In the case of the FC/supercapacitor hybrid source, the stepped energy is automatically supplied or absorbed by the supercapacitor because the proposed control algorithm is based on the regulated dc bus voltage. Then, the supercapacitor module functions as

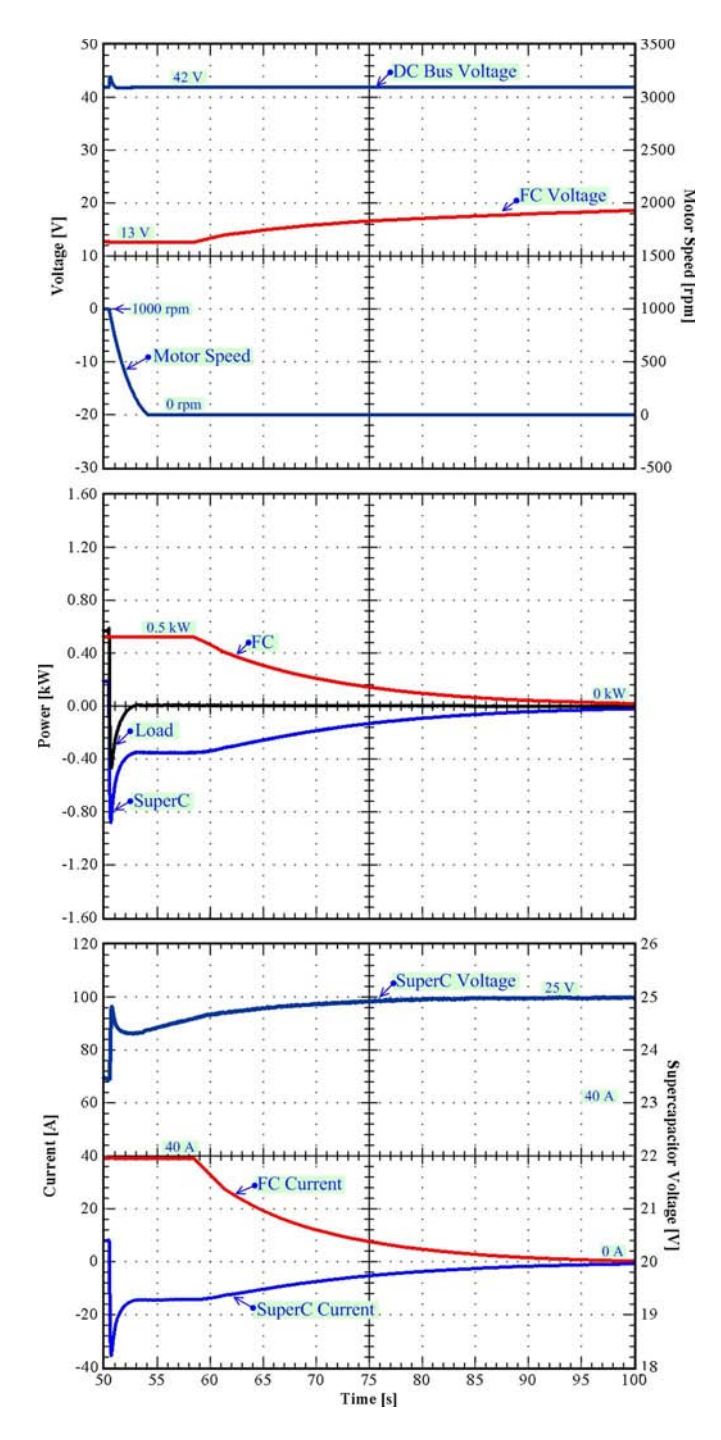


Fig. 13. FC/supercapacitor hybrid source response during motor braking from 1000 r/min.

the one supplying or absorbing the energy that is required to achieve the dc bus voltage.

V. CONCLUSION

The advantages of an FC hybrid vehicle could include improved vehicle performance and fuel economy and lower system cost. The degree of hybridization benefits from 1) FC efficiency characteristics; 2) FC downsizing; 3) displacing FC tasks with the secondary source functionality; or 4) energy recovery through regenerative braking. This paper has studied

the role of the energy-storage device in FC hybrid vehicles to understand their potential impact on dynamic performances.

Experimental verifications with a small-scale hybrid test bench in the laboratory have evidently shown the possibility of improving the performance of the whole system and validated the proposed control algorithms: the FC/battery hybrid source and the FC/supercapacitor hybrid source.

In general, the FC/supercapacitor hybrid has better performance because the supercapacitor can more effectively assist the FC to meet the transient power demand (the supercapacitor can be charged or discharged at a high current, in which the battery cannot function), and high-current charges and discharges from the battery will reduce its lifetime as well.

Nonetheless, an FC hybrid vehicle with supercapacitors as the only energy storage will be deficient or even malfunction during the vehicle startup because of the startup time of a PEMFC of around 5–10 min, in which the battery has higher specific energy than the supercapacitor. Consequently, a more practical answer will be an FC/battery/supercapacitor hybrid power source [45] to increase the battery lifetime due to the reduction of high-current charges and discharges.

ACKNOWLEDGMENT

The authors would like to thank S. Lekapat, who is in charge of the process of the "Franco-Thai on Higher Education and Research Joint Project" and of the research funding for this paper.

REFERENCES

- P. Thounthong, B. Davat, and S. Raël, "Drive friendly," *IEEE Power Energy Mag.*, vol. 6, no. 1, pp. 69–76, Jan./Feb. 2008.
- [2] K. Rajashekara, J. Grieve, and D. Daggett, "Hybrid fuel cell power in aircraft," *IEEE Ind. Appl. Mag.*, vol. 14, no. 4, pp. 54–60, Jul./Aug. 2008.
- [3] W. M. Yan, H. S. Chu, M. X. Lu, F. B. Weng, G. B. Jung, and C. Y. Lee, "Degradation of proton exchange membrane fuel cells due to CO and CO₂ poisoning," *J. Power Sources*, vol. 188, no. 1, pp. 141–147, Mar. 2009.
- [4] A. Khaligh, A. M. Rahimi, Y. J. Lee, J. Cao, A. Emadi, S. D. Andrews, C. Robinson, and C. Finnerty, "Digital control of an isolated active hybrid fuel cell/Li-ion battery power supply," *IEEE Trans. Veh. Technol.*, vol. 56, no. 6, pp. 3709–3721, Nov. 2007.
- [5] P. Thounthong, S. Raël, and B. Davat, "Control strategy of fuel cell/supercapacitors hybrid power sources for electric vehicle," *J. Power Sources*, vol. 158, no. 1, pp. 806–814, Jul. 2006.
- [6] J. M. Corrêa, F. A. Farret, V. A. Popov, and M. G. Simões, "Sensitivity analysis of the modeling used in simulation of proton exchange membrane fuel cells," *IEEE Trans. Energy Convers.*, vol. 20, no. 1, pp. 211–218, Jan./Mar. 2005.
- [7] P. Thounthong, B. Davat, S. Raël, and P. Sethakul, "Fuel cell high-power applications," *IEEE Ind. Electron. Mag.*, vol. 3, no. 1, pp. 32–46, Mar. 2009.
- [8] K. P. Adzakpa, K. Agbossou, Y. Dubé, M. Dostie, M. Fournier, and A. Poulin, "PEM fuel cells modeling and analysis through current and voltage transient behaviors," *IEEE Trans. Energy Convers.*, vol. 23, no. 2, pp. 581–591, Jun. 2008.
- [9] C. Wang and M. H. Nehrir, "Load transient mitigation for stand-alone fuel cell power generation systems," *IEEE Trans. Energy Convers.*, vol. 22, no. 4, pp. 864–872, Dec. 2007.
- [10] R. Gaynor, F. Mueller, F. Jabbari, and J. Brouwer, "On control concepts to prevent fuel starvation in solid oxide fuel cells," *J. Power Sources*, vol. 180, no. 1, pp. 330–342, May 2008.
 [11] W. Schmittinger and A. Vahidi, "A review of the main parameters influ-
- [11] W. Schmittinger and A. Vahidi, "A review of the main parameters influencing long-term performance and durability of PEM fuel cells," *J. Power Sources*, vol. 180, no. 1, pp. 1–14, May 2008.
- [12] B. Wahdame, D. Candusso, X. François, F. Harel, M. C. Péra, D. Hissel, and J. M. Kauffmann, "Analysis of a fuel cell durability test based on

- design of experiment approach," *IEEE Trans. Energy Convers.*, vol. 23, no. 4, pp. 1093–1104, Dec. 2008.
- [13] P. Thounthong, S. Raël, and B. Davat, "Control strategy of fuel cell and supercapacitors association for distributed generation system," *IEEE Trans. Ind. Electron.*, vol. 54, no. 6, pp. 3225–3233, Dec. 2007.
- [14] P. Corbo, F. Migliardini, and O. Veneri, "An experimental study of a PEM fuel cell power train for urban bus application," *J. Power Sources*, vol. 181, no. 2, pp. 363–370, Jul. 2008.
- [15] S. M. Lukic, J. Cao, R. C. Bansal, F. Rodriguez, and A. Emadi, "Energy storage systems for automotive applications," *IEEE Trans. Ind. Electron.*, vol. 55, no. 6, pp. 2258–2267, Jun. 2008.
- [16] M. M. Flynn, P. Mcmullen, and O. Solis, "Saving energy using flywheels," IEEE Ind. Appl. Mag., vol. 14, no. 6, pp. 69–76, Nov./Dec. 2008.
- [17] A. Emadi, Y. J. Lee, and K. Rajashekara, "Power electronics and motor drives in electric, hybrid electric, and plug-in hybrid electric vehicles," *IEEE Trans. Ind. Electron.*, vol. 55, no. 6, pp. 2237–2245, Jun. 2008.
- [18] J. Bauman and M. Kazerani, "A comparative study of fuel-cell-battery, fuel-cell-ultracapacitor, and fuel-cell-battery-ultracapacitor," *IEEE Trans. Veh. Technol.*, vol. 57, no. 2, pp. 760–769, Mar. 2008.
- [19] M. Ceraolo, A. di Donato, and G. Franceschi, "A general approach to energy optimization of hybrid electric vehicles," *IEEE Trans. Veh. Technol.*, vol. 57, no. 3, pp. 1433–1441, May 2008.
- [20] A. Szumanowski and Y. Chang, "Battery management system based on battery nonlinear dynamics modeling," *IEEE Trans. Veh. Technol.*, vol. 57, no. 3, pp. 1425–1432, May 2008.
- [21] P. Thounthong, S. Raël, and B. Davat, "Control algorithm of fuel cell and batteries for distributed generation system," *IEEE Trans. Energy Convers.*, vol. 23, no. 1, pp. 148–155, Mar. 2008.
- [22] M. B. Camara, H. Gualous, F. Gustin, and A. Berthon, "Design and new control of DC/DC converters to share energy between supercapacitors and batteries in hybrid vehicles," *IEEE Trans. Veh. Technol.*, vol. 57, no. 5, pp. 2721–2735, Sep. 2008.
- [23] A. Payman, S. Pierfederici, and F. Meibody-Tabar, "Energy control of supercapacitor/fuel cell hybrid power source," *Energy Convers. Manage.*, vol. 49, no. 6, pp. 1637–1644, Jun. 2008.
- [24] A. F. Burke, "Batteries and ultracapacitors for electric, hybrid, and fuel cell vehicles," *Proc. IEEE*, vol. 95, no. 4, pp. 806–820, Apr. 2007.
- [25] J. R. Miller and A. F. Burke, "Electrochemical capacitors: Challenges and opportunities for real-world applications," *Electrochem. Soc. Interface*, vol. 17, no. 1, pp. 53–57, Spring 2008.
- [26] Y. S. Lee, W. Y. Wang, and T. Y. Kuo, "Soft computing for battery state-of-charge (BSOC) estimation in battery string systems," *IEEE Trans. Ind. Electron.*, vol. 55, no. 1, pp. 229–239, Jan. 2008.
- [27] A. Kusko and J. DeDad, "Stored energy—Short-term and long-term energy storage methods," *IEEE Ind. Appl. Mag.*, vol. 13, no. 4, pp. 66–72, Jul./Aug. 2007.
- [28] M. Uzunoglu and M. S. Alam, "Modeling and analysis of an FC/UC hybrid vehicular power system using a novel-wavelet-based load sharing algorithm," *IEEE Trans. Energy Convers.*, vol. 23, no. 1, pp. 263–272, Mar. 2008.
- [29] P. Thounthong, S. Raël, and B. Davat, "Test of a PEM fuel cell with low voltage static converter," *J. Power Sources*, vol. 153, no. 1, pp. 145–150, Jan. 2006.
- [30] S. Jain and V. Agarwal, "An integrated hybrid power supply for distributed generation applications fed by nonconventional energy sources," *IEEE Trans. Energy Convers.*, vol. 23, no. 2, pp. 622–631, Jun. 2008.
- [31] S. Y. Choe, J. W. Ahn, J. G. Lee, and S. H. Baek, "Dynamic simulator for a PEM fuel cell system with a PWM DC/DC converter," *IEEE Trans. Energy Convers.*, vol. 23, no. 2, pp. 669–680, Jun. 2008.
- [32] P. Thounthong, B. Davat, S. Raël, and P. Sethakul, "Fuel starvation: Analysis of a PEM fuel-cell system," *IEEE Ind. Appl. Mag.*, vol. 15, no. 4, pp. 52–59, Jul./Aug. 2009.
- [33] R. Chandrasekaran, W. Bi, and T. F. Fuller, "Robust design of battery/fuel cell hybrid systems—Methodology for surrogate models of Pt stability and mitigation through system controls," *J. Power Sources*, vol. 182, no. 2, pp. 546–557, Aug. 2008.
- [34] D. Gao, Z. Jin, and Q. Lu, "Energy management strategy based on fuzzy logic for a fuel cell hybrid bus," *J. Power Sources*, vol. 185, no. 1, pp. 311–317, Oct. 2008.
- [35] F. Baalbergen, P. Bauer, and J. A. Ferreira, "Energy storage and power management for typical 4Q-load," *IEEE Trans. Ind. Electron.*, vol. 56, no. 5, pp. 1485–1498, May 2009.
- [36] A. Khaligh, "Realization of parasitics in stability of DC-DC converters loaded by constant power loads in advanced multiconverter automotive systems," *IEEE Trans. Ind. Electron.*, vol. 55, no. 6, pp. 2295–2304, Jun. 2008.

- [37] A. Di Napoli, F. Crescimbini, L. Solero, F. Caricchi, and F. G. Capponi, "Multiple-input DC–DC power converter for power-flow management in hybrid vehicles," in *Conf. Rec. 37th IEEE IAS Annu. Meeting*, Pittsburgh, PA, Oct. 13–17, 2002, vol. 3, pp. 1578–1585.
- [38] L. Solero, A. Lidozzi, and J. A. Pomilio, "Design of multiple-input power converter for hybrid vehicles," *IEEE Trans. Power Electron.*, vol. 20, no. 5, pp. 1007–1016, Sep. 2005.
- [39] I. Sadli, P. Thounthong, J. P. Martin, S. Raël, and B. Davat, "Behaviour of a PEMFC supplying a low voltage static converter," *J. Power Sources*, vol. 156, no. 1, pp. 119–125, May 2006.
- vol. 156, no. 1, pp. 119–125, May 2006.

 [40] Z. Jiang and R. A. Dougal, "A compact digitally controlled fuel cell/battery hybrid power source," *IEEE Trans. Ind. Electron.*, vol. 53, no. 4, pp. 1094–1104, Jun. 2006.
- [41] M. Y. Ayad, S. Pierfederici, S. Raël, and B. Davat, "Voltage regulated hybrid DC power source using supercapacitors as energy storage device," *Energy Convers. Manage.*, vol. 48, no. 7, pp. 2196–2202, Jul. 2007.
- [42] P. Thounthong, S. Raël, and B. Davat, "Supercapacitors as an energy storage for fuel cell automotive hybrid electrical system," *Int. J. Elect. Eng. Trans.*, vol. 1, no. 1, pp. 21–25, 2005.
- [43] M. Kim, Y. J. Sohn, W. Y. Lee, and C. S. Kim, "Fuzzy control based engine sizing optimization for a fuel cell/battery hybrid mini-bus," *J. Power Sources*, vol. 178, no. 2, pp. 706–710, Apr. 2008.
- [44] P. Thounthong, S. Raël, and B. Davat, "Analysis of supercapacitor as second source based on fuel cell power generation," *IEEE Trans. Energy Convers.*, vol. 24, no. 1, pp. 247–255, Mar. 2009.
- [45] P. Thounthong, S. Raël, and B. Davat, "Energy management of fuel cell/battery/supercapacitor hybrid power source for vehicle applications," *J. Power Sources*, vol. 193, no. 1, pp. 376–385, Aug. 2009.



Phatiphat Thounthong (M'09) received the B.S. and M.E. degrees in electrical engineering from King Mongkut's Institute of Technology North Bangkok (KMITNB), Bangkok, Thailand, in 1996 and 2001, respectively, and the Ph.D. degree in electrical engineering from the Institut National Polytechnique de Lorraine, Nancy, France, in 2005.

From 1997 to 1998, he was an electrical engineer with the E.R. Metal Works Ltd. (EKARAT Group), Thailand. From 1998 to 2002, he was an Assistant Lecturer with KMITNB. He is currently an Assistant

Professor and the Director of the Department of Teacher Training in Electrical Engineering, Faculty of Technical Education, King Mongkut's University of Technology North Bangkok (KMUTNB), where he is also the Head of the Renewable Energy Research Laboratory (sponsored by KMUTNB and the French Embassy in Bangkok). His current research interests include power electronics, electric drives, and electrical devices (fuel cells, batteries, and supercapacitors). He is the principal author of more than 50 journal and conference papers, as well as a book entitled Fuel Cell Energy Source for Electric Vehicle Applications (New York: Nova Science, 2008). He has contributed one chapter on "Utilizing Supercapacitors to Improve System Performances of Fuel Cell Power Source" for Recent Advances in Supercapacitors (Kerala: Transworld Research Network, 2006), one chapter on "A PEM Fuel Cell Power Source for Electric Vehicle Applications with Supercapacitor or Battery as Auxiliary Source" for Progress in Fuel Cell Research (New York: Nova Science, 2007), and one chapter on "Fuel Cell Converters for High Power Applications" for Polymer Electrolyte Membrane Fuel Cells and Electrocatalysts (New York: Nova Science, 2009)

Dr. Thounthong is a member of the Thai-French Technical Association.



Viboon Chunkag received the B.S. degree (with honors) in electrical engineering from King Mongkut's Institute of Technology North Bangkok, Bangkok, Thailand, in 1979, the M.E. degree in electrical engineering from Kasetsart University, Bangkok, in 1985, and the Ph.D. degree in electrical engineering from the University of Bath, Bath, U.K., in 1995.

He is currently the Dean of the Faculty of Engineering, King Mongkut's University of Technology North Bangkok. His research interests include power

electronic circuits and devices.



Panarit Sethakul received the B.S. degree in electrical engineering from King Mongkut's Institute of Technology North Bangkok, Bangkok, Thailand, in 1979 and the Dipl.-Ing. degree in electrical engineering from Wuppertal University, Wuppertal, Germany, in 1986.

He is currently the Dean of the Faculty of Technical Education, King Mongkut's University of Technology North Bangkok. His research interests include power electronics and drives and renewable energy sources.



Melika Hinaje received the M.S. degree in electrical engineering from the University of Nancy, Nancy, France, in 2002 and the Ph.D. degree from the Institut National Polytechnique de Lorraine (INPL), Nancy, in 2005.

Since 2006, she has been an Assistant Professor with the INPL. Her research activities with the Groupe de Recherche en Electrotechnique et Electronique de Nancy, Department of Electrical Engineering, INPL, concern fuel cells.



Bernard Davat (M'89) received the Engineer degree from Ecole Nationale Supérieure d'Electrotechnique, d'Electronique, d'Informatique, d'Hydraulique et des Telecommunications, Toulouse, France, in 1975 and the Ph.D. and Docteur d'Etat degrees in electrical engineering from the Institut National Polytechnique de Toulouse in 1978 and 1984, respectively.

From 1980 to 1988, he was a Researcher with the French National Center for Scientific Research, Laboratoire d'Electrotechnique et d'Electronique In-

dustrielle. Since 1988, he has been a Professor with the Institut National Polytechnique de Lorraine, Nancy, France. His current research interests include power electronics and drives and new electrical devices (fuel cells and supercapacitors).

ARTICLE IN PRESS

Journal of Power Sources xxx (2010) xxx-xxx

Contents lists available at ScienceDirect

Journal of Power Sources

journal homepage: www.elsevier.com/locate/jpowsour



Energy management of fuel cell/solar cell/supercapacitor hybrid power source

Phatiphat Thounthong^{a,*}, Viboon Chunkag^b, Panarit Sethakul^a, Suwat Sikkabut^c, Serge Pierfederici^d, Bernard Davat^d

- ^a Department of Teacher Training in Electrical Engineering, King Mongkut's University of Technology North Bangkok, 1518, Piboolsongkram Road, Bangsue, Bangkok 10800, Thailand
- ^b Department of Electrical Engineering, King Mongkut's University of Technology North Bangkok, 1518, Piboolsongkram Road, Bangsue, Bangkok 10800, Thailand
- c Thai-French Innovation Institute, King Mongkut's University of Technology North Bangkok, 1518, Piboolsongkram Road, Bangsue, Bangkok 10800, Thailand
- d Groupe de Recherche en Electrotechnique et Electronique de Nancy (GREEN: UMR 7037), Nancy Université, INPL-ENSEM, 2, Avenue de la Forêt de Haye, Vandœuvre-lés-Nancy, Lorraine 54516, France

ARTICLE INFO

Article history: Received 19 October 2009 Received in revised form 14 December 2009 Accepted 18 January 2010 Available online xxx

Keywords: Converter Energy management Fuel cell Photovoltaic array Supercapacitor Voltage control

ABSTRACT

This study presents an original control algorithm for a hybrid energy system with a renewable energy source, namely, a polymer electrolyte membrane fuel cell (PEMFC) and a photovoltaic (PV) array. A single storage device, i.e., a supercapacitor (ultracapacitor) module, is in the proposed structure. The main weak point of fuel cells (FCs) is slow dynamics because the power slope is limited to prevent fuel starvation problems, improve performance and increase lifetime. The very fast power response and high specific power of a supercapacitor complements the slower power output of the main source to produce the compatibility and performance characteristics needed in a load. The energy in the system is balanced by d.c.-bus energy regulation (or indirect voltage regulation). A supercapacitor module functions by supplying energy to regulate the d.c.-bus energy. The fuel cell, as a slow dynamic source in this system, supplies energy to the supercapacitor module in order to keep it charged. The photovoltaic array assists the fuel cell during daytime. To verify the proposed principle, a hardware system is realized with analog circuits for the fuel cell, solar cell and supercapacitor current control loops, and with numerical calculation (dSPACE) for the energy control loops. Experimental results with small-scale devices, namely, a PEMFC (1200 W, 46 A) manufactured by the Ballard Power System Company, a photovoltaic array (800 W, 31 A) manufactured by the Ekarat Solar Company and a supercapacitor module (100 F, 32 V) manufactured by the Maxwell Technologies Company, illustrate the excellent energy-management scheme during load cycles. © 2010 Elsevier B.V. All rights reserved.

1. Introduction

Currently, most of the energy demand in the world is met by fossil and nuclear power plants. A small part is drawn from renewable energy technologies such as wind, solar, fuel cell, biomass and geothermal energy [1,2]. Wind energy, solar energy and fuel cells have experienced a remarkably rapid growth in the past ten years [3–5] because they are pollution-free sources of power. Additionally, they generate power near the load centres, which eliminates the need to run high-voltage transmission lines through rural and urban landscapes.

The cost of solar photovoltaic and fuel cell electricity is still high [6–8]. Nevertheless, with ongoing research, development and utilization of these technologies around the world, the costs of solar cells and fuel cell energy are expected to fall in the next few years. As for solar cell and fuel cell electricity producers, they now sell power

0378-7753/\$ – see front matter © 2010 Elsevier B.V. All rights reserved. doi:10.1016/j.jpowsour.2010.01.051

freely to end-users through truly open access to the transmission lines. For this reason, they are likely to benefit as much as other producers of electricity. Another benefit in their favour is that the cost of renewable energy falls as technology advances, whereas the cost of electricity from conventional power plants rises with inflation. The difference in their trends indicates that hydrogen and solar power will be more advantageous in future.

In the near future, the utility power system at a large scale will be supplied by renewable energy sources and storage device(s), i.e., hybrid energy systems, in order to increase their reliability and make them more effective. The specific properties of fuel cells and solar cells are as follows:

• The amount of power the fuel cell system delivers is controlled by the amount of current drawn from the system if the proper conditions for cell operation are maintained. When a large load is applied to the cells, the sudden increase in the current can cause the system to stall if the depleted oxygen or hydrogen cannot be replenished immediately and sufficiently. Cell starvation can lead to a system stall, permanent cell damage or

^{*} Corresponding author. Tel.: +66 2 913 2500x3332; fax: +66 2 587 8255. E-mail addresses: Phatiphat.Thounthong@ensem.inpl-nancy.fr, phtt@kmutnb.ac.th (P. Thounthong).

G Model

POWER-12837; No. of Pages 12

ARTICLE IN PRESS

P. Thounthong et al. / Journal of Power Sources xxx (2010) xxx-xxx

Nomenclature

a.c. alternating current
d.c. direct current
FC fuel cell
PV photovoltaic
SC supercapacitor

 C_{Bus} total capacitance at d.c.-bus (F)

*C*_{SC} total capacitance of supercapacitor module (F)

 i_{Load} d.c.-bus load current (A) i_{FC} fuel cell current (A)

 i_{FCREF} fuel cell current reference (set-point) (A) i_{Sol} solar cell (photovoltaic) current (A) i_{SolREF} solar cell current reference (set-point) (A)

 i_{SC} supercapacitor current (A)

*i*_{SCREF} supercapacitor current reference (set-point) (A)

p_{Load} load power (W)p_{FC} fuel cell power (W)

 p_{FCa} fuel cell output power to d.c.-bus (W) p_{FCREF} fuel cell power reference (set-point) (W)

 p_{FCMax} maximum fuel cell power (W) p_{Sol} solar cell (photovoltaic) power (W) p_{Sola} solar cell output power to d.c.-bus (W) p_{SolREF} solar cell power reference (set-point) (W)

p_{SolMax} maximum solar cell power (W)p_{SC} supercapacitor power (W)

p_{SCa} supercapacitor output power to d.c.-bus (W)
p_{SCREF} supercapacitor power reference (set-point) (W)

 p_{SCMax} maximum supercapacitor power (W)

 v_{Bus} d.c.-bus voltage (V) v_{FC} fuel cell voltage (V)

 v_{Sol} solar cell (photovoltaic) voltage (V)

 v_{SC} supercapacitor voltage (V)

y_{Bus} d.c.-bus energy (J)

 y_{BusREF} d.c.-bus energy reference (set-point) (J)

 y_{SC} supercapacitor energy (J)

 y_{SCREF} supercapacitor energy reference (set-point) (J) y_{T} total energy at d.c.-bus and supercapacitor (J) equivalent series resistance in fuel cell converter

 (Ω)

 r_{Sol} equivalent series resistance in solar cell converter

 (Ω)

r_{SC} equivalent series resistance in supercapacitor con-

verter (Ω)

u input variable vectorx state-variable vectory output vector

 $\varphi(\cdot)$, $\psi(\cdot)$, $\phi(\cdot)$ smooth mapping functions

reduced cell lifetime. To protect the fuel cells from overloading and starvation, especially during transient conditions, excessive oxygen and hydrogen can be supplied to the cells during the steady-state operation, which increases the reserve of available power in anticipation of a load increase. This strategy, however, is conservative and leads to increased parasitic losses, decreased air utilization and thereby compromised system performance. Therefore, the fuel cell power or current slope must be limited to prevent a fuel cell stack from experiencing the fuel starvation phenomenon and to optimize the system, for example, $4 \, \text{A s}^{-1}$ for a $0.5 \, \text{kW}$, $12.5 \, \text{V}$ PEMFC [9], and $5, 10 \, \text{and} \, 50 \, \text{A s}^{-1}$ for a $20 \, \text{kW}$, $48 \, \text{V}$ PEMFC [10].

 The output power of solar cells fluctuates considerably depending on solar radiation, weather conditions and temperature [11,12]. Therefore, in order to supply electric power to fluctuating loads with a hybrid system composed of the above-mentioned fuel cell and solar cell, an electric energy-storage system is needed to compensate for the gap between the output from the renewable energy sources and the load, in addition to the collaborative load sharing among those energies [13–15].

Moreover, hydrogen as an energy storage media has the potential to address both daily and seasonal buffering requirements. Systems that employ an electrolyzer to convert excess electricity to hydrogen coupled with hydrogen storage and regeneration using a fuel cell can, in principle, provide power with zero (or near zero) emissions. Hydrogen production by solar energy is a 'renewable-regenerative system' [4], and this process is known as the electrolysis process. The basic principle is the following: when the photovoltaic input power exceeds the load power demand, the system controller determines that the energy should be directed to hydrogen production. In this kind of operation, i.e., a solar-based renewable-regenerative system, almost half of the solar input energy is directed to hydrogen production and converted with 60% energy efficiency [4].

Based on present storage device technology, battery design has to supply the trade-off between specific energy, specific power and cycle life. The difficulty in obtaining high values of these three parameters has led to some suggestions that the energy-storage system of distributed generation systems should be a hybridization of an energy source and a power source [16,17]. The energy source, mainly fuel cells and solar cells in this study, has high specific energy, whereas the power source has high specific power. The power sources can be recharged from the main energy source(s) when there is less demand. The power source that has received wide attention is the supercapacitor (or 'ultracapacitor', or 'electrochemical double-layer capacitor') [18–20].

The enhancements in the performance of renewable energy source power systems that are gained by adding energy storage are all derived from the ability to shift the system output. Firmingup the renewable system is accomplished by ensuring that energy is available when there is a demand for it rather than being limited by the availability of the renewable resource. As a result, the system output may need to be shifted to periods when the hydrogen and/or the sun, for example, are not available [21]. Depending on the size and type of the energy-storage system and the load, it may be possible to provide all of the power needed to support the load. A much more common scenario is for the energy storage to simply provide enough power for applications, like peak shaving, without having full load support capability. The energy-storage system may also provide sufficient energy to ride out electric service interruptions that range from a few seconds to a few hours. This is especially important for service disruptions that occur when the renewable resource is not available.

In this study, a fuel cell/photovoltaic/supercapacitor hybrid power source is proposed. A power electronic converter structure, energy management and innovative energy control law are presented. To authenticate the proposed principle, the hardware system is realized by analog circuits and digital estimation with a dSPACE controller. Experimental results obtained with small-scale devices illustrate the system performance.

2. Renewable energy hybrid system

2.1. System configuration

The power converter structure of the system is shown in Fig. 1. Fuel cell and solar cell power-generating systems may provide direct or alternating current (d.c. or a.c.) to satisfy application-specific power needs (Fig. 1). The current, voltage and power quality

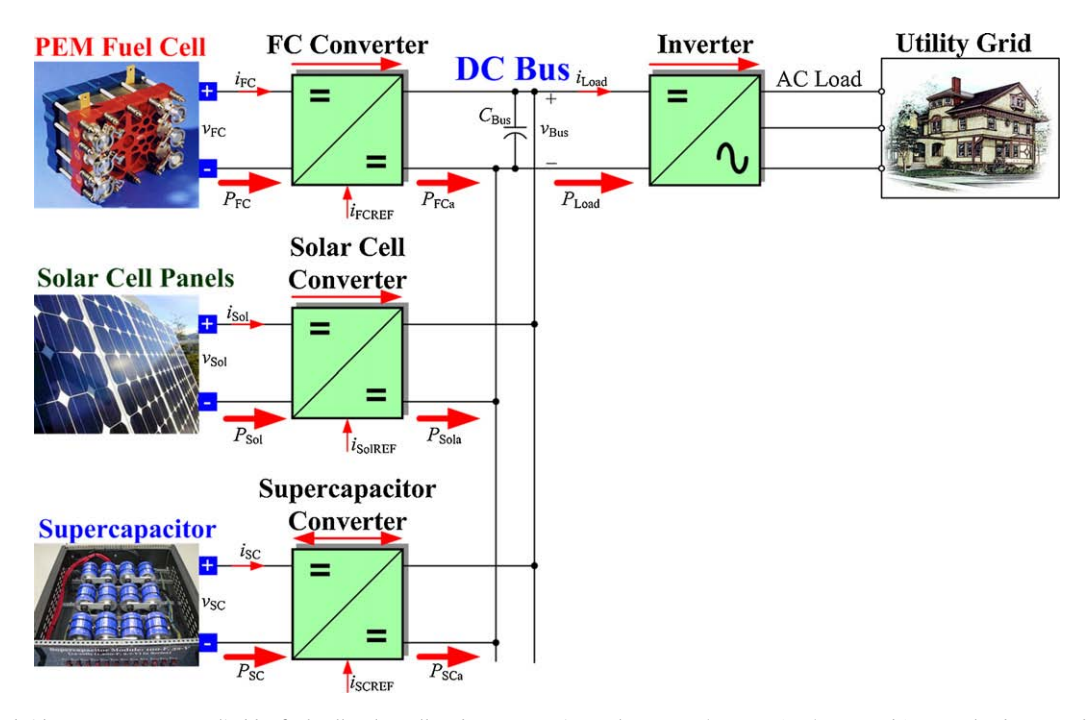


Fig. 1. Proposed hybrid energy system supplied by fuel cell, solar cell and supercapacitor, where $p_{\text{Load}} (= v_{\text{Bus}} \times i_{\text{Load}})$, v_{Bus} and i_{Load} are load power, d.c.-bus voltage and d.c.-bus load current, respectively. $p_{\text{FC}} (= v_{\text{FC}} \times i_{\text{FC}})$, v_{FC} and i_{FC} are fuel cell power, voltage and current, respectively. $p_{\text{SO}} (= v_{\text{SO}} \times i_{\text{SO}})$, v_{SO} and i_{SO} are solar cell power, voltage and current, respectively. $p_{\text{FC}} (= v_{\text{FC}} \times i_{\text{SO}})$, v_{SC} and i_{SC} are supercapacitor power, voltage, and current, respectively. $p_{\text{FC}} (= v_{\text{FC}} \times i_{\text{SO}})$, $v_{\text{SC}} (= v_{\text{SC}} \times i_{\text{SC}})$, $v_{\text{SC}} (= v_$

are controlled by electronic power-conditioning systems. Generally, voltage regulators and d.c.-d.c. converters (chopper circuits) are used to control and adjust the fuel cell and photovoltaic d.c. output voltages to useful values [22,23].

The voltages of the fuel cell and solar cell vary with the current drawn by the load and decrease significantly at high load currents [24]. Therefore, a power-electronics system is needed to process the raw output power from the stack or panel and provide power to the load at a constant d.c. or a.c. voltage. Typically, the power-electronics systems include multiple interconnected power converters: for example, a d.c.–d.c. converter is often followed by a d.c.–a.c. converter for stationary applications [25]. The switching scheme in such power converters can be based on pulsewidth modulation (PWM), resonant, quasi-resonant, soft-switched, or line-commutated switching [26–28]. Furthermore, the topological structures of these converters can vary dramatically [29].

The supercapacitor bank is always connected to the d.c.-bus by means of a two-quadrant d.c.-d.c. converter (bidirectional converter), a 'supercapacitor converter'. The supercapacitor power can be positive or negative, which allows energy to be transferred in both directions [30].

An inverter is used to convert the d.c. voltage to a useful a.c. voltage. It may operate as grid-independent or with grid-synchronization. Then, the solar cell supplies all its output power to the d.c.-bus, and the fuel cell supplies a slowly fluctuating power difference between the load power $p_{\rm Load}$ demand and the solar cell output power. A supercapacitor storage device can compensate for both a sudden change in the load demand and rapidly fluctuating solar cell output power caused by solar radiation; therefore, the load is supplied with stable power.

As depicted in Fig. 1, the proposed system has a multi-source structure (or cascade scheme). The cascaded structure can lead to interactions between converters that cause the system to be unstable, if they are designed separately. This problem has been studied during the past decade. In this case, to study interactions between the converters, impedance criteria are often used to determine the

stability of the cascaded system. Nonetheless, the technique only proves the asymptotic stability around a given operating point. The large signal stability properties or the behaviour of the system in the case of outsized disturbances are not considered in this model. In this paper, a non-linear control algorithm based on the differential flatness principle of the renewable power plant is proposed. Design controller parameters are independent of the operating point. Interactions between the converters are taken into account by the controllers, and high dynamics in perturbation rejection are accomplished.

2.2. Energy management

For reasons of safety and dynamics, the fuel cell, solar cell and supercapacitor converters are usually controlled primarily by inner current-regulation loops [17]. The dynamics of current-regulation loops are much faster than those of outer control loops, which are described later. Therefore, the fuel cell current $i_{\rm FC}$, the solar cell current $i_{\rm SOl}$ and the supercapacitor current $i_{\rm SC}$ are considered to follow their references $i_{\rm FCREF}$, $i_{\rm SolREF}$ and $i_{\rm SCREF}$ perfectly.

Energy management of multi-power sources has already been studied recently, for example, Feroldi et al. [31] studied control (based on efficiency map) of a fuel cell/supercapacitor hybrid power source for vehicle applications, Payman et al. [32] studied control of a regulated d.c. voltage supplied by a fuel cell and supercapacitor storage device based on a differential flatness system, and Thounthong et al. addressed a regulated d.c.-bus voltage fuel cell/supercapacitor hybrid source [33], a regulated d.c.-bus voltage fuel cell/battery/supercapacitor hybrid source [34] and an unregulated d.c.-bus voltage fuel cell/battery hybrid source [14].

Thus, in the proposed system depicted in Fig. 1, there are two-voltage variables, or two-energy variables, to be regulated. The d.c.-bus energy y_{Bus} is the most important variable, and the supercapacitor storage energy y_{SC} is the next most important. Therefore, based on the previous work described above, it is proposed to utilize supercapacitors, which are the fastest energy source in the pro-

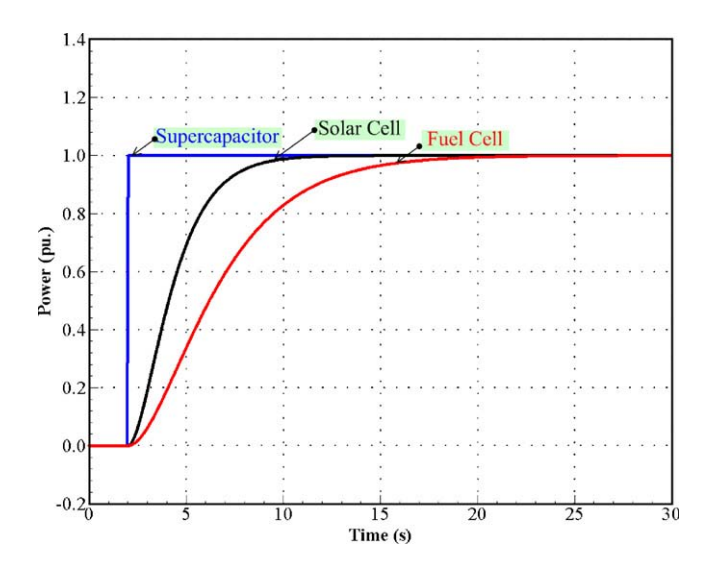


Fig. 2. Dynamic classification for proposed hybrid power source.

posed system, to supply the energy for the d.c.-bus [33,34]. Thus, the fuel cell (as the slowest dynamic device) and solar cell supply energy for both the d.c.-bus capacitor C_{Bus} and the supercapacitors C_{SC} to keep them charged.

At the d.c. link, there are three sources that supply energy at the same time. Therefore, the dynamics of the three sources must be classified in order to guarantee system stability [34], as illustrated in Fig. 2. Note that the power unit in Fig. 2 is the normalized unit (or per-unit [pu]). Thus, the defined dynamic classification depicted in Fig. 2 is obtained from the simulation result using Matlab-Simulink, and the experimental results of the power source dynamics are presented after the performance validation section. The supercapacitor is operated as the highest dynamic power source to provide the micro-cycles and the fast dynamic power supply. It can withstand a very large number of charge-discharge cycles without degradation (or virtually infinite cycles) [33,35]. The fuel cell generator is operated as the lowest dynamic power source. The fuel cell current or power slope must be limited to avoid the fuel starvation phenomenon. The fuel cell limited current or power slope has been experimentally determined to be the highest slope of an operating fuel cell system, where no fuel starvation occurs in order to improve its lifetime [33,34]. The photovoltaic generator is between the fuel cell and supercapacitor in the dynamic classification.

2.2.1. Principle of differential flatness theory

A non-linear control algorithm based on the flatness properties [36–38] of the system is proposed. According to the flatness-control law, the tuning controller parameters are independent of the operating point [32]. According to Fliess et al. [39,40], an independent dynamic system is considered to be differentially flat if an output y is given by:

$$\mathbf{y} = \phi(\mathbf{x}, \mathbf{u}, \dot{u}, \dots, u^{(\alpha)}), \quad \mathbf{y} \in \mathbb{R}^{m}$$
(1)

such that the state \boldsymbol{x} and controls \boldsymbol{u} (or inputs) can be written as:

$$\mathbf{x} = \varphi(\mathbf{y}, \dot{\mathbf{y}}, ..., \mathbf{y}^{(\beta)}), \quad \mathbf{x} \in \mathbb{R}^{n}$$
(2)

$$\mathbf{u} = \psi(\mathbf{v}, \dot{\mathbf{v}}, \dots, \mathbf{v}^{(\beta+1)}), \quad \mathbf{u} \in \mathbb{R}^{m}$$
(3)

where $\varphi(\cdot)$, $\psi(\cdot)$, $\phi(\cdot)$ are the smooth mapping functions, α and β are a finite number of their time derivatives, and $(n, m) \in \mathbb{N}$. Moreover, it is assumed that $m \le n$.

The output \mathbf{y} is called a *flat output*. Thus, a dynamic system is, in nature, differentially flat if it is equivalent to a system without dynamics, i.e., a static system. In other words, there are no differential constraints in output space. The apparent advantage of a

differentially flat system is that every trajectory in the output space is feasible; therefore, trajectory generation is theoretically simpler in terms of the flat outputs. For this reason, by using the flatness estimation in power electronic applications, interactions between the converters are taken into account by the flatness-control law and high dynamics in perturbation elimination are achieved.

2.2.2. d.c.-Bus energy control

Based on the flatness-control, the electrostatic energy y_{Bus} stored in the total d.c.-bus capacitor C_{Bus} is considered as the flat output variable (Eq. (1)), i.e.:

$$y_{\text{Bus}} = \frac{1}{2} C_{\text{Bus}} v_{\text{Bus}}^2 \tag{4}$$

It is assumed that the supercapacitor current follows its reference value perfectly. Thus:

$$i_{SC} = i_{SCREF} = \frac{p_{SC}}{\nu_{SC}} = \frac{p_{SCREF}}{\nu_{SC}}$$
 (5)

where p_{SCREF} is the control variable of the reduced system described in Eq. (3).

Therefore, the state variable v_{Bus} may be put into a form similar to that in Eq. (2):

$$v_{\text{Bus}} = \sqrt{\frac{2y_{\text{Bus}}}{C_{\text{Bus}}}} = \varphi_1(y) \tag{6}$$

To obtain a relationship between the control variable p_{SC} and the flat output variable y_{Bus} , the differential equation verified by the reduced model from Fig. 1 is written as:

$$\dot{y}_{\text{Bus}} = p_{\text{FCa}} + p_{\text{Sola}} + p_{\text{SCa}} - p_{\text{Load}} \tag{7}$$

where

$$p_{FCa} = p_{FC} - r_{FC} \left(\frac{p_{FC}}{\nu_{FC}}\right)^2 \tag{8}$$

$$p_{\text{Sola}} = p_{\text{Sol}} - r_{\text{Sol}} \left(\frac{p_{\text{Sol}}}{v_{\text{Sol}}} \right)^2 \tag{9}$$

$$p_{SCa} = p_{SC} - r_{SC} \left(\frac{p_{SC}}{\nu_{SC}}\right)^2 \tag{10}$$

 $r_{\rm FC}$ is the total equivalent series resistance in the fuel cell converter. Here, only static resistance loss is considered [32]. $r_{\rm Sol}$ is the total equivalent series resistance in the solar cell converter. $r_{\rm SC}$ is the total equivalent series resistance in the supercapacitor converter.

It follows that:

$$p_{\text{SCREF}} = 2p_{\text{SCMax}} \left[1 - \sqrt{1 - \left(\frac{\dot{y}_{\text{Bus}} + p_{\text{Load}} - p_{\text{FCa}} - p_{\text{Sola}}}{p_{\text{SCMax}}} \right)} \right]$$
$$= \psi_1(y, \dot{y}) \tag{11}$$

where

$$p_{\text{SCMax}} = \frac{v_{\text{SC}}^2}{4r_{\text{SC}}} \tag{12}$$

$$p_{\text{Load}} = v_{\text{Bus}} i_{\text{Load}} = \sqrt{\frac{2y_{\text{Bus}}}{C_{\text{Bus}}}} i_{\text{Load}}$$
 (13)

 p_{SCMax} is the limited maximum power from the supercapacitor module.

Thus, it is apparent that $p_{SC} = \psi_1(y, \dot{y})$, which corresponds with Eq. (3), and the proposed reduced system with the control variable p_{SC} can be considered to be a flat system associated with y_{Bus} as the flat output variable.

To ensure the control of the flat output variable $y_{\rm Bus}$ to its reference trajectory $y_{\rm BusREF}$, the following control law is based on the

ARTICLE IN PRESS

P. Thounthong et al. / Journal of Power Sources xxx (2010) xxx-xxx

Fig. 3. Proposed d.c.-bus energy control loop for fuel cell/solar cell/supercapacitor hybrid source.

well-known second-order control law:

 $(\dot{y}_{\text{Bus}} - \dot{y}_{\text{BusREF}}) + K_{11}(y_{\text{Bus}} - y_{\text{BusREF}})$

$$+K_{12} \int_0^t (y_{\text{Bus}} - y_{\text{BusREF}}) d\tau = 0$$
 (14)

where K_{11} , and K_{12} are the controller parameters. Defining $e_{yBus} = y_{Bus} - y_{BusREF}$, $K_{11} = 2\zeta\omega_n$, and $K_{12} = \omega_n^2$ gives:

$$\ddot{e}_{\text{vBus}} + 2\zeta \omega_n \dot{e}_{\text{vBus}} + \omega_n^2 e_{\text{vBus}} = 0 \tag{15}$$

It is obvious that the control system is stable for K_{11} , $K_{12} > 0$. Based on the power electronic constant switching frequency $f_{\rm S}$ and a cascade control structure, the outer control loop (here the d.c.-bus energy control) must operate at a cut-off frequency $f_{\rm e} \ll f_{\rm C}$ (a cut-off frequency of the supercapacitor current loop or power loop) $\ll f_{\rm S}$ [41]. The d.c.-bus energy control loop detailed above is portrayed in Fig. 3.

The d.c.-bus energy control law generates a supercapacitor power reference $p_{\rm SCREF}$. This signal is then divided by the measured supercapacitor voltage $v_{\rm SC}$ and limited to maintain the supercapacitor voltage within an interval $[V_{\rm SCMin}, V_{\rm SCMax}]$ by limiting the supercapacitor charging current or discharging current, as presented in the block "SuperC Current Limitation Function" [33]. The higher voltage value $V_{\rm SCMax}$ of this interval corresponds to the maximum voltage of the storage device. Generally, the lower voltage value $V_{\rm SCMin}$ is chosen as $V_{\rm SCMax}/2$, which causes only 25% of the energy in the supercapacitor bank to remain [33]; as a result, the supercapacitor discharge becomes ineffective. This results in the supercapacitor current reference $i_{\rm SCREF}$.

2.2.3. Supercapacitor energy control

The classical electrostatic energy storage y_{SC} in the supercapacitor is expressed by:

$$y_{SC} = \frac{1}{2} C_{SC} v_{SC}^2 \tag{16}$$

where C_{SC} is the supercapacitor capacitance (refer to Fig. 1), and v_{SC} is the supercapacitor voltage.

Again, based on the flatness-control, the total electrostatic energy y_T stored in the total d.c.-bus capacitor C_{Bus} and the supercapacitor C_{SC} is taken as the flat output variable (Eq. (1)), i.e.:

$$y_{\rm T} = y_{\rm Bus} + y_{\rm SC} = \frac{1}{2}C_{\rm Bus}v_{\rm Bus}^2 + \frac{1}{2}C_{\rm SC}v_{\rm SC}^2$$
 (17)

It is again assumed that the fuel cell and photovoltaic currents follow their reference values perfectly. Thus:

$$i_{FC} = i_{FCREF} = \frac{p_{FC}}{\nu_{FC}} = \frac{p_{FCREF}}{\nu_{FC}}$$
 (18)

$$i_{\text{Sol}} = i_{\text{SolREF}} = \frac{p_{\text{Sol}}}{v_{\text{Sol}}} = \frac{p_{\text{SolREF}}}{v_{\text{Sol}}}$$
(19)

where p_{FCREF} and p_{SolREF} are the control variables of the reduced system (Eq. (3)).

Thus, the state variable v_{SC} may be put into a form similar to that of Eq. (2):

$$v_{SC} = \sqrt{\frac{2(y_{T} - y_{Bus})}{C_{SC}}} = \varphi_{2}(y)$$
 (20)

The differential equation verified by the reduced model from Fig. 1 is:

$$\dot{y}_{\rm T} = p_{\rm Ta} - p_{\rm Load} \tag{21}$$

where

$$p_{\text{Ta}} = p_{\text{FCa}} + p_{\text{Sola}} = p_{\text{T}} - r_{\text{T}} \left(\frac{p_{\text{T}}}{v_{\text{T}}}\right)^2 \tag{22}$$

For a fuel cell and a solar cell that are combined as an energy source to supply energy to a d.c.-bus and supercapacitor, v_T is defined as presented in Eq. (22) and r_T represents the total losses in the fuel cell and photovoltaic converters.

Therefore:

$$p_{\text{TREF}} = 2p_{\text{TMax}} \left[1 - \sqrt{1 - \left(\frac{\dot{y}_{\text{T}} + p_{\text{Load}}}{p_{\text{TMax}}}\right)} \right] = \psi_2(y, \dot{y})$$
 (23)

where

$$p_{\text{TMax}} = \frac{v_{\text{T}}^2}{4r_{\text{T}}} \tag{24}$$

In fact

$$p_{\text{TMax}} = p_{\text{FCMax}} + p_{\text{FCMax}} \tag{25}$$

 p_{FCMax} is the maximum fuel cell power. p_{SolMax} is the maximum photovoltaic power.

Photovoltaic power systems require some specific estimation algorithms to deliver the maximum power point (MPP) because the output features of a solar cell vary with environmental changes in irradiance and temperature. Many previous investigations have presented different techniques for maximum power point tracking (MPPT) of photovoltaic arrays [42–44]. It is beyond the scope of this study to present the MPPT algorithm here, though it is similar to Eq. (14). Because the supercapacitor energy storage has a large capacity and the supercapacitor energy is defined as a slower dynamic variable than the d.c.-bus energy variable, the total (supercapacitor) energy control law is defined as:

$$(\dot{y}_{\rm T} - \dot{y}_{\rm TREF}) + K_{21}(y_{\rm T} - y_{\rm TREF}) = 0$$
 (26)

The supercapacitor energy control loop is shown in Fig. 4. The total energy control law generates a total power reference p_{TREF} . First, p_{TREF} is considered to be the photovoltaic power reference p_{SolarREF} . It must be limited in level, within an interval maximum p_{SolarMax} (MPP) and minimum p_{SolarMin} (set to 0 W), and have limited dynamics to respect constraints in the dynamic classification (Fig. 2). Here, the second-order delay [34] is selected as a photovoltaic power dynamic limitation, as illustrated in Fig. 4. Second, the difference between the total power reference p_{TREF} and the

P. Thounthong et al. / Journal of Power Sources xxx (2010) xxx-xxx

Fig. 4. Proposed supercapacitor energy control loop for fuel cell/solar cell/supercapacitor hybrid source.

photovoltaic power reference $p_{\rm SolarREF}$ is the fuel cell power reference $p_{\rm FCREF}$. It must be limited in level, within an interval maximum $p_{\rm FCMax}$ and minimum $p_{\rm FCMin}$ (set to 0 W), and be limited in dynamics to respect the dynamic classification constraints in Fig. 2. Again, second-order delay is selected as a fuel cell power dynamic limitation.

3. Performance validation

3.1. Test bench description

In order to authenticate the proposed original hybrid energy management, a small-scale test bench has been implemented, as presented in Fig. 5. The fuel cell system used in this effort is a Ballard Nexa fuel cell system (1.2 kW, 46 A). It is supplied using pure hydrogen with a regulated pressure of 10 bar from bottles under a pressure of 150 bar and with clean dry air from a compressor. The photovoltaic array (800 W, 31 A) was obtained by connecting four panels (200 W, 7.78 A) in series. The solar cell panels were developed and manufactured by the Ekarat Solar Company. They were installed on the roof of the laboratory building, as illustrated in Fig. 5. The supercapacitor module (100 F, 32 V, based on Maxwell Technologies Company) was obtained by connecting 12 cells BCAP1200 (capacitance: 1200 F; maximum voltage: 2.7 V) in series, as shown in Fig. 5.

The fuel cell converter (1200 W) is composed of four-phase boost converters connected in parallel using the interleaving technique [45] and is selected to adapt the low d.c. voltage delivered

by the fuel cell, which is approximately $26\,V$ at rated power, to the $60\,V$ d.c.-bus. Thus, each boost converter is composed of a high-frequency input inductor ($420\,\mu H$), four output filtering capacitors connected in parallel (each capacitor is an aluminum electrolytic capacitor ($470\,\mu F$), thus the total capacitance is $1880\,\mu F$), a diode (Schottky diode RURG3020: $200\,V$, $30\,A$), and a main power switch (power metal–oxide–semiconductor field-effect transistor IRFP264N MOSFET: $250\,V$, $38\,A$). The frequency of the pulse-width modulation (PWM) that drives each boost converter is $25\,k Hz$.

The solar cell converter (800 W) is composed of two-phase boost converters connected in parallel by the interleaving technique and is selected to adapt the low d.c. voltage delivered by the solar panels, which is approximately 25 V at rated power, to the 60 V d.c.-bus. Thus, each boost converter is composed of a high-frequency input inductor (140 μ H), four output filtering capacitors connected in parallel (total capacitance: 4400 μ F), a diode (Schottky diode RURG3020: 200 V, 30 A), and a main power switch (power metal–oxide–semiconductor field–effect transistor IRFP264N MOS-FET: 250 V, 38 A). The frequency of the PWM that drives each boost converter is 25 kHz.

The supercapacitor converter is composed of four-phase bidirectional converters connected in parallel by the interleaving technique. Thus, each two-quadrant converter is composed of a high-frequency input inductor (290 μ H), an output filtering capacitor (aluminum electrolytic capacitors: 680 μ F), two power switches (power metal–oxide–semiconductor field-effect transistor IRFP264N MOSFET: 250 V, 38 A), and two diodes (Schottky diode RURG3020: 200 V, 30 A). The frequency of the PWM that drives



Fig. 5. Hybrid power source test bench.

Please cite this article in press as: P. Thounthong, et al., J. Power Sources (2010), doi:10.1016/j.jpowsour.2010.01.051

ARTICLE IN PRESS

P. Thounthong et al. / Journal of Power Sources xxx (2010) xxx-xxx

 Table 1

 d.c.-bus energy control loop parameters.

Parameter	Value	
$ u_{BusREF} $	60	V
C_{Bus}	12,200	μF
K ₁₁	450	$rad s^{-1}$
K ₁₂	22,500	$ m rads^{-2}$
$r_{ ext{FC}}$	0.14	Ω
r_{Sol}	0.12	Ω
$r_{ m SC}$	0.10	Ω
V_{SCMax}	32	V
V_{SCMin}	15	V
$I_{SCRated}$	150	A

each bidirectional converter is 25 kHz. The supercapacitor current, which flows across the storage device, can either be positive or negative, which allows energy to be transferred in both directions.

3.2. Control description

Measurements of the fuel cell current $i_{\rm FC}$, the solar cell current $i_{\rm Sol}$, the supercapacitor current $i_{\rm SC}$, the load current $i_{\rm Load}$, the d.c. link voltage $v_{\rm Bus}$, the fuel cell voltage $v_{\rm FC}$, the solar cell voltage $v_{\rm Sol}$, and the supercapacitor voltage $v_{\rm SC}$ are collected with zero-flux Hall effect sensors.

The fuel cell, the solar cell and the supercapacitor current-regulation loops were realized by analog circuits to function at a high bandwidth. Parameters associated with the d.c.-bus energy regulation loop and the supercapacitor energy regulation loop can be seen in Tables 1 and 2, respectively. The fuel cell power dynamic delay is shown in Table 2; this value was experimentally determined as the highest power slope of the FC system, where no fuel starvation occurs. It must be noted here that, for the small-

Table 2 Supercapacitor energy control loop parameters.

Parameter	Value	
$\nu_{ m SCREF}$	25	V
C_{SC}	100	F
K_{21}	0.1	WJ^{-1}
p_{SolMax} (rated)	800	W
$p_{\rm SolMin}$	0	W
I _{SolMax} (rated)	28	A
I_{SolMin}	0	A
ζ_2	1	
ω_{n2}	0.8	$\rm rads^{-1}$
p_{FCMax}	500	W
p_{FCMin}	0	W
I _{FCMax} (rated)	46	A
I_{FCMin}	0	A
ζ1	1	
ω_{n1}	0.4	rad s ⁻¹

test bench, the fuel cell maximum power $p_{\rm FCMax}$ is set at 500 W; but, the rated fuel cell power considered here is 1200 W. Further, these two energy control loops, which generate current references $i_{\rm FCREF}$, $i_{\rm SolREF}$ and $i_{\rm SCREF}$ are implemented on the real time card dSPACE DS1104 through the mathematical environment of Matlab–Simulink with a sampling frequency of 25 kHz.

3.3. Experimental results

The studied d.c.-bus of 60 V is only connected to an electronic load. To validate the dynamics of the power (current) regulation loops for each power source, Figs. 6–8 present waveforms that are obtained during the stepped power demand. Fig. 6 illustrates the fuel cell power demand, power response, voltage and current. Fig. 7 contains the photovoltaic power demand, power response,

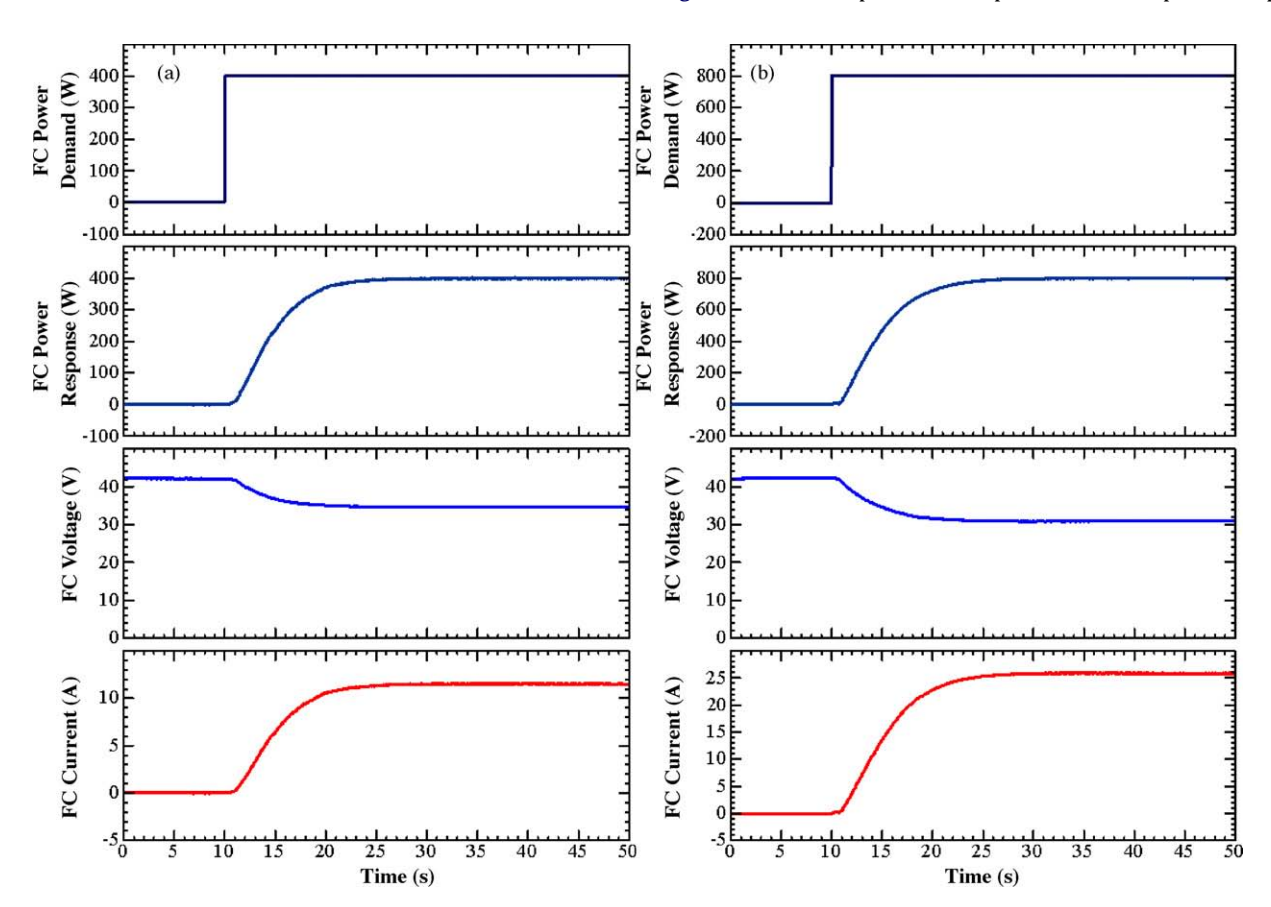


Fig. 6. Dynamic identification of fuel cell power control loop.

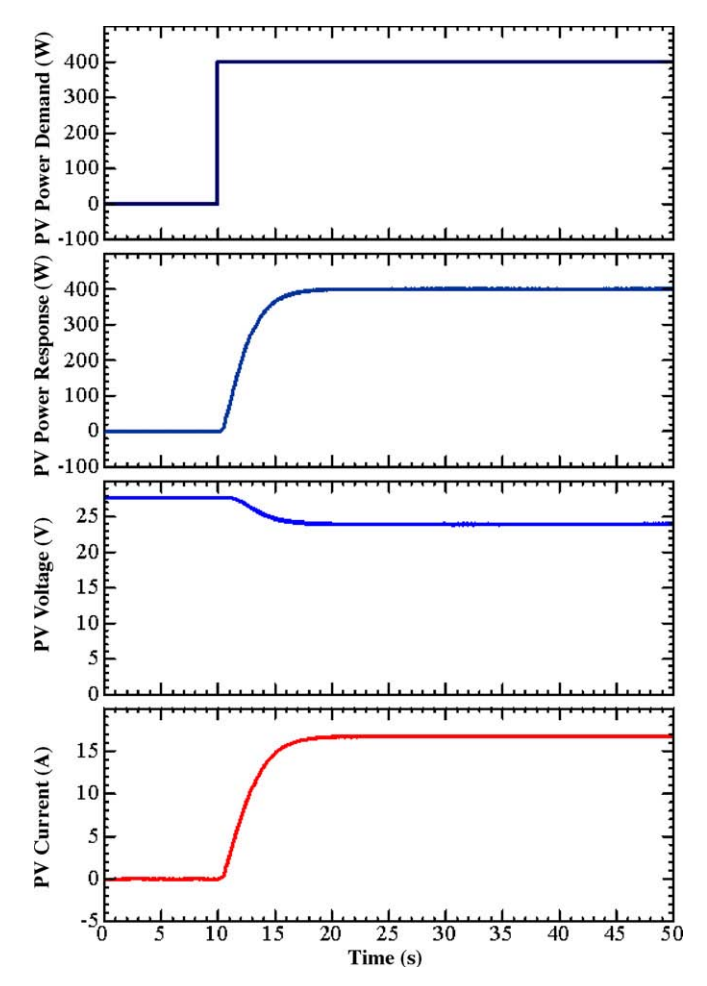


Fig. 7. Dynamic identification of photovoltaic power control loop.

voltage and current. Finally, Fig. 8 illustrates the supercapacitor power demand, power response, voltage and current. Because the fuel cell and photovoltaic powers are intentionally limited by the control algorithm (refer to Fig. 4: 'solar cell dynamic power limitation' and 'fuel cell power dynamic limitation'), a smooth transition of the power responses of the fuel cell and photovoltaic sources is observed, while the supercapacitor power dynamics are very fast. The supercapacitor can supply power from 0 to 400 W in 50 ms. It is clear that the fast response of the supercapacitor storage device can be operated with the fuel cell and solar cell main generators in order to improve system performance. The data in Fig. 6 also confirm that the fuel cell is controlled to avoid the fuel starvation phenomenon.

Because flatness-based control is model-based, it may have some sensitivity to errors in the model parameters. To authenticate its robustness, the flatness-based control was tested with the exact model parameters ($r_{\rm FC}$ = 0.14 Ω , $r_{\rm Sol}$ = 0.12 Ω , $r_{\rm SC}$ = 0.10 Ω) and in the lossless parameters case (r_{FC} = 0 Ω , r_{Sol} = 0 Ω , r_{SC} = 0 Ω). In the case of no losses, this leads to a drastically less complex estimation of the control law (Eqs. (8)–(11)). Comparisons (robustness) between the accurate parameters and the error parameters are given in Fig. 9. They generate waveforms that are obtained during the large load step from 0 to 500 W and show the d.c.-bus voltage, the load power (disturbance), the supercapacitor power, and the supercapacitor voltage (storage SOC). Because the power of the fuel cell and the solar cells are intentionally limited, the supercapacitor supplies the transient load power demand. Similar waveforms are seen in Fig. 9(a) and (b). The d.c.-bus voltage (d.c. link stabilization) is minimally influenced by the large step in load power. Clearly the performance of the control system is hardly affected by the considered error in model parameters. Experimental testing demonstrates that errors in these parameters have relatively little effect on regulation performance. It is therefore conclude that the non-linear differential flatness-based approach provides an absolutely robust controller in this application.

Waveforms obtained during the large load cycle are presented in Fig. 10. The data show the d.c.-bus voltage, the fuel cell voltage, the photovoltaic voltage, the load power, the supercapacitor power, the fuel cell power, the photovoltaic power, the supercapacitor current, the fuel cell current, the photovoltaic current, and the supercapacitor voltage (or the supercapacitor SOC). In the initial state, the small load power is equal to $100\,\mathrm{W}$, and the storage device is fully charge, i.e., $v_{\mathrm{SC}} = 25\,\mathrm{V}$; as a result, both the fuel cell and supercapacitor powers are zero, and the photovoltaic source supplies power for the load of $100\,\mathrm{W}$. At $t = 40\,\mathrm{s}$, the load power steps to the final constant power of around $900\,\mathrm{W}$ (positive load power transition). The following observations are made:

- The supercapacitor supplies most of the 900W power that is required during the transient step load.
- Simultaneously, the photovoltaic power increases with limited dynamics to a maximum power point (MPP) of around 300 W, which is limited by the maximum power point tracker (MPPT).
- Concurrently, the fuel cell power increases with limited dynamics to a maximum power of 500 W.
- The input from the supercapacitor, which supplies most of the transient power that is required during the stepped load, slowly decreases and the unit remains in a discharge state after the load step because the steady-state load power (approximately 900 W) is greater than the total power supplied by the fuel cell and photovoltaic array.

At t = 100 s, the supercapacitor voltage is equal to 19 V. As a result, the supercapacitor supplies its stored energy y_{SC} to the d.c.-bus. This energy $y_{SC,Supply}$ is estimated to be:

$$y_{\text{SC_Supply}} = \frac{1}{2}C_{\text{SC}}v_{\text{SC}}^{2}(t = 40 \text{ s}) - \frac{1}{2}C_{\text{SC}}v_{\text{SC}}^{2}(t = 100 \text{ s})$$

$$= 13.20 \text{ kJ}$$
(27)

The load power is reduced from the high constant power of 900 W to the low constant power of 100 W (negative load power transition). As a result, the supercapacitor changes from discharging to charging and demonstrates the following four phases:

- First, the fuel cell and photovoltaic array still supply their constant maximum powers to drive the load and to charge the supercapacitor.
- Second, at t = 110 s, the supercapacitor is approaching full charge, i.e., $v_{SC} = 23$ V. Consequently, the fuel cell power is reduced with limited power dynamics.
- Third, at $t = 120 \, \text{s}$, the supercapacitor is nearly fully charged, i.e., $v_{\text{SC}} = 24 \, \text{V}$. As a result, the photovoltaic power is reduced with limited power dynamics.
- Fourth, at $t = 160 \, \text{s}$, the supercapacitor is fully charged, i.e., $v_{\text{SC}} = v_{\text{SCREF}} = 25 \, \text{V}$. After slowly decreasing, the photovoltaic power remains at a constant power of 100 W for the load power demanded. Furthermore, the fuel cell and supercapacitor powers are zero.

It is evident that the d.c.-bus voltage waveform is stable during the large load cycle, which is critically important when employing supercapacitors to improve the dynamic performance of the whole system using the proposed control law.

Finally, Fig. 11 presents waveforms that are obtained during the long load cycles measured on 5 December, 2009. The waveforms are

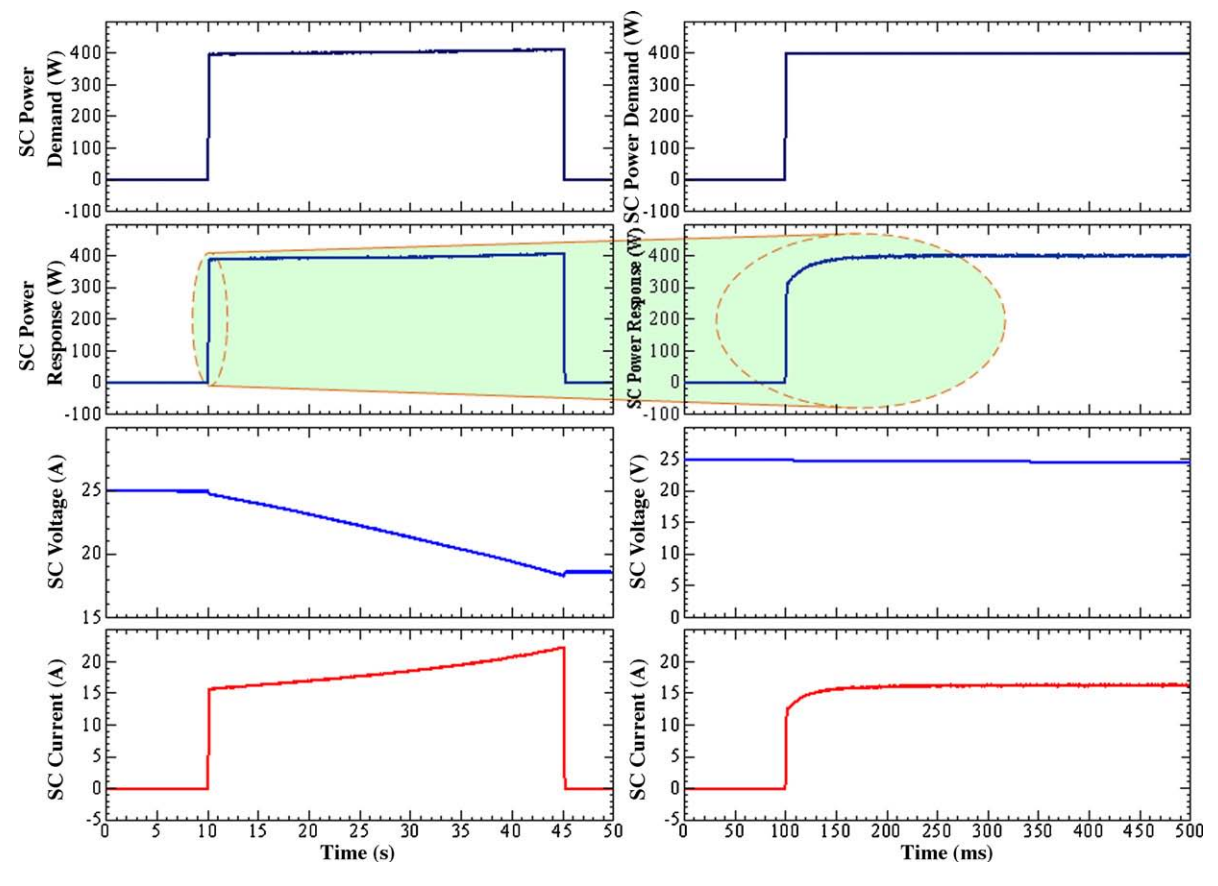


Fig. 8. Dynamic identification of supercapacitor power control loop.

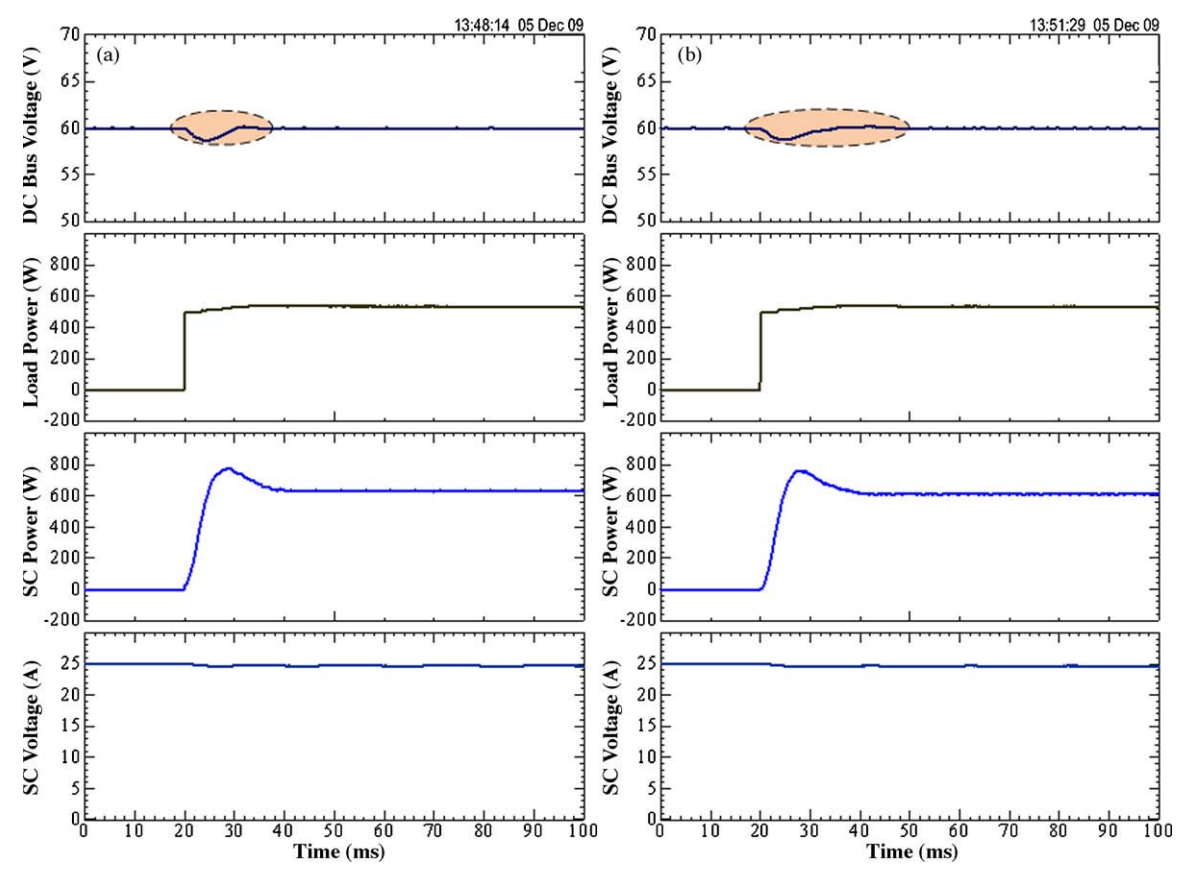


Fig. 9. Comparison of d.c. link stabilization of hybrid energy source during large load step. (a) exact model (r_{EC} = 0.14 Ω , r_{Sol} = 0.12 Ω , r_{SC} = 0.10 Ω) and (b) error model (robustness) (r_{EC} = 0 Ω , r_{Sol} = 0 Ω , r_{SC} = 0 Ω).

P. Thounthong et al. / Journal of Power Sources xxx (2010) xxx-xxx

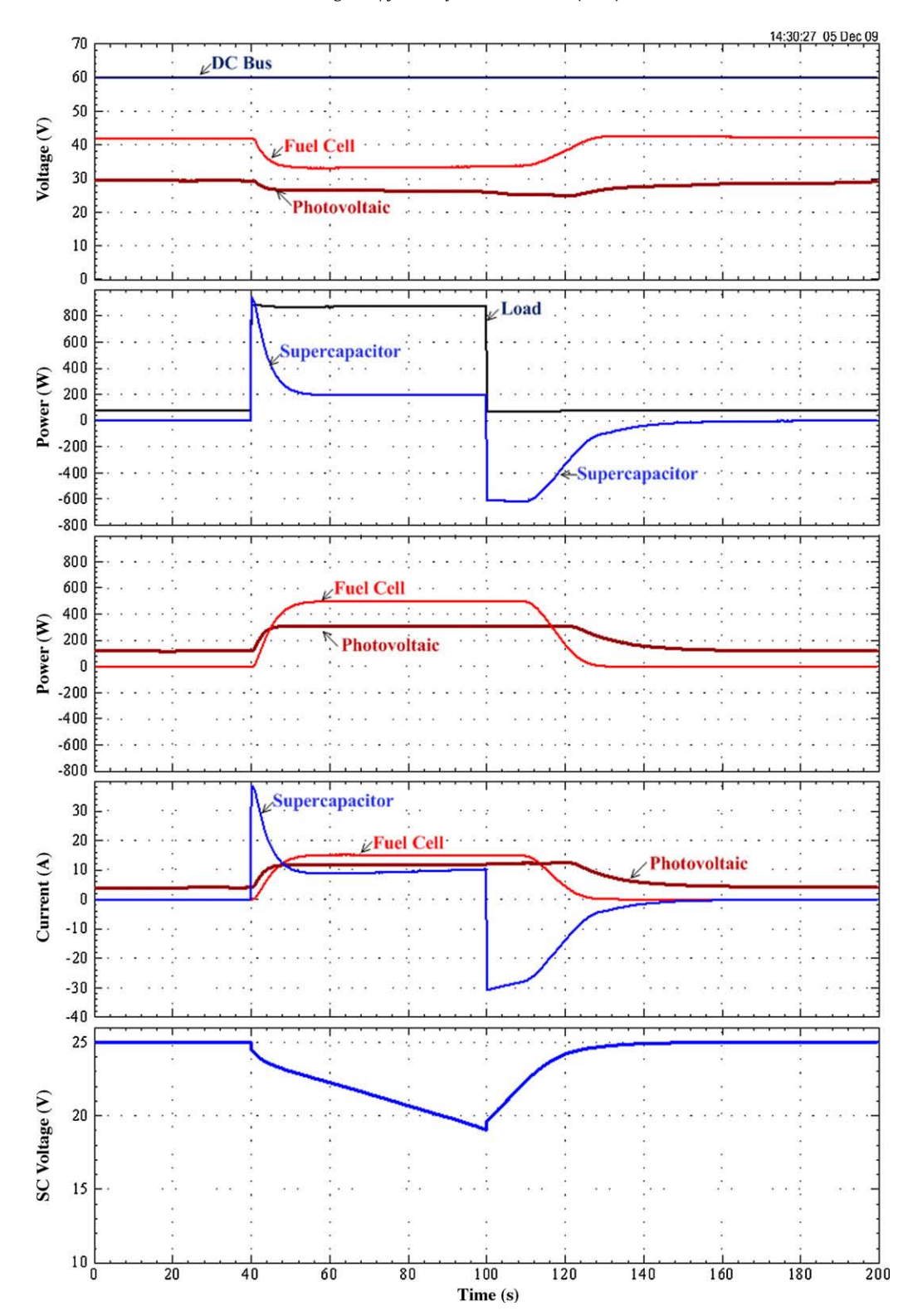


Fig. 10. Hybrid source response during load cycle.

similar to the test bench results in Fig. 10. During the experiment, the FC maximum power was set to 500 W, and the PV maximum power (depending on solar radiation, weather conditions and temperature) was limited by the MPPT. For example, at 15:01:40, the PV maximum power was approximately equal to 180 W; at 15:02:30, the PV maximum power was about 180 W; at 15:03:20, the PV maximum power was around 180 W; and from 15:05:50 to 15:08:20, the PV maximum power was reduced to 0 W, because of the cloudy

conditions. In particular, it was found that the power plant was always energy balanced $p_{\text{Load}}(t) \approx p_{\text{FC}}(t) + p_{\text{Sol}}(t) + p_{\text{SC}}(t)$ by the proposed original control algorithm.

The important variable necessary to balance the energy in this complex system is the d.c.-bus energy or voltage. From the experimental validation, the d.c.-bus voltage is automatically controlled at the constant set-point, i.e., $\nu_{\text{Bus}} = 60 \, \text{V}$. This experiment confirms that the energy in the system is well managed. The fuel cell and

Please cite this article in press as: P. Thounthong, et al., J. Power Sources (2010), doi:10.1016/j.jpowsour.2010.01.051

10

P. Thounthong et al. / Journal of Power Sources xxx (2010) xxx-xxx

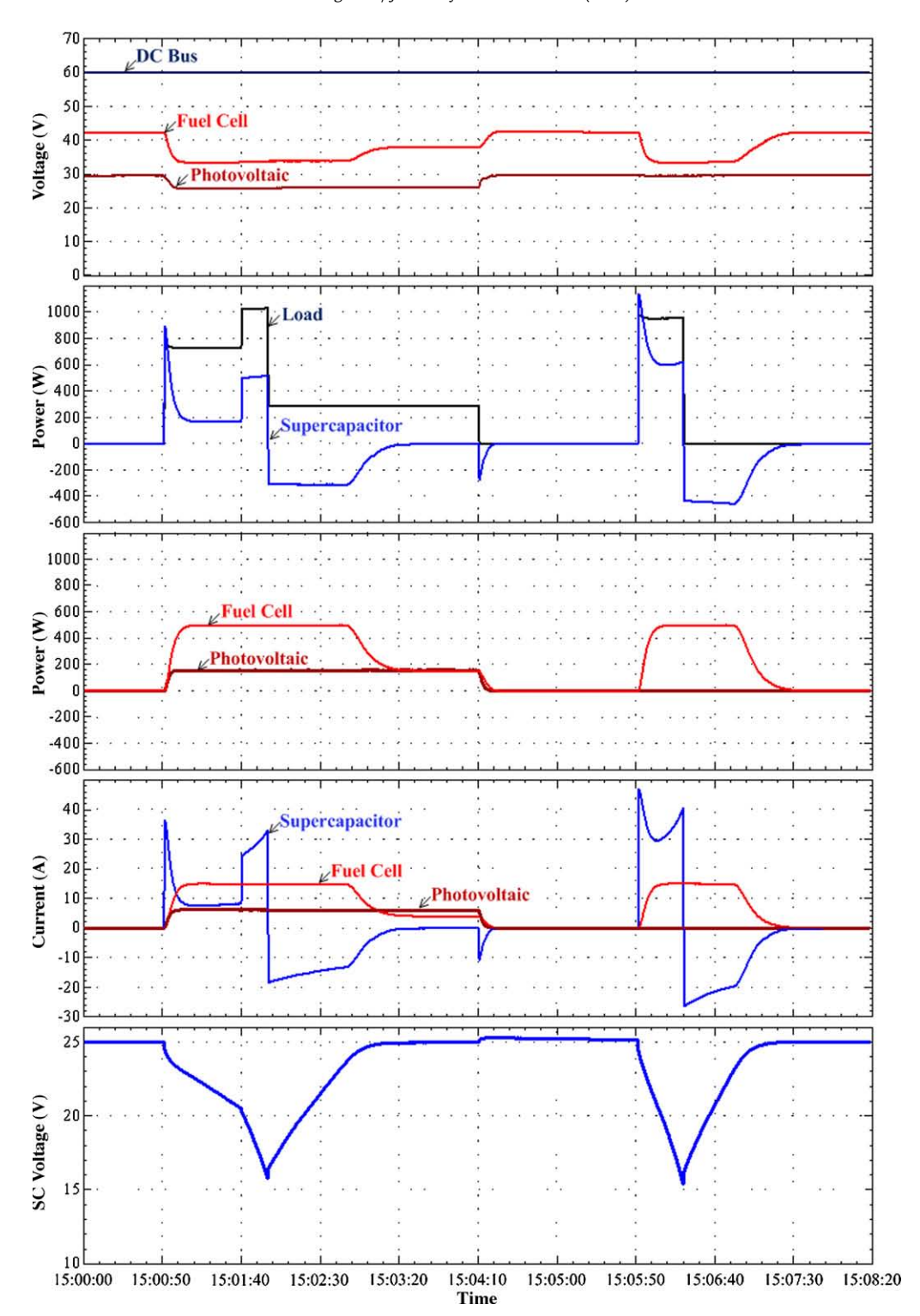


Fig. 11. Hybrid source response during long load cycles.

solar cell powers are limited at their maximum powers, and the fuel cell power dynamics are controlled; as a result, there is no fuel starvation problem and the fuel cell stack lifetime is increased [46–48].

4. Conclusions

Energy management of multi-power sources has been proposed as a solution for a hybrid energy system that uses renewable energy from solar cells, fuel cells and a supercapacitor as an energy storage device. A supercapacitor can advance the load, following the characteristics of the main sources by providing a stronger power response to changes in the system load. During essential steps in the load, the supercapacitor provides the energy balance needed during load transition periods. Adding energy storage to the distributed power systems improves power quality and efficiency.

Experimental verification with a small-scale hybrid test bench (Nexa Ballard fuel cell power generator: 1.2 kW, 46 A; Ekarat Solar Cell power module: 800 W, 31 A; Maxwell supercapacitor storage device: 100 F, 32 V) has demonstrated the excellent performance of

POWER-12837; No. of Pages 12

ARTICLE IN PRESS

P. Thounthong et al. / Journal of Power Sources xxx (2010) xxx-xxx

the whole system, and has validated the proposed energy management principle.

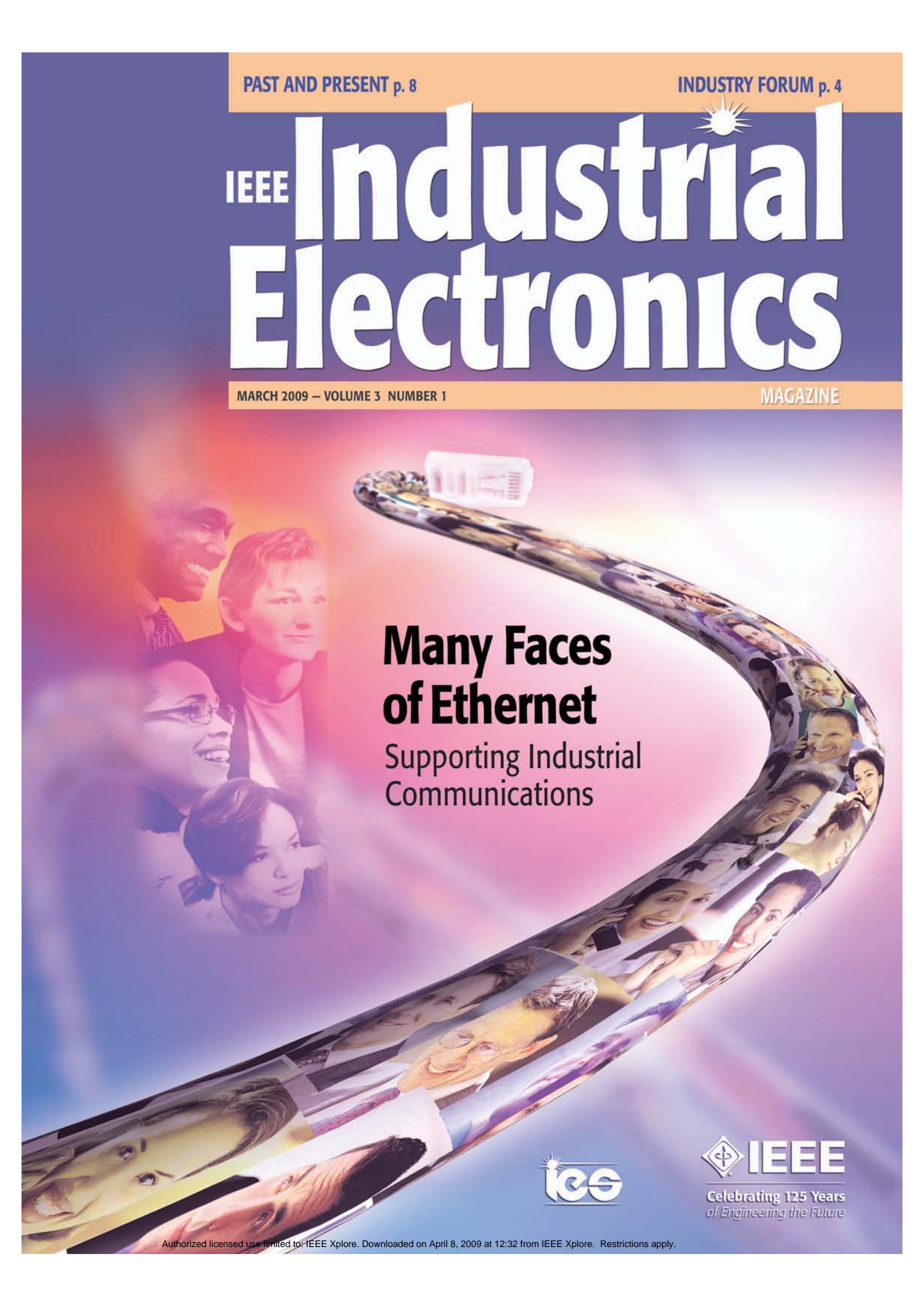
Acknowledgments

The authors gratefully acknowledge the French National Center for Scientific Research (CNRS), the Groupe de Recherche en Electrotechnique et Electronique de Nancy (GREEN: UMR 7037), the Thailand Research Fund (TRF Grant number: MRG5180348), and the Thai-French Innovation Institute (TFII) for supporting this project. The research work was undertaken in the "Franco-Thai Cooperation Program in Higher Education and Research Year: 2009–2011".

References

- [1] R. Toonssen, N. Woudstra, A.H.M. Verkooijen, J. Power Sources 194 (October (1)) (2009) 456–466.
- [2] K. Rajashekara, J. Grieve, D. Daggett, IEEE Ind. Appl. Mag. 14 (July–August (4)) (2008) 54–60.
- [3] N.W. Miller, D. Guru, K. Clark, IEEE Ind. Appl. Mag. 14 (March–April (4)) (2009) 54–61.
- [4] A. Bergen, L. Pitt, A. Rowe, P. Wild, N. Djilali, J. Power Sources 186 (2009) 158-166.
- [5] G.S. Aglietti, S. Redi, A.R. Tatnall, T. Markvart, IEEE Trans. Energy Convers. 24 (June (2)) (2009) 442–451.
- [6] H. Patel, V. Agarwal, IEEE Trans. Energy Convers. 24(March (1)) (2009) 256–263.
- [7] J.R. Salgado, M.A.D. Aguilar, J. Power Sources 186 (2009) 455–463.
- [8] J.P. Mock, S.A. Schmid, J. Power Sources 190 (2009) 133–140.
- [9] P. Thounthong, B. Davat, S. Raël, P. Sethakul, IEEE Ind. Appl. Mag. 15 (July-August (4)) (2009) 52–59.
- [10] P. Corbo, F. Migliardini, O. Veneri, J. Power Sources 181 (July) (2008) 363–370.
- [11] M. Kolhe, IEEE Trans. Energy Convers. 24 (June (2)) (2009) 511–519.
- [12] T. Senjyu, M. Datta, A. Yona, C.H. Kim, IEEE Trans. Energy Convers. 24 (June (2)) (2009) 520–528.
- [13] A.J. del Real, A. Arce, C. Bordons, J. Power Sources 193 (2009) 315–321.
- [14] P. Thounthong, S. Raël, B. Davat, IEEE Trans. Energy Convers. 23 (January (1)) (2008) 148–155.
- [15] N. Kakimoto, H. Satoh, S. Takayama, K. Nakamura, IEEE Trans. Energy Convers. 24 (June (2)) (2009) 465–473.
- [16] A. Cooper, J. Furakawa, L. Lam, M. Kellaway, J. Power Sources 188 (2009) 642–649.
- [17] P. Thounthong, V. Chunkag, P. Sethakul, B. Davat, M. Hinaje, IEEE Trans. Veh. Technol. 58 (8) (Oct. 2009) 3892–3904.
- [18] E. Schaltz, A. Khaligh, P.O. Rasmussen, IEEE Trans. Veh. Technol. 58 (8) (Oct. 2009) 3882–3891.
- [19] J. Bernard, S. Delprat, F.N. Büchi, T.M. Guerra, IEEE Trans. Veh. Technol. 58 (September (7)) (2009) 3168–3176.
- [20] J. Bauman, M. Kazerani, IEEE Trans. Veh. Technol. 58 (September (7)) (2009) 3186–3197.

- [21] P. Thounthong, S. Raël, B. Davat, IEEE Trans. Ind. Electron. 54 (December (6)) (2007) 3225–3233.
- [22] S.J. Chiang, H.J. Shieh, M.C. Chen, IEEE Trans. Ind. Electron. 56 (November (11)) (2009) 4344–4353.
- [23] A.F. Segura, E. Durán, J.M. Andújar, J. Power Sources 193 (2009) 276–284.
- [24] M. Ferraro, F. Sergi, G. Brunaccini, G. Dispenza, L. Andaloro, V. Antonucci, J. Power Sources 193 (2009) 342–348.
- [25] A.E. Auld, J. Brouwer, K.M. Smedley, S. Samuelsen, IEEE Trans. Energy Convers. 24 (September (3)) (2009) 617–625.
- [26] P. Thounthong, S. Raël, IEEE Ind. Electron. Mag. 3 (September (3)) (2009) 25–37.
- [27] Y. Lembeye, V.D. Bang, G. Lefèvre, J.P. Ferrieux, IEEE Trans. Energy Convers. 24 (March (1)) (2009) 203–210.
- [28] S.Y. Choe, J.W. Ahn, J.G. Lee, S.H. Baek, IEEE Trans. Energy Convers. 23 (June (2)) (2008) 669–680.
- [29] P. Thounthong, B. Davat, S. Raël, P. Sethakul, IEEE Ind. Electron. Mag. 3 (March (1)) (2009) 32–46.
- [30] S.M. Muyeen, R. Takahashi, T. Murata, J. Tamura, IEEE Trans. Energy Convers. 24 (September (3)) (2009) 740–749.
- [31] D. Feroldi, M. Serra, J. Riera, J. Power Sources 190 (2009) 387-401.
- [32] A. Payman, S. Pierfederici, F. Meibody-Tabar, Energy Convers. Manage. 49 (June (6)) (2008) 1637–1644.
- [33] P. Thounthong, S. Raël, B. Davat, IEEE Trans. Energy Convers. 24 (March (1)) (2009) 247–255.
- [34] P. Thounthong, S. Raël, B. Davat, J. Power Sources 193 (August (1)) (2009) 376–385.
- [35] R. Nozu, M. Iizuka, M. Nakanishi, M. Kotani, J. Power Sources 186 (2009) 570–579.
- [36] M.A. Danzer, J. Wilhelm, H. Aschemann, E.P. Hofer, J. Power Sources 176 (2008) 515–522.
- [37] H. Aschemann, D. Schindele, IEEE Trans. Ind. Electron. 55 (November (11))
- (2008) 3855–3864.
 [38] A. Gensior, H. Sira-Ramírez, J. Rudolph, H. Güldner, IEEE Trans. Ind. Electron. 56 (February (2)) (2009) 360–370.
- [39] M. Fliess, J. Lévine, Ph. Martin, P. Rouchon, Int. J. Control. 61 (6) (1995) 1327–1361.
- [40] M. Fliess, J. Lévine, Ph. Martin, P. Rouchon, IEEE Trans. Automat. Control. 44 (May (5)) (1999) 922–937.
- (May (3)) (1999) 922–937. [41] C.P. Mudannayake, M.F. Rahman, IEEE Ind. Appl. Mag. 15 (July–August (4))
- (2009) 14–25. [42] S. Lalouni, D. Rekioua, T. Rekioua, E. Matagne, J. Power Sources 193 (2009)
- 899–907. [43] G. Carannante, C. Fraddanno, M. Pagano, L. Piegari, IEEE Trans. Ind. Electron. 56 (November (11)) (2009) 4374–4380.
- (November (11)) (2009) 4473–4430. [44] N. Femia, G. Petrone, G. Spagnuolo, M. Vitelli, IEEE Trans. Ind. Electron. 56 (November (11)) (2009) 4473–4482.
- [45] D.J. Perreault, J.G. Kassakian, IEEE Trans. Circuits Syst. I, Fundam. Theory Appl. 44 (August (8)) (1997) 728–734.
- [46] N. Yousfi-Steiner, Ph. Moçotéguy, D. Candusso, D. Hissel, J. Power Sources 194 (October (1)) (2009) 130–145.
- (October (1)) (2009) 130–145. [47] J. Hasikos, H. Sarimveis, P.L. Zervas, N.C. Markatos, J. Power Sources 193 (August (1)) (2009) 258–268.
- [48] F. Ettingshausen, J. Kleemann, M. Michel, M. Quintus, H. Fuess, C. Roth, J. Power Sources 194 (December (2)) (2009) 899–907.





MARCH 2009 - VOLUME 3 NUMBER 1

Features

Digital Current-Control Schemes

Comparing the Performance of Digital Signal Processor-Based Current Controllers for Three-Phase Active Power Filters Leonardo Rodrigues Limongi, Radu Bojoi, Giovanni Griva, and Alberto Tenconi

32 Fuel Cell High-Power Applications

An Overview of Power Converters for a Clean Energy Conversion Technology Phatiphat Thounthong, Bernard Davat, Stéphane Raël, and Panarit Sethakul

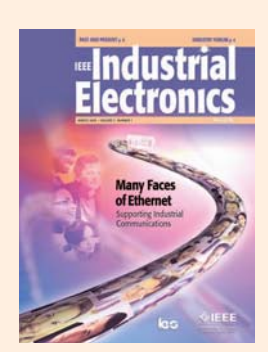
Departments and Columns

- **EDITOR'S COLUMN**
- **MESSAGE FROM THE PRESIDENT**
- **INDUSTRY FORUM**
- 8 PAST AND PRESENT
- **SOCIETY NEWS** 47
- **62 CHAPTER NEWS**
- **EDUCATION NEWS**
- **BOOK NEWS**
- **68 NEW PRODUCTS**
- 69 CALENDAR

SCOPE—IEEE Industrial Electronics Magazine (IEM) publishes peer-reviewed articles that present emerging trends and practices in industrial electronics product research and development, key insights, and tutorial surveys in the field of interest to the membership of the IEEE Industrial Electronics Society (IEEE/IES). IEM will be limited to the scope of the IES, which is given as theory and applications of electronics, controls, communications, instrumentation, and computational intelligence to industrial and manufacturing systems and processes.

IEEE Industrial Electronics Magazine (ISSN 1932-4529) is published quarterly by The Institute of Electrical and Electronics Engineers, Inc. Headquarters: 3 Park Avenue, 17th Floor, New York, NY 10016-5997, USA +1 212 419 7900. Responsibility for the contents rests upon the authors and not upon the IEEE, the Society, or its members. The magazine is a membership benefit of the IEEE Industrial Electronics Society, and subscriptions are included in magazine is a membership benefit of the IEEE Industrial Electronics Society, and subscriptions are included in Society fee. Replacement copies for members are available for \$20 (one copy only). Nonmembers can purchase individual copies for \$53.00. Nonmember subscription prices are available on request. Copyright and Reprint Permissions: Abstracting is permitted with credit to the source. Libraries are permitted to photocopy beyond the limits of the U.S. Copyright law for private use of patrons: 1) those post-1977 articles that carry a code at the bottom of the first page, provided the per-copy fee indicated in the code is paid through the Copyright Clearance Center, 222 Rosewood Drive, Danvers, MA 01970, USA; and 2) pre-1978 articles without fee. For other copying, reprint, or republication permission, write to: Copyrights and Permissions Department, IEEE Service Center, 445 Hoes Lane, Piscataway, NJ 08854 U.S.A. Copyright © 2009 by The Institute of Electrical and Electronics Engineers, Inc. All rights reserved. Periodicals postage paid at New York, NY and at additional mailing offices. Postmaster: Send address changes to IEEE Industrial Electronics Magazine, IEEE, 445 Hoes Lane, Piscataway, NJ 08854 USA. Canadian GST #125634188 Printed in USA

Digital Object Identifier 10.1109/MIE.2009.931893



ON THE COVER: @ DIGITAL VISION & EYEWIRE

EDITOR-IN-CHIEF

Dr. Marco Liserre, Politecnico di Bari, Italy

EDITORIAL BOARD

Prof. Kamal Al-Haddad Ecole de Technologie Superieur, Canada

Prof. Seta Bogosyan — *Educational/Chapter News* University of Alaska Fairbanks, USA

Prof. Bimal K. Bose University of Tennessee, USA

Dr. Chandan Chakraborty Indian Institute of Technology, India

Dr. Michael W. Condry — Industry Forum Intel, USA

Prof. Hiroshi Fujimoto — *New Products* Yokohama National University, Japan

Prof. Okyay Kaynak Bogazici University, Turkey

Prof. Marian Kazmierkowski — Book News Warsaw University of Technology, Poland

Dr. Mariusz Malinowski — Society News Warsaw University of Technology, Poland

Prof. Kouhei Ohnishi Keio University, Japan

Dr. Alberto Pigazo University of Cantabria, Spain

Dr. Thilo Sauter

Austrian Academy of Sciences, Austria

Prof. Bogdan M. (Dan) Wilamowski Auburn University, UŚA

Dr. Richard Zurawski Atut Technology, USA

IEEE PERIODICALS/MAGAZINES DEPARTMENT

Geri Krolin-Taylor Senior Managing Editor Janet Dudar

Senior Art Director

Gail A. Schnitzer Assistant Art Director

Theresa L. Smith

Production Coordinator Susan Schneiderman

Business Development Manager

+1 732 562 3946

Felicia Spagnoli Advertising Production Manager

Peter M. Tuohy

Production Director

Dawn Melley

Editorial Director

Fran Zappulla Staff Director, Publishing Operations

Fuel Cell High-Power Applications

An Overview of Power Converters for a Clean Energy Conversion **Technology**

PHATIPHAT THOUNTHONG, BERNARD DAVAT, STÉPHANE RAËL, and PANARIT SETHAKUL

MARCH 2009

nergy consumption plays an important role in our modern civilization and daily life, which is heavily dependent on burning fossil fuels. The increasing threat of the fast depletion of resources such as petroleum, coal, and natural gas forces people to seek regenerative energy sources, such as solar, wind, geothermal, and hydroelectric energies. Another way of saving valuable natural resources and solving the environmental problem is to develop cleaner and more efficient energy conversion devices. In recent years, fuel cell (FC) research and development have received much attention for their higher energy conversion efficiency and lower or nongreenhousegas emissions than thermal engines in the processes of converting fuel into usable energies [1]-[3]. The power and energy efficiency of an FC is highly dependent on thermodynamics, electrode kinetics, and reactant mass transfer, as well as materials and components for assembling the FC. These factors have been addressed throughout the FC history and are now still the major challenges for FC research and development [4]-[6].

In industry, United Technologies Corporation (UTC) Fuel Cells is involved in FC systems for space and defense applications. UTC Fuel Cells activity began in 1958 and led to the development of the first practical FC application used to generate electrical power and potable water for the Apollo space missions. Since 1966, all of the more than 100 manned U.S. space flights, including the Space Shuttle, have operated with FCs supplied by UTC companies. In 1991, UTC Fuel Cells manufactured its first PureCell 200 power plant, the world's first and only commercial FC power. The Pure-Cell 200 FC produces 200-kW of electricity and 700,000 BTUs of heat. The unit can be powered by natural gas, propane, butane, hydrogen, naphtha, or gases from waste. Since their first flight in 1981, UTC Fuel Cells power plants have provided electric power for more than 100 shuttle missions. They shipped a 50-kW hydrogen-air

FC power plant to the U.S. Department of Energy (DOE) and the Ford Motor Company. In 1998, UTC Fuel Cells delivered a 100-kW methanol power plant, with 40% efficiency, to Nova Bus for installation in a 40-ft, hybrid drive electric bus under a DOE/Georgetown University contract [7], [8].

General Motors is involved in the development of FCs for stationary power as well as the more obvious automotive markets [9]-[11]. In February 2004, they began the first phase of installation operations in Texas at Dow Chemical Company, the largest facility in the world. These FC systems are used to generate 35 MW of electricity [12].

posed approximately 170 years ago when William Robert Grove conceived the first FC in 1839, which produced water and electricity by supplying hydrogen and oxygen into a sulfuric acid bath in the presence of porous platinum electrodes [1]. The process by which this is done is very similar to the electrochemical process by which a battery generates power; at one electrode, a fuel such as hydrogen is oxidized, and at the other electrode an oxidant such as oxygen is reduced. The reactions exchange ions through a solid or liquid electrolyte and electrons through an external circuit, as shown in Figure 1 [15], [16].

Fuel cells produce dc voltage outputs, and they are always connected to electric power networks through power conditioning units such as dc/dc and dc/ac converters.

Axane (France) is also working on FC technology. Three markets that are likely to provide large commercial outlets [13], [14] are:

- portable multiapplication generators (500 W-10 kW)
- stationary applications (more than 10 kW)
- mobile applications for small hybrid vehicles (5-20 kW).

FCs produce dc voltage outputs, and they are always connected to electric power networks through power conditioning units such as dc/dc and dc/ac converters. Power conversion and control functions form the basis of what has come to be known as the field of power electronics. In recent years, power electronics technology has been spurred by needs for efficient control of industrial applications and the development of more reliable lightweight switching power supplies for a sophisticated system. This article reviews the current research of power electronic converters for FC high-power applications.

FC Technology

An FC is a device that converts the chemical energy of a fuel directly to electrical energy. Its concept was pro-

The theoretical value of a single cell voltage of FC is 1.23 V. It is never reached even at no load. At the rated current, the voltage of an elementary cell is about 0.6–0.7 V [17]–[19]. Therefore, an FC is always an assembly of elementary cells that constitute a stack, as Figure 2 depicts.

There are many different types of FCs, with the principal differences between them being the type of electrolyte and/or the type of fuel that they use. For instance, both the phosphoric acid FC (PAFC) and the molten carbonate FC (MCFC) have a liquid electrolyte, whereas a solid oxide FC (SOFC) has a solid, ceramic electrolyte [20]-[22]. A proton exchange or polymer electrolyte membrane FC (PEMFC) and a direct methanol FC (DMFC) may have the same solid polymer electrolyte, but the DMFC uses liquid methanol for fuel whereas the PEMFC uses gaseous hydrogen [23], [24].

Currently, there are three general areas of application for FC technology: portable power, distributed power, and transportation. For each application, it is generally found that one type of FC is better suited than the others to satisfy the requirements of

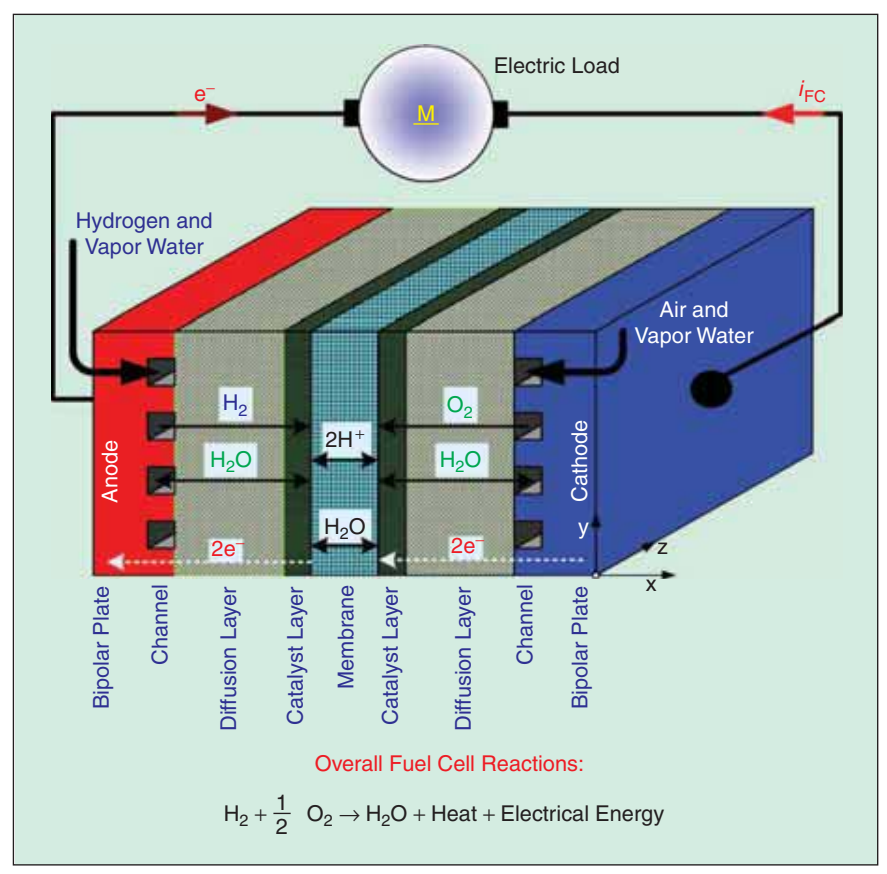


FIGURE 1 - Different layers of an elementary cell of PEMFC.

the application. The DMFCs are attractive for several applications in view of their lower weight and volume. The DMFCs are increasingly being developed to replace or support batteries, mainly for the high energy density of methanol. The DMFCs are promising candidates as portable power sources because they do not require any fuel processing and operate at low temperatures (30–60 °C) [25]–[27]. The SOFC, because of its high pow-

er density and high grade waste heat that may be used in cogeneration applications, is a front-runner in distributed power applications at the industrial level [28]–[31]. The PEMFC has many of the qualities required of an automotive power system including relatively low operating temperature, high power density, and rapid startup [32]–[34]. In addition, PEMFC may also be used in residential and commercial power systems [35].

An FC stack requires fuel, oxidant, and coolant in order to

operate. The composition, pressure, and flow rate of each of these streams must be regulated. In addition, the gases must be humidified and the coolant temperature must be controlled. To achieve this, the FC stack must be surrounded by a fuel system, fuel delivery system, air system, stack cooling system, and humidification system. Once operating, the output power generated by the FCs must be conditioned



FIGURE 2 – An PEMFC (16 cells, 500 W, 50 A, and around 11 V) manufactured by the Centre for Solar Energy and Hydrogen Research Baden-Württemberg (ZSW) Company. It is being functioned at the GREEN laboratory.

and absorbed by a load (converter). Suitable alarms must shut down the process if unsafe operating conditions occur, and a cell voltage monitoring system must monitor FC stack performance. These functions are performed by electrical control systems. As an example, Figure 3 shows a simplified diagram of the PEMFC system. When an FC operates, its fuel (hydrogen and air) flows are controlled by an FC controller, which receives current demand. This current demand is the FC current reference i_{FCREF} (see Figure 3) coming from the energy management controller. The fuel flows must be adjusted to match the reactant delivery rate to the usage rate by the FC controller [36], [37].

FC Characteristics

As mentioned earlier, an FC power source is always connected to the dc bus by a step-up converter. Switching characteristics of the PEMFC (500 W, 40 A) at steady-state when connecting with a boost converter are presented in Figure 4. It can be seen that the PEMFC contains a complex impedance component, which it is not purely resistive at a high switching frequency of 25 kHz [36].

Thounthong et al. [38] (who worked with a 500-W PEMFC system by ZSW Company), Corrêa et al. [39], [40] (who worked with a 500-W Ballard and 500-W Avista PEMFC system), and Zhu et al. [41] (who worked with a 500-W PEMFC system) have demonstrated

that the electrical response time of an FC is generally fast, being mainly associated with the speed at which the chemical reaction is capable of restoring the charge that has been drained by the load. On the other hand, because an FC system is composed of many mechanical devices, the whole FC system has slow transient response and slow output power ramping [42], [43].

For clarity about the FC dynamics, Figure 5 illustrates a Nexa PEMFC system (1.2 kW, 46 A), and Figure 6 depicts the FC voltage response to a current

demand of the Nexa PEMFC stack. The tests operate in two different ways: current step and controlled current slope of $2 \text{ A} \cdot \text{s}^{-1}$. One can scrutinize the voltage drop in Figure 6(a), compared to Figure 6(b), because fuel flows (particularly the delay of air flow) have difficulties following the current step. This characteristic is called fuel starvation phenomenon [1], [44]-[47]. The same kind of FC dynamic responses can be seen in [48]. This condition of operation is evidently dangerous for the FC stack, as already demonstrated by Taniguchi et al. [49]. To utilize the FC in dynamic applications, its current or power slope must be limited, for example, $4 \text{ A} \cdot \text{s}^{-1}$ for a PEMFC (0.5 kW, 12.5 V) [50]; a 2.5 $kW \cdot s^{-1}$ for a PEMFC (40 kW, 70 V) [51]; and 500 $W \cdot s^{-1}$ for a PEMFC (2.5 kW, 22 V) [52].

Therefore, the constraints to operate an FC are as follows:

- The FC power or current must be kept within an interval (rated value, minimum value or zero).
- 2) The FC current must be controlled as a unidirectional current.
- 3) The FC current slope must be limited to a maximum absolute value (for example, 4 A·s⁻¹ [53]), to prevent an FC stack from the fuel starvation phenomenon.
- 4) Switching frequency of the FC current must be greater than 1.25 kHz, and the FC ripple current must be lower than around 5% of rated value, to ensure minor impact to the FC conditions [54], [55].

FC Power Conditioning

The power conditioning system provides regulated dc or ac power appropriate for the application. It is the major component of an FC distributed system. The output of the FC is an unregulated dc voltage (see Figure 6), and it needs to be conditioned in order to be of practical use. The power conditioner section converts the FC power to usable power for different applications. The power conditioning unit also controls electricity's frequency and maintains harmonics to an acceptable level. The purpose of conditioners is to adapt the electrical current from FC to suit the electrical

needs of the application. FC operates giving direct current and at a low voltage; thereby, the step-up (boost) converter (dc/dc converter, named here FC converter) is always selected to adapt the low dc voltage delivered

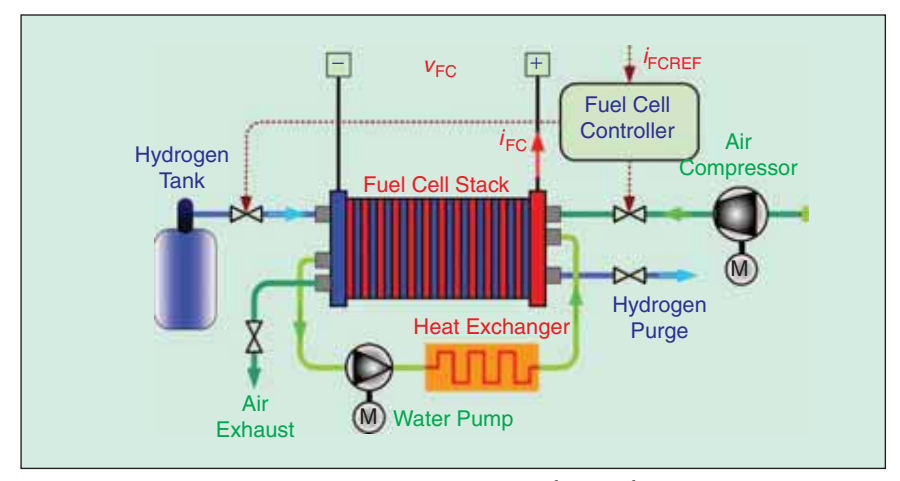


FIGURE 3 – Simplified diagram of the PEMFC system. $v_{\rm FC}$, $i_{\rm FC}$, and $i_{\rm FCREF}$ are the FC voltage, current, and current demand, respectively.

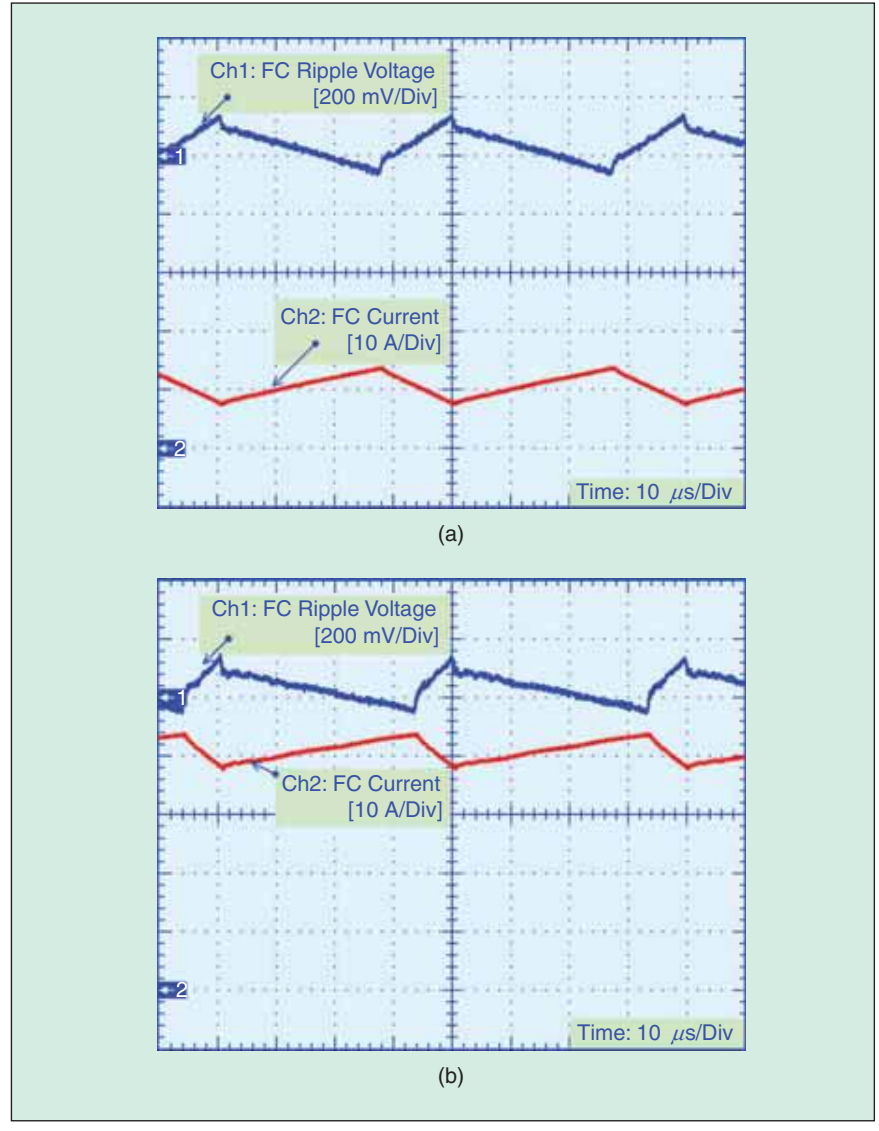


FIGURE 4– Switching characteristics of a 500 W PEMFC of 25 kHz at the FC current supply of (a) 10 A and (b) 40 A (rated current).

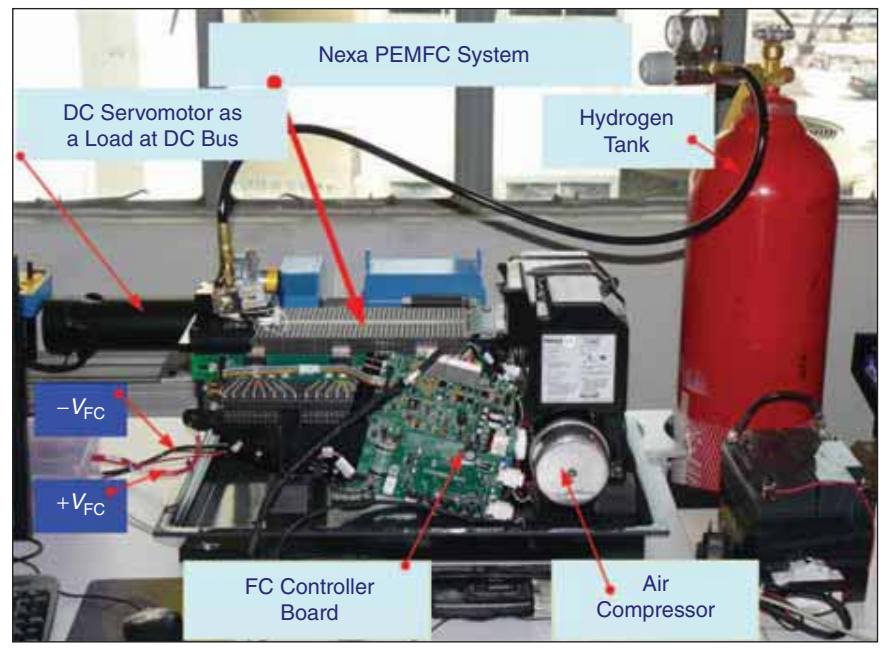


FIGURE 5 - A Nexa PEMFC (1.2 kW, 46 A). It is being functioned at the TFII laboratory.

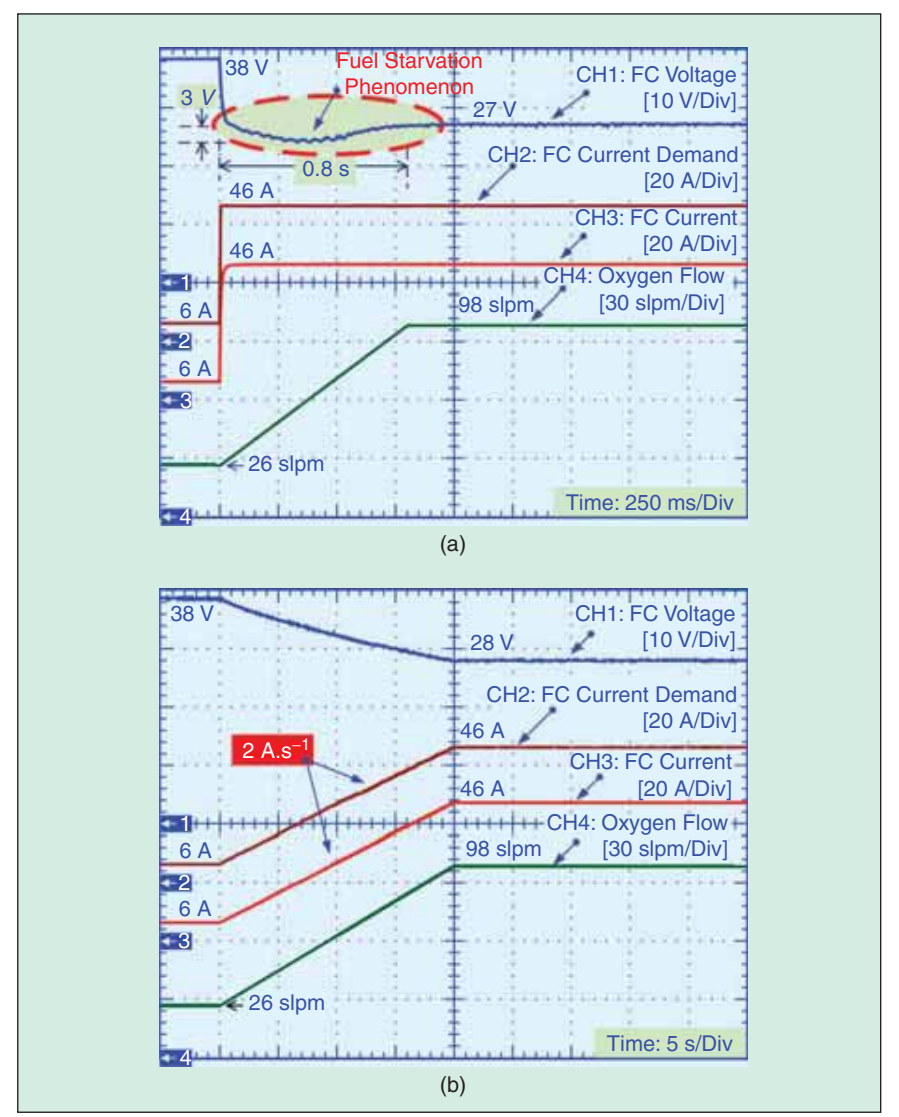


FIGURE 6 – FC dynamic characteristics to (a) current step and (b) controlled current slope of 2 A·s⁻¹.

by the FC to the utility dc bus followed by an inverter (Figure 7) [56]. In general, the load for the boost stage is a filter and the inverter system.

The inverter is used for the interfacing of the FC system to the power grid to provide the grid with voltage/current with proper frequency phase and magnitude where the input for the inverter comes from the boost converter stage and the inverter (with the filter) becomes the load for the boost converter. The power conditioner is also used for the grid connection of the FC. An electrical power-generating system that uses FC as the primary source of electricity generation and is intended to operate synchronously, and in parallel with the electric utility network is a gridconnected FC system [57], [58]. Such systems may also include storage devices and other generating sources and may operate on site loads independent of the utility network during outages.

To employ the FC as a main power source in dynamic applications (such as an electric vehicle [59]-[61] and railway vehicle [62]-[64]), the electrical system must have at least an auxiliary power source (storage device) to improve the dynamic performances of the whole system, when electrical loads at a dc bus demand high power in a short time (for example, vehicle acceleration and deceleration), as portrayed in Figure 8. Moreover, one can take advantage of this auxiliary power source to achieve an actual hybrid source to disassociate mean power sizing from peak transient power sizing, the aim being a reduction in volume and weight, and in the case of FCs used as main energy source, the possibility of regenerative braking [38], [65]. For example, some authors have described the study of the FC/battery hybrid power source [66]-[70] and the FC/supercapacitor hybrid power source [71]-[73].

For the past ten years, much research has been conducted on the utilizations of FCs in high power applications. Today, the required FC power is in the range of $1\,\mathrm{kW}$ to $2\,\mathrm{MW}$:

■ 1–2 kW for unmanned aircrafts [74] and 40–700 kW for manned aircraft [75]–[78]

- 50–100 kW for urban cars [9], [33], [79]-[85]
- 100-200 kW for buses and light trams [7], [86]–[88]
- 600 kW-1 MW for tramways and locomotives [62]-[64], [89]-[92] (for example four motors of 180-kW peak are installed on a tramway, two motors per boggy. The total power installed is 800 kW)
- 480 kW-2 MW for distributed generation systems (grid parallel connection) [8], [93].

To increase the power and voltage levels, several configurations for the FC association can be envisaged as depicted in Figure 9 [93]-[98]. For association of the converter inputs, we can connect several FC in series and then connect them to a converter or each FC to a converter. The FC parallel connection is currently complicated because of complexity of controlling the output power distribution in each FC. For association of converter outputs, the output of a converter can be connected in series for a high output voltage or in parallel for a low output voltage.

FC Power Converter

Different power converter topologies can be used for the power electronic interface between the FC and the utility dc bus. For the dc link

A large research effort is underway to develop the FC for applications ranging from small portable electronic devices to automotive transport, as well as residential combined heat and power supplies.

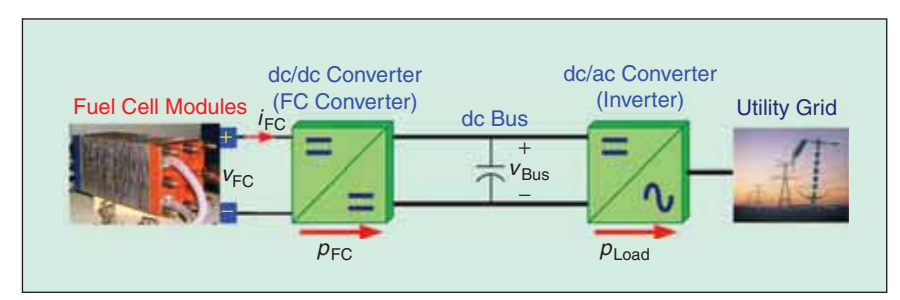


FIGURE 7 – FC power system.

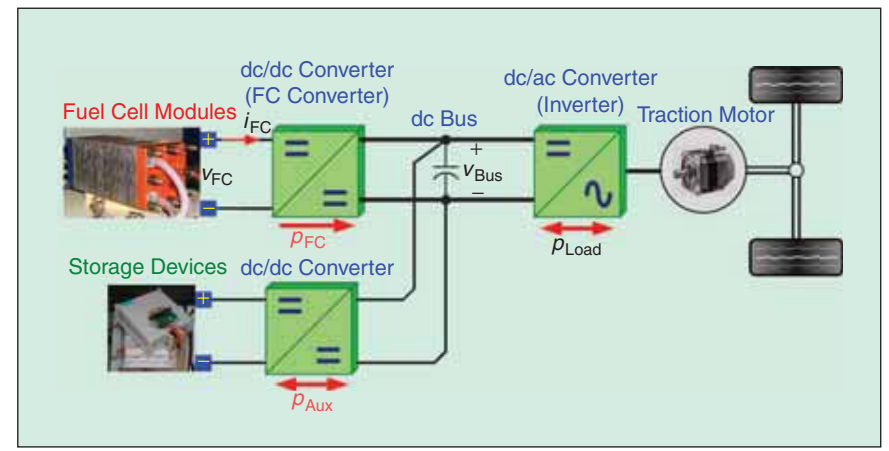


FIGURE 8 - Fuel cell powered vehicle.

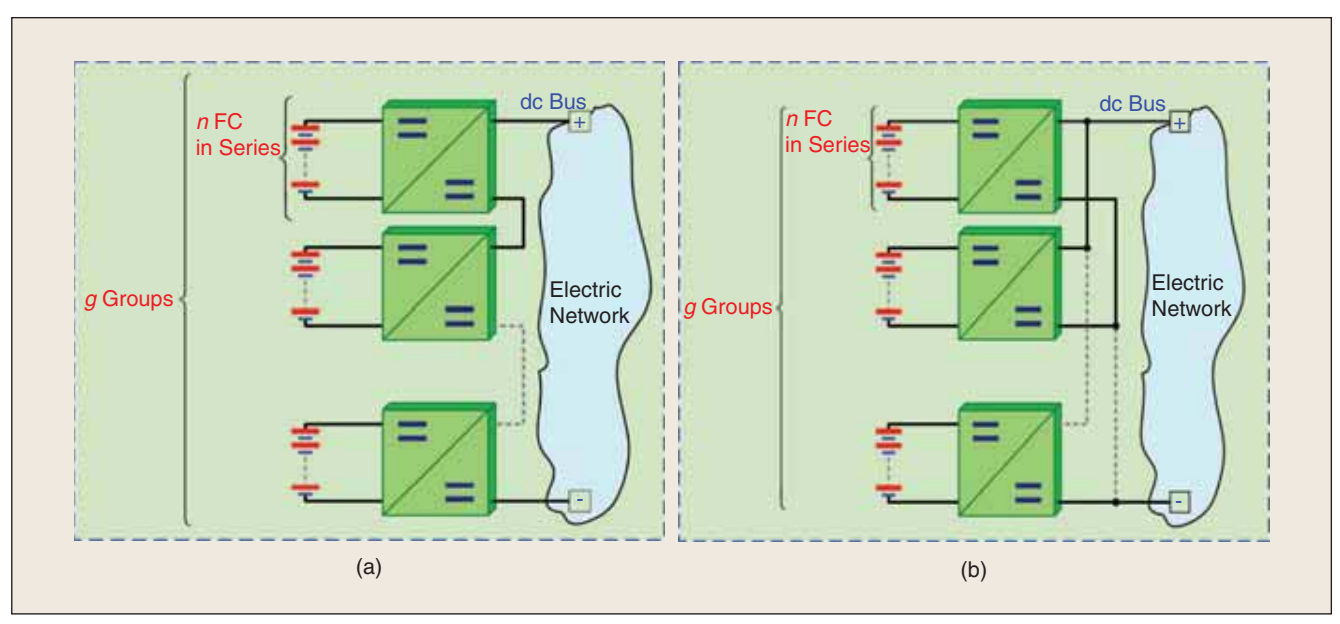


FIGURE 9 - Modular stack FC architectures connected to the dc bus: (a) output connected in series and (b) output connected parallel. n: number of FC in series in each group, g: number of FC-converter groups.

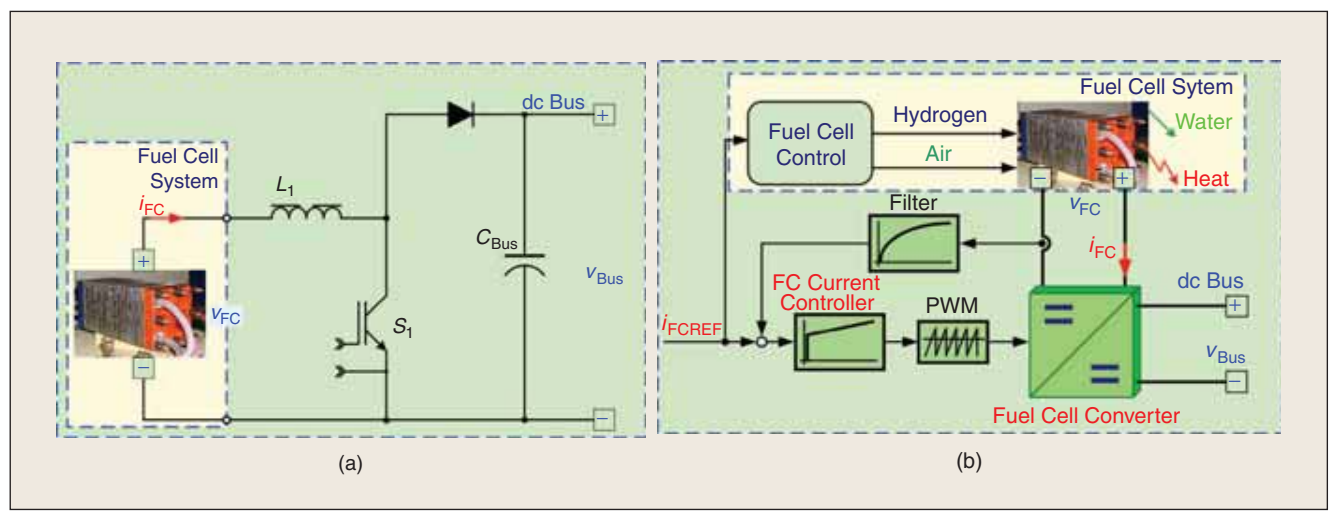


FIGURE 10 - Classical fuel cell boost converter: (a) power circuit and (b) FC current regulation loop.

voltage level, it is depending on its applications:

- 270 V or 350 V for the standard on the all-electric aircraft [78]
- 48 V [99], 120 V [100], or 400–480 V [30], [93], [101] for stand-alone or parallel grid connections
- 42 V (PowerNet) a new standard voltage for automobile systems [34], [102], [103]
- 270–540 V for electric (FC) vehicles [60], [65], [82]
- 350 V (transit bus systems) to 750 V (tramway and locomotive systems) [7], [63], [64], [87], [89]–[92], [104]. Basically, low-voltage, high-current structures are needed because of the FC electrical characteristics. A classical boost converter is often selected as an FC converter [38], [93], [99]–[101],

[105]-[107], because it can be operated in the current control mode in a continuous condition mode, as portrayed in Figure 10. Then, one does not need a blocking diode and passive filter between an FC and a converter. Based on the load conditions, the boost converter can be commanded to draw a specific amount of current from the FC with a ripple well defined by the frequency, size of the inductor, and duty ratio. The FC boost converter sizes of 0.5 kW [38]; 1 kW [100], [101], [105]; 5 kW [99]; 27 kW [106]; and 50 kW [93] have been studied. However, a classical boost converter will be limited when the power increases or for higher step-up ratios. In that way, the use of paralleling power converters with interleaved technique may offer some better performances.

Fuel Cell i_{FC} i_{L_1} i_{L_1} i_{D_1} $i_{C_{Bus}}$ i_{C_{B

Module 1

FIGURE 11 – Multiphase paralleled step-up converters for FC high-power applications.

Parallel Power Converter with Interleaved Switching Algorithm

The subject of paralleling power converters was on the sideline of design engineering tasks for decades. Latest efforts in standardization, miniaturization, and the proliferation of high current, low voltage power supplies have directed additional attention to various techniques to parallel power modules. The fundamental difficulty using parallel power processing circuits is to ensure that the load current is properly distributed among the parallel connected power modules. Only then can the design be optimized for the highest

reliability and lowest cost by ensuring equal temperature rise and by minimizing the power rating of the individual components.

The major problems of using a single dc/dc converter connected with FC in high power applications are as follows:

- difficulty of the design of magnetic component: ferrite core and Litz-
- high FC ripple current, which may lead to reduce its stack lifetime.

Therefore, by paralleling converters with interleaving technique, these problems can be avoided [108]-[111]. A high-power dc distributed power system supplied by FC invokes the need to parallel power modules with interleaving technique. Active ripple cancellation methods can yield even higher performance. Today, the active method of interleaving is well known [94], [96], [98]. In the interleaving method, the modules operate at the same switching frequency. Their switching waveforms are displaced in phase over a switching period with respect to one another by $2\pi/N$ radians, with *N* being the number of converters in parallel. It is important to note here that, according to [54] and [55], a high FC current ripple plays an important role in its catalyst lifetime. Especially,

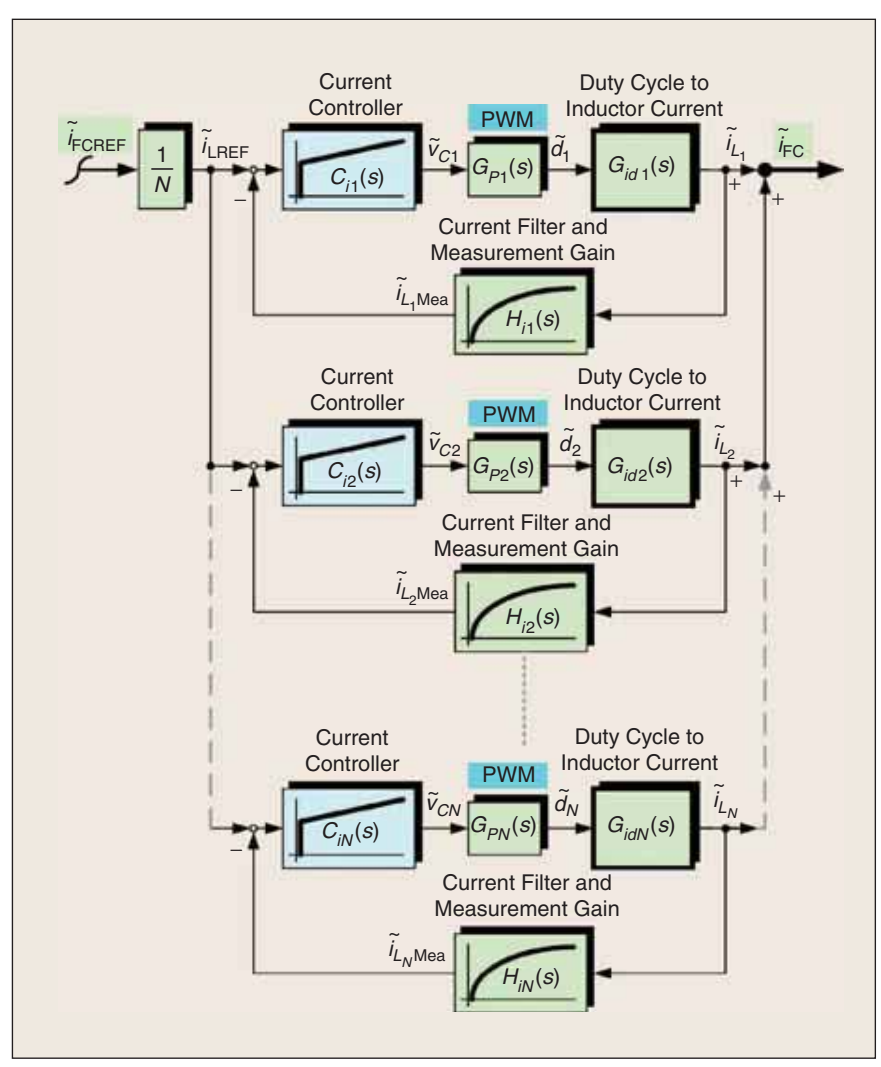


FIGURE 12 – Current sharing technique of N-phase parallel modules (here, boost converters).

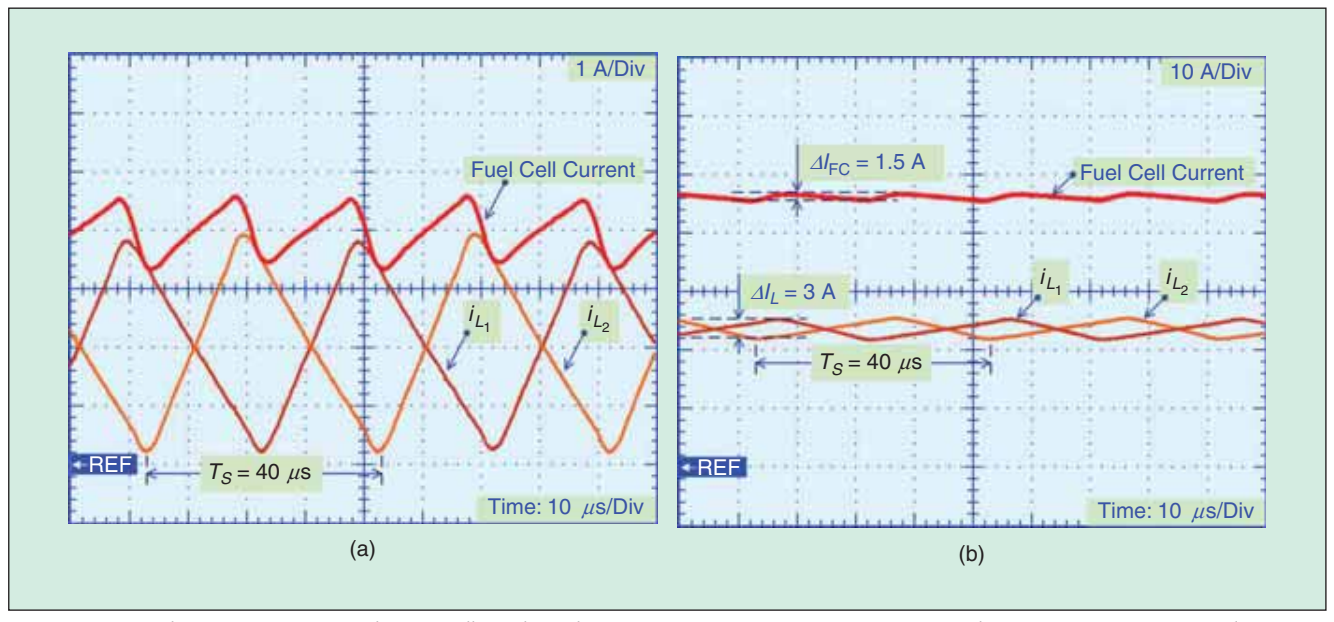


FIGURE 13 – Steady-state waveforms of the two-cell interleaved converter system at an FC current command of (a) 4 A ($v_{FC} = 35.8 \text{ V}$) and (b) 46 A rated current ($v_{FC} = 26.3 \text{ V}$).

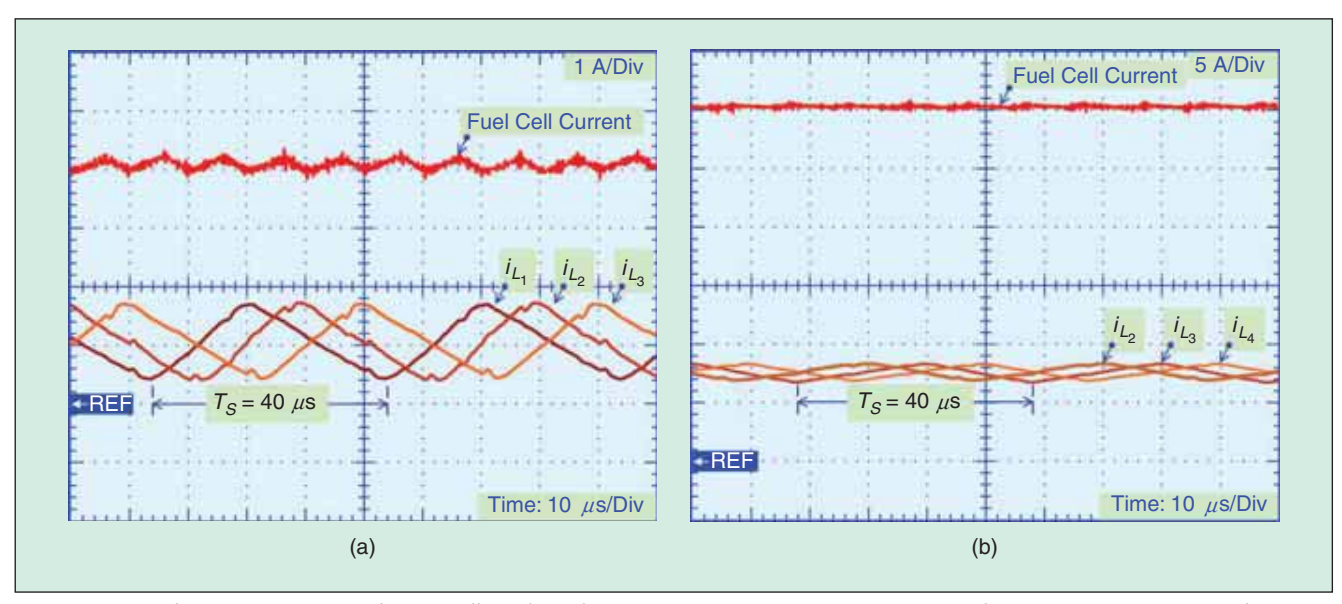


FIGURE 14 – Steady-state waveforms of the four-cell interleaved converter system at an FC current command of (a) 4 A ($v_{FC} = 35.8 \text{ V}$) and (b) 30 A ($v_{FC} = 28.9 \text{ V}$).

sharp current rise/fall and large magnitude of current ripple should be avoided. The multiphase parallel converters

for FC high-power applications are depicted in Figure 11.

The most sophisticated and most accurate current sharing implementations rely on a closed loop

negative feedback system, very similar to those control loops used to regulate

the output voltage of a power supply, as portrayed in Figure 12 [112], [113]. To make this approach work, two piec-

There are three general areas of application for FC technology: portable power, distributed power, and transportation.

es of information must be available in the system. One is the actual inductor currents of the modules and the other is the desired amount of FC current reference $i_{\rm FCREF}$. Since the goal is

to evenly distribute the FC current, the desired FC current is the FC current divided by the number of parallel modules. Therefore the task is two fold; measure

the inductor currents and generate the average inductor current set-points.

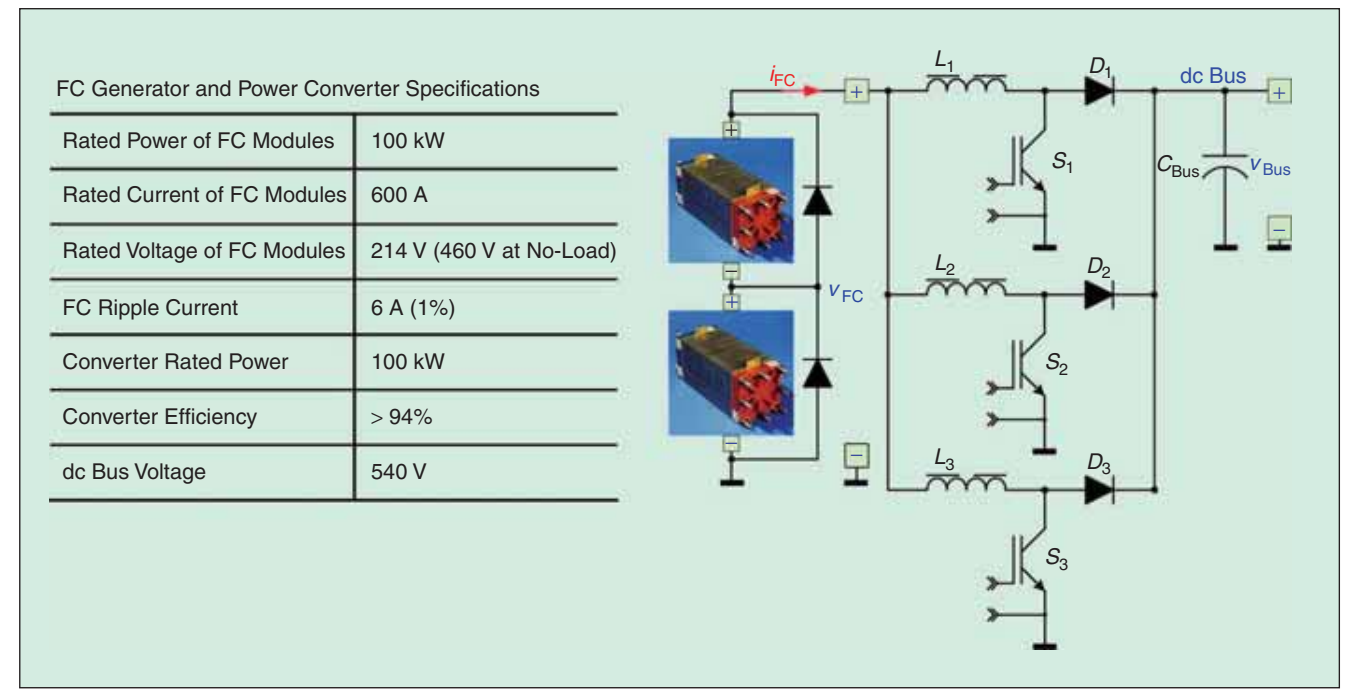


FIGURE 15 - 100-kW FC converter of three-phase interleaved boost converters with two FC modules in series [98].

According to Thounthong et al. [114], [115], who worked with a Ballard Nexa PEMFC unit (1.2-kW, 46-A, see Figure 5), they have already demonstrated the experimental results of the two- and four-phase paralleled boost converters for FC applications. The oscilloscope waveforms in Figures 13 and 14 portray the steady-state characteristics of the interleaved converters at different FC current demands. the load at dc bus being adjusted in order to obtain a constant dc bus voltage of 60 V (here rated value). Figure 13 illustrates the FC current, and the first and the second inductor currents of the two-phase parallel converter at the average FC current reference of 4 A and 46 A (rated current), respectively [114]. Figure 14(a) presents the FC current and the first, second, and third inductor currents of the four-phase parallel converters at the average FC current reference of 4 A. For the last test, Figure 14(b) shows the FC current and the second, third, and fourth inductor currents of the 4-phase parallel converters at the average FC current reference of 30 A [115].

One can observe again that the FC current is the sum of the inductor currents and that the FC ripple current is 1/N the individual inductor ripple currents. Absolutely, the FC ripple current of the four-cell interleaved converter is lower than the two-cell interleaved converter. So, the FC ripple current of

The PEMFC is well suited to automotive power applications and may be used in residential and commercial power systems.

the four-cell interleaved converter is nearly zero. It means that the FC mean current is close to the FC rms current. In addition, it can be seen the FC ripple frequency is *N*-times the switching frequency of 25 kHz.

According to Hwang et al. [116], an FC converter size of 1 kW with fourphase interleaved boost cells had been also presented. For an FC converter size of 150 kW (technical specification:

 $V_{\mathrm{FC}} = 250\text{--}450 \ \mathrm{V}, \ V_{\mathrm{Bus}} = 548 \ \mathrm{V}, \ \mathrm{weigh}$ 50 kg) with two-phase interleaved boost converters had been fabricated and tested [117]. Its volume and weight is less than one third of a single phase boost converter, the FC ripple current is less than 10%, and its efficiency is over 97%. According to Vulturescu et al. [98], the design of an FC converter size of 100 kW with three-phase interleaved boost converters with two

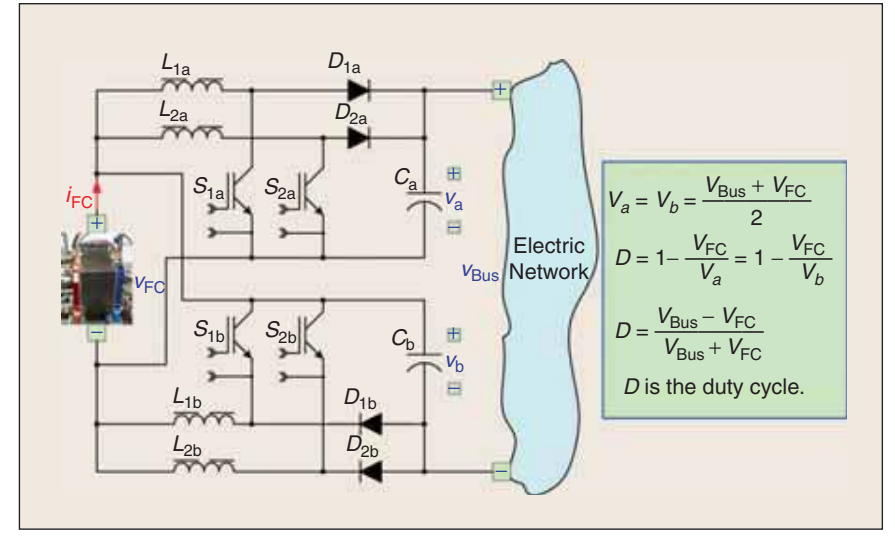


FIGURE 16 - 120-kW two-blanches interleaved double dual boost converters [96].

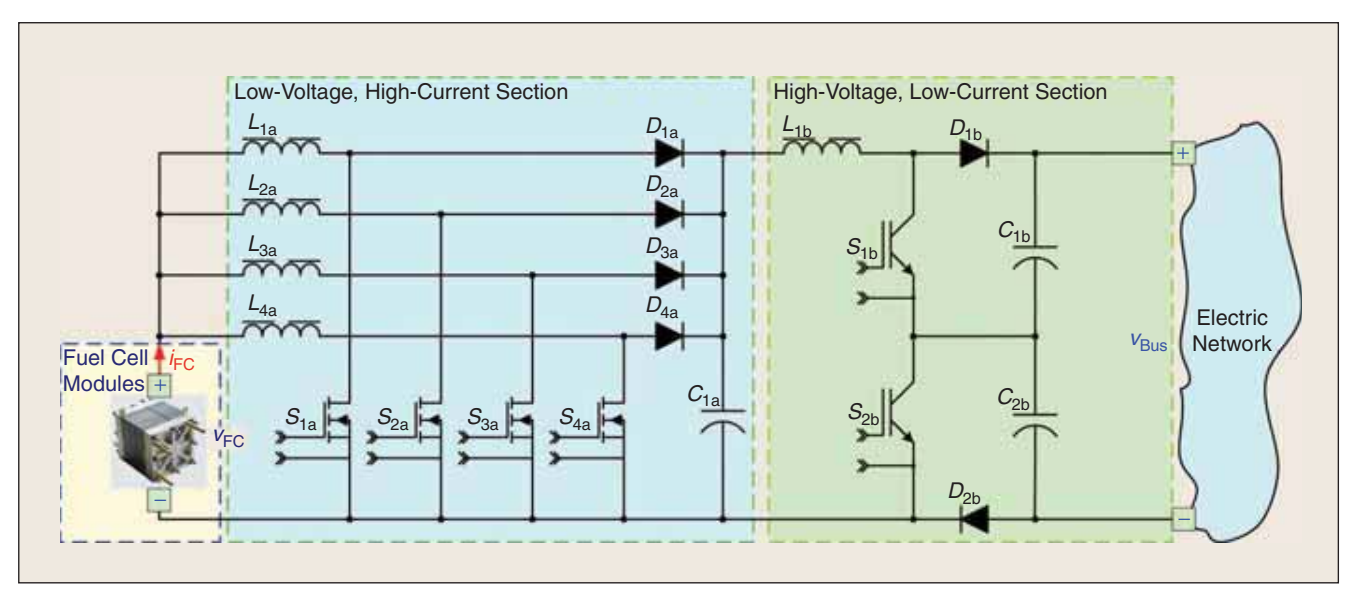


FIGURE 17 – 200-kW cascade-parallel boost converter for the FC power converter.

FCs hold great promise as a clean energy conversion technology.

FC modules in series has been studied for French urban transportation networks, as depicted in Figure 15. In addition, a three-phase interleaved boost modules based on the commercial standard Lopak5 of insulated gate bipolar transistors (IGBTs) by Asea Brown Boveri Ltd. (ABB) for 250–1,000-kW FC converter at the dc link voltage

of 750 V has been proposed in [118]. For the FC urban car, the 94-kW FC converter with the multiphase interleaved boost converters at the dc link voltage of 320 V had been designed and used in the HydroGen3 FC vehicle of General Motors (GM) Company [119].

To increase the higher voltage conversion ratio, Viet et al. [96] have

proposed the two-blanches interleaved double dual (IDD) boost converters for an FC converter: 20–120 kW, as shown in Figure 16. One summarizes that this scheme can boost the FC input voltage from 60–700 V utility dc bus at the FC current of 333 A (20 kW).

Another possibility to increase the voltage conversion ratio of the FC high-power converter is cascade-parallel boost converter, as Figure 17 illustrates. This similar concept has been proposed in [120]–[122]. One might suppose that this power converter can

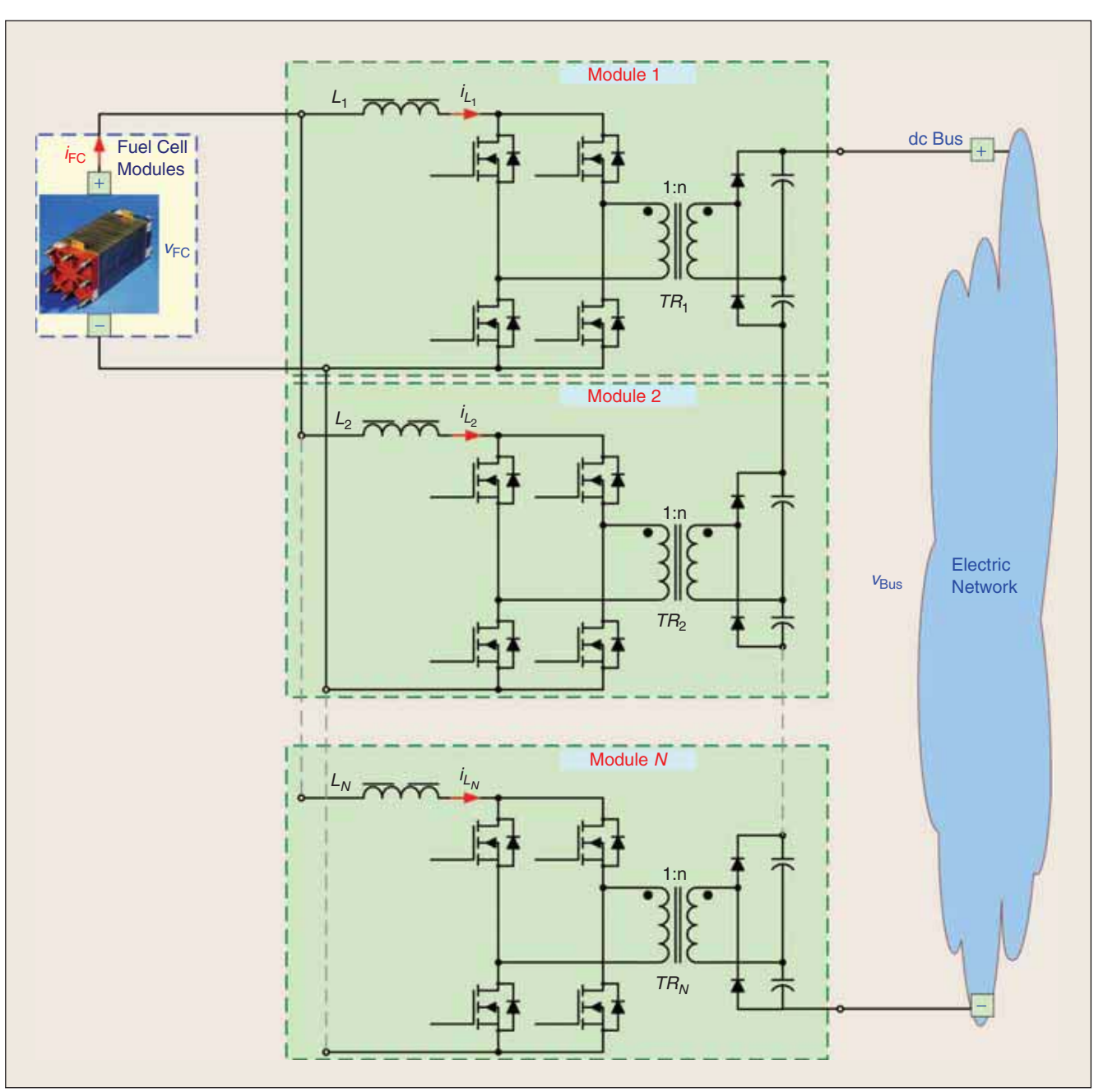


FIGURE 18 – Interleaved current-fed full bridge converters with a parallel input and a series output for FC high power applications.

operate up to 200 kW with the voltage conversion ratio of eight.

For ground isolation and high voltage step-up ratio (but more complicated), interleaved boost/flyback [123], [124], push-pull [125]–[127], and half bridge and full bridge [128]–[132] can be considered as candidate topologies for the FC converter. Advantages and disadvantages of these converters are discussed in [127], [128], and [132]. The most popular ground isolation circuit today for high-power applications is the full-bridge dc/dc converter, because of reasonable device voltage ratings and soft switching possibility [133], [134].

Considering the ripple and direct current control requirement, an isolated current-fed full bridge converter topology shows some promise [134]-[136]. It has small current ripple and high efficiency. To reduce the size of the magnetic components and further improve the converter efficiency, a multiphase interleaved current-fed full-bridge converter is proposed in [113], as shown in Figure 18. By paralleling input of the converter system, input current, and hence the power, can be equally shared between the modules of the converter system. Therefore, current stress on the semiconductor devices on the input side is reduced. On the other hand, the series connection on the output side results in lower voltage ratings for output capacitors and diodes. Furthermore, phase shifted pulse-width modulation (PWM) is used for the interleaved full-bridge converter. So, the input current ripple frequency and the output voltage ripple frequency increase. Hence, for the same input current and output voltage ripple requirement, smaller input inductors and output capacitors can be used.

The advantages of the parallel converter with interleaving technique are as follows:

- Size and volume of passive devices (inductor and capacitor) are reduced.
- 2) Ripple of the input and output waveforms are reduced.
- 3) Ripple frequency of the input and output waveforms are increased
- Power converter is modular. It enhances reliability of the system, and increases converter power

The power and energy efficiency of an FC is highly dependent on the thermodynamics, electrode kinectics, and reactant mass transfer, as well as materials and components for assembling the FC.

rating by paralleling phases, not by paralleling multiple devices.

- 5) Thermal management is simple. The primary driver in all paralleling schemes for lower power applications is the decentralized heat dissipation of the parallel power converters.
- 6) Current ratings of power electronic components are reduced, because current ratings are proportional to the continuous power rating of the circuit.

Conclusions

FCs hold great promise as a clean energy conversion technology. A large research effort is underway to develop the FC for applications ranging from small portable electronic devices to automotive transport, as well as residential combined heat and power supplies. These applications have a large emerging market and widespread adoption should lead to a reduced dependence on fossil fuels as well as encourage the development of a hydrogen economy.

FCs produce low dc voltage, so that it is most often connected to electric networks through a step-up dc/dc converter. This article first introduces electrical characteristics, power electronic requirements, and different types of FCs and is then followed by a discussion of the various topologies of step-up dc/dc converters used for FCs' power-conditioning system. The examinations of several different approaches to power-conditioning systems for single and multiple FC combinations have been reviewed.

High-power dc distributed power systems supplied by FC invokes the need to parallel power modules with interleaving technique. By method of the parallel converter modules with interleaving algorithm for an FC generator for high-power applications, inductor size (ferrite core and Litzwire) are simple to design and fabricate, and the FC ripple current can be virtually reduced to zero. As a result, the FC mean current is nearly equal to the FC rms current. The main drawback of the multiphase approach is added circuit complexity, requiring measurement and balancing of each phase current as the larger number of control components illustrates.

Acknowledgments

Based on research carried out over several years, some work in the reviewed article were supported in part by the French National Center for Scientific Research (CNRS), the Nancy Research Group in Electrical Engineering (GREEN: UMR 7037), Thai-French Innovation Institute (TFII), King Mongkut's University of Technology North Bangkok (KMUTNB), and the Thailand Research Fund (TRF) under Grant MRG5180348.

Biographies

Phatiphat Thounthong received the B.S. and M.E. degrees in electrical engineering from King Mongkut's Institute of Technology North Bangkok, Thailand, in 1996 and 2001, respectively, and the Ph.D. degree in electrical engineering from Institut National Polytechnique de Lorraine (INPL), Nancy, France, in 2005. From 1998 to 2002, he was an assistant lecturer at King Mongkut's University of Technology North Bangkok, where he is currently a lecturer. He has published more than 30 papers in international journals, refereed conferences, and two book chapters. His current research interests include power electronics, electric drives, and electrical devices (fuel cells, batteries, and supercapacitor).

There are many different types of FCs, with the principal differences between them being the type of electrolyte and/or the type of fuel that they use.

Bernard Davat received the engineering degree from Ecole Nationale Supérieure d'Electrotechnique, d'Electronique, d'Informatique, d'Hydraulique et des Telecommunications (ENSEEIHT), Toulouse, France, in 1975, and the Ph.D. and Docteur d'Etat degrees in electrical engineering from Institut National Polytechnique de Toulouse (INPT), Toulouse, in 1978 and 1984, respectively. Since 1988, he has been a professor INPL. He is the author of Power Semiconductor Converters and has published more than 50 papers in international journals and refereed conferences. His research interests include power electronics, drives, and new electrical devices (fuel cells, batteries, and supercapacitor). He is a Member of the IEEE.

Stéphane Raël received the M.E. degree in electrical engineering from the Ecole Nationale Supérieure des Ingénieurs Electriciens de Grenoble, Grenoble, France, in 1992 and the Ph.D. degree in electrical engineering from the Institut National Polytechnique de Grenoble (INPG), Grenoble, France, in 1996. He is a professor at the Institut National Polytechnique de Lorraine (INPL), Nancy, France. His research interests include power electronic components, supercapacitor, batteries, and fuel cells.

Panarit Sethakul received the B.S. and M.S. degrees in electrical engineering from King Mongkut's University of Technology North Bangkok, Thailand, in 1979 and 1982, respectively, and the Dipl.-Ing. from the University of Wuppertal, Germany in 1986. Since 2005, he has been an assistant professor at King Mongkut's University of Technology North Bangkok. He is currently a director of the Thai-French Innovation Institute (TFII),

Bangkok, Thailand. His research interests are electrical machine drives and power electronics.

References

- [1] P. Thounthong, B. Davat, and S. Raël, "Drive friendly," *IEEE Power Energy Mag.*, vol. 6, no. 1, pp. 69–76, 2008.
- [2] M. C. Péra, D. Candusso, D. Hissel, and J. M. Kauffmann, "Power generation by fuel cells," *IEEE Ind. Electron. Mag.*, vol. 1, no. 3, pp. 28–37, 2007
- [3] M. Tekin, D. Hissel, M. C. Péra, and J. M. Kauff-mann, "Energy-management strategy for embedded fuel-cell systems using fuzzy logic," *IEEE Trans. Ind. Electron.*, vol. 54, pp. 595–603, Feb. 2007.
- [4] W. Schmittinger and A. Vahidi, "A review of the main parameters influencing long-term performance and durability of PEM fuel cells," J. Power Sources, vol. 180, pp. 1–4, May 2008.
- [5] C. Casati, P. Longhi, L. Zanderighi, and F. Bianchi, "Some fundamental aspects in electrochemical hydrogen purification/compression," *J. Power Sources*, vol. 180, pp. 103–113, May 2008.
- [6] C. Kim, K. J. Kim, and M. Y. Ha, "Performance enhancement of a direct borohydride fuel cell in practical running conditions," *J. Power Sources*, vol. 180, pp. 154–161, May 2008.
- [7] S. Varigonda and M. Kamat, "Control of stationary and transportation fuel cell systems: Progress and opportunities," *Comput. Chem. Eng.*, vol. 30, pp. 1735–1748, Sept. 2006.
- [8] Y. Kishinevsky and S. Zelingher, "Coming clean with fuel cells," *IEEE Power Energy Mag.*, vol. 1, pp. 20–25, Nov./Dec. 2003.
- [9] R. von Helmolt and U. Eberle, "Fuel cell vehicles: Status 2007," *J. Power Sources*, vol. 165, pp. 833–843, Mar. 2007.
- [10] V. P. McConnell, "Downsized footprint and material changes for GM's fourth-generation fuel cell technology," *Fuel Cells Bull.*, vol. 2007, pp. 12–15, Jan. 2007.
- [11] K. Bonhoff, "The clean energy partnership Berlin-CEP," J. Power Sources, vol. 181, pp. 350– 352, July 2008.
- [12] General Motors Corporation. Dow—GM Make World's First Significant Fuel Cell Application a Reality [Online]. Available: http://www. gm.com/company/gmability/adv_tech/500_ stationary
- [13] D. Lecocq, "Tomorrow's energy today with Axane," Fuel Cells Bull., vol. 2004, pp. 13–15, Mar. 2004
- [14] Axane Company. Axane: Products [Online]. Available: http://www.axane.fr/axane/ gb/produits/evopac/concept.html
- [15] R. J. Wai, C. Y. Lin, R.Y. Duan, and Y. R. Chang, "High-efficiency dc-dc converter with high voltage gain and reduced switch stress," *IEEE Trans. Ind. Electron.*, vol. 54, pp. 354–364, Feb. 2007.
- [16] S. Y. Choe, J. W. Ahn, J. G. Lee, and S. H. Baek, "Dynamic simulator for a PEM fuel cell system

- with a PWM dc/dc converter," *IEEE Trans. Energy Conversion*, vol. 23, pp. 669–680, June 2008
- [17] I. Sadli, P. Thounthong, J. P. Martin, S. Raël, and B. Davat, "Behaviour of a PEMFC supplying a low voltage static converter," *J. Power Sources*, vol. 156, pp. 119–125, May 2006.
- [18] S. C. Page, A. H. Anbuky, S. P. Krumdieck, and J. Brouwer, "Test method and equivalent circuit modeling of a PEM fuel cell in a passive state," *IEEE Trans. Energy Conversion*, vol. 22, pp. 764–773, Sept. 2007.
- [19] S. Pasricha, M. Keppler, S. R. Shaw, and M. H. Nehrir, "Comparison and identification of static electrical terminal fuel cell models," *IEEE Trans. Energy Conversion*, vol. 22, pp. 746–754, Sept. 2007.
- [20] S. R. Choudhury and R. Rengaswamy, "Characterization and fault diagnosis of PAFC cathode by EIS technique and a novel mathematical model approach," *J. Power Sources*, vol. 161, pp. 971–986, Oct. 2006.
- [21] C. Wang and M. H. Nehrir, "A physically based dynamic model for solid oxide fuel cells," *IEEE Trans. Energy Conversion*, vol. 22, pp. 887–897, Dec. 2007.
- [22] M. Suzuki, N. Shikazono, K. Fukagata, and N. Kasagi, "Numerical analysis of coupled transport and reaction phenomena in an anode-supported flat-tube solid oxide fuel cell," J. Power Sources, vol. 180, pp. 29–40, May 2008.
- [23] D. H. Ko, M. J. Lee, W. H. Jang, and U. Krewer, "Non-isothermal dynamic modelling and optimization of a direct methanol fuel cell," J. Power Sources, vol. 180, pp. 71–83, May 2008.
- [24] M. Paquin and L. G. Fréchette, "Understanding cathode flooding and dry-out for water management in air breathing PEM fuel cells," *J. Power Sources*, vol. 180, pp. 440–451, May 2008.
- [25] U. A. Icardi, S. Specchia, G. J. R. Fontana, G. Saracco, and V. Specchia, "Compact direct methanol fuel cells for portable application," *J. Power Sources*, vol. 176, pp. 460–467, Feb. 2008.
- [26] J. Y. Park, J. H. Lee, J. Kim, S. Han, and I. Song, "Stable operation of air-blowing direct methanol fuel cells with high performance," *J. Power Sources*, vol. 179, pp. 1–8, Apr. 2008.
- [27] S. K. Kamarudin, W. R. W. Daud, S. L. Ho, and U. A. Hasran, "Overview on the challenges and developments of micro-direct methanol fuel cells (DMFC)," J. Power Sources, vol. 163, pp. 743–754, Jan. 2007.
- [28] P. C. Buddingh, V. Scaini, and L. F. Casey, "Utilizing waste hydrogen for energy recovery using fuel cells and associated technologies," *IEEE Trans. Ind. Applicat.*, vol. 42, pp. 186–194, Jan./Feb. 2006.
- [29] K. Sedghisigarchi and A. Feliachi, "Impact of fuel cells on load-frequency control in power distribution systems," *IEEE Trans. Energy Con*version, vol. 21, pp. 250–256, Mar. 2006.
- [30] J. Lee, J. Jo, S. Choi, and S. B. Han, "A 10-kW SOFC low-voltage battery hybrid power conditioning system for residential use," *IEEE Trans. Energy Conversion*, vol. 21, pp. 575–585, June 2006.
- [31] Y. H. Li, S. S. Choi, and S. Rajakaruna, "An analysis of the control and operation of a solid oxide fuel-cell power plant in an isolated system," *IEEE Trans. Energy Conversion*, vol. 20, pp. 381–387, June 2005.
- [32] P. Corbo, F. Migliardini, and O. Veneri, "An experimental study of a PEM fuel cell power train for urban bus application," *J. Power Sources*, vol. 181, pp. 363–370, July 2008.
- [33] W. Mitchell, B. J. Bowers, C. Garnier, and F. Boudjemaa, "Dynamic behavior of gasoline fuel cell electric vehicles," *J. Power Sources*, vol. 154, pp. 489–496, Mar. 2006.

- [34] A. Emadi, Y. J. Lee, and K. Rajashekara, "Power electronics and motor drives in electric, hybrid electric, and plug-in hybrid electric vehicles, IEEE Trans. Ind. Electron., vol. 55, pp. 2237-2245,
- [35] M. H. Nehrir, C. Wang, and S. R. Shaw, "Fuel cells: promising devices for distributed generation," IEEE Power Energy Mag., vol. 4, pp. 47-53, Jan./Feb. 2006.
- [36] P. Thounthong, S. Raël, and B. Davat, "Test of a PEM fuel cell with low voltage static converter," J. Power Sources, vol. 153, pp. 145-150, Jan.
- [37] P. T. Krein, R. S. Balog, and X. Geng, "Highfrequency link inverter for fuel cells based on multiple-carrier PWM," IEEE Trans. Power Electron., vol. 19, pp. 1279-1288, Sept. 2004.
- [38] P. Thounthong, S. Raël, and B. Davat, "Control strategy of fuel cell and supercapacitors association for distributed generation system, IEEE Trans. Ind. Electron., vol. 54, pp. 3225-3233, Dec. 2007.
- [39] J. M. Corrêa, F. A. Farret, L. N. Canha, and M. G. Simões, "An electrochemical-based fuel-cell model suitable for electrical engineering automation approach," IEEE Trans. Ind. Electron., vol. 51, pp. 1103-1112, Oct. 2004.
- [40] J. M. Corrêa, F. A. Farret, V. A. Popov, and M. G. Simões. "Sensitivity analysis of the modeling s used in simulation of proton exchange membrane fuel cells," IEEE Trans. Energy Conversion, vol. 20, pp. 211-218, Jan./ Mar. 2005.
- [41] T. Zhu, S. R. Shaw, and S. B. Leeb, "Transient recognition control for hybrid fuel cell systems," IEEE Trans. Energy Conversion, vol. 21, pp. 195-201, Mar. 2006.
- [42] F. Jurado, "Novel fuzzy flux control for fuel-cell inverters," IEEE Trans. Ind. Electron., vol. 52, no. 6, pp. 1707-1710, Dec. 2005.
- [43] C. Wang and M. H. Nehrir, "Load transient mitigation for stand-alone fuel cell power generation systems," IEEE Trans. Energy Conversion, vol. 22, pp. 864-872, Dec. 2007.
- [44] P. Thounthong, S. Raël, and B. Davat, "DC bus voltage regulation supplied by fuel cell/ supercapacitor hybrid source." ECTI Trans. Electrical Eng., Electron., and Commun., vol. 4, pp. 90-95, Aug. 2006.
- [45] R. Gaynor, F. Mueller, F. Jabbari, and J. Brouwer, "On control concepts to prevent fuel starvation in solid oxide fuel cells," J. Power Sources, vol. 180, pp. 330-342, May 2008.
- [46] M. Meiler, O. Schmid, M. Schudy, and E. P. Hofer, "Dynamic fuel cell stack model for realtime simulation based on system identification," J. Power Sources, vol. 176, pp. 523-528, Feb. 2008.
- [47] J. T. Pukrushpan, A. G. Stefanopoulou, and H. Peng, "Controlling fuel cell breathing," IEEE Control Syst. Mag., vol. 24, no. 2, pp. 30-46, Apr.
- [48] P. Thounthong, S. Raël, and B. Davat, "Fuel cell and supercapacitors for automotive hybrid electrical system," ECTI Trans. Elect. Eng., Electron. Commun., vol. 3, pp. 20-30, Feb. 2005.
- [49] A. Taniguchi, T. Akita, K. Yasuda, and Y. Miyazaki, "Analysis of electrocatalyst degradation in PEMFC caused by cell reversal during fuel starvation," J. Power Sources, vol. 130, pp. 42-49, May 2004.
- [50] P. Thounthong, "Control of fuel cell/battery hybrid source for electric vehicle applications, ECTI Trans. Elect. Eng., Electron. Commun., vol. 5, pp. 192-198, Aug. 2007.
- [51] P. Rodatz, G. Paganelli, A. Sciarretta, and L. Guzzella, "Optimal power management of

- an experimental fuel cell/supercapacitorpowered hybrid vehicle," Control Eng. Practice, vol. 13, no. 1, pp. 41-53, Jan. 2005.
- [52] P. Corbo, F. E. Corcione, F. Migliardini, and O. Veneri, "Experimental study of a fuel cell power train for road transport application," J. Power Sources, vol. 145, pp. 610-619, Aug. 2005.
- [53] P. Thounthong, S. Raël, and B. Davat, "Supercapacitors as an energy storage for fuel cell automotive hybrid electrical system." J. Elect. Eng. Transport., vol. 1, pp. 21-25, no. 1, 2005.
- [54] R. S. Gemmen, "Analysis for the effect of inverter ripple current on fuel cell operating condition,' Trans. ASME, J. Fluids Eng., vol. 125, pp. 576-585, May 2003.
- [55] W. Choi, G. Joung, P. N. Enjeti, and J. W. Howze, "An experimental evaluation of the effects of ripple current generated by the power conditioning stage on a proton exchange membrane fuel cell stack," Trans. ASME, J. Mater. Eng. Perform., vol. 13, pp. 257-264, June 2004.
- [56] A. Sakhare, A. Davari, and A. Feliachi, "Fuzzy logic control of fuel cell for stand-alone and grid connection," J. Power Sources, vol. 135, pp. 165-176, Sept. 2004.
- [57] K. Sedghisigarchi and A. Feliachi, "Dynamic and transient analysis of power distribution systems with fuel cells-Part II: control and stability enhancement," IEEE Trans. Energy Conversion, vol. 19, pp. 429-434, June 2004.
- [58] D. B. Nelson, M. H. Nehrir, and V. Gerez, "Economic evaluation of grid-connected fuel-cell systems," IEEE Trans. Energy Conversion, vol. 20, pp. 452-458, June 2005.
- [59] P. Thounthong and B. Davat, "A PEM fuel cell power source for electric vehicle applications with supercapacitor or battery as auxiliary," in Progress in Fuel Cell Research, P. V. Alemo, Ed. Commack, NY: Nova, 2007, ch. 8.
- [60] S. M. Lukic, J. Cao, R. C. Bansal, F. Rodriguez, and A. Emadi, "Energy storage systems for automotive applications," IEEE Trans. Ind. Electron., vol. 55, pp. 2258-2267. June 2008.
- [61] M. J. Kim and H. Peng, "Power management and design optimization of fuel cell/battery hybrid vehicles," J. Power Sources, vol. 165, pp. 819-832, Mar. 2007.
- [62] R. Lallemand, A. De Bernardinis, G. Coquery, J. P. Ousten, S. Raël, and B. Davat, "Active load for fuel cell system dedicated to transportation applications," in Proc. EPE'03, Toulouse, France, Oct. 2003.
- [63] T. Furuya, K. Kondo, and T. Yamamoto, "Experimental study on a PEMFC fed railway vehicle motor drive system," in Proc. 41st IEEE-IAS, 8-12 Oct. 2006, pp. 1249-1252.
- [64] T. Montani, "Electric energy storage evaluation for urban rail vehicles," in Proc. EPE'03, Toulouse, France, Oct. 2003.
- [65] L. U. Gökdere, K. Benlyazid, R. A. Dougal, E. Santi, and C. W. Brice, "A virtual prototype for a hybrid electric vehicle," Mechatronics, vol. 12, pp. 575-593, May 2002.
- [66] P. Thounthong, S. Raël, and B. Davat, "Control algorithm of fuel cell and batteries for distributed generation system," IEEE Trans. Energy Conversion, vol. 23, pp. 148-155, Mar. 2008.
- [67] J. Gonzales and G. Tamizhmani, "High efficiency fuel cell based uninterruptible power supply for digital equipment," J. Power Sources, vol. 153, pp. 151-156, Jan. 2006.
- [68] P. Corbo, F. E. Corcione, F. Migliardini, and O. Veneri, "Experimental assessment of energymanagement strategies in fuel-cell propulsion systems," J. Power Sources, vol. 157, pp. 799-808, July 2006.
- [69] A. Folkesson, C. Andersson, P. Alvfors, M. Alaküla, and L. Overgaard, "Real life testing of a hybrid PEM fuel cell bus," J. Power Sources, vol. 118, no. 1-2, pp. 349-357, May 2003.

- [70] K. S. Jeong, W. Y. Lee, and C. S. Kim, "Energy management strategies of a fuel cell/battery hybrid system using fuzzy logics," J. Power Sources, vol. 145, pp. 319-326,
- [71] P. Thounthong, S. Raël, and B. Davat, "Control strategy of fuel cell/supercapacitors hybrid power sources for electric vehicle," J. Power Sources, vol. 158, no. 1, pp. 806-814, July
- [72] R. Kötz, J. C. Sauter, P. Ruch, P. Dietrich, F. N. Büchi, P. A. Magne, and P. Varenne, "Voltage balancing: Long-term experience with the 250 V supercapacitor module of the hybrid fuel cell vehicle HY-LIGHT," J. Power Sources, vol. 174, pp. 264-271, Nov. 2007.
- [73] M. Uzunoglu and M. S. Alam, "Dynamic modeling, design, and simulation of a combined PEM fuel cell and ultracapacitor system for standalone residential applications," IEEE Trans. Energy Conversion, vol. 21, pp. 767-775, Sept. 2006.
- [74] T. H. Bradley, B. A. Moffitt, D. N. Mavris, and D. E. Parekh, "Development and experimental characterization of a fuel cell powered aircraft," J. Power Sources, vol. 171, pp. 793-801, Sept. 2007.
- [75] N. Lapena-Rey, J. Mosquera, E. Bataller, F. Ortı, C. Dudfield, and A. Orsillo, "Environmentally friendly power sources for aerospace applications," J. Power Sources, vol. 181, pp. 353-362, July 2008.
- [76] T. L. Cable and S. W. Sofie, "A symmetrical, planar SOFC design for NASA's high specific power density requirements," J. Power Sources, vol. 174, pp. 221-227, Nov. 2007.
- [77] A. K. Sehra and W. Whitlow, Jr., "Propulsion and power for 21st century aviation," Progress Aerosp. Sciences, vol. 40, pp. 199-235, May-July 2004.
- [78] J. Dollmayer, N. Bundschuh, and U. B. Carl, "Fuel mass penalty due to generators and fuel cells as energy source of the all-electric aircraft," Aerosp. Sci. Technol., vol. 10, pp. 686-694. Dec. 2006.
- [79] M. Granovskii, I. Dincer, and M. A. Rosen, "Economic and environmental comparison of conventional, hybrid, electric and hydrogen fuel cell vehicles," J. Power Sources, vol. 159, pp. 1186-1193, Sept. 2006.
- [80] W. Kempton and T. Kubo, "Electric-drive vehicles for peak power in Japan," Energy Policy, vol. 28, pp. 9-18, Jan. 2000.
- [81] T. Aicher, B. Lenz, F. Gschnell, U. Groos, F. Federici, L. Caprile, and L. Parodi, "Fuel processors for fuel cell APU applications," J. Power Sources, vol. 154, pp. 503-508, Mar. 2006.
- [82] O. Bitsche and G. Gutmann, "Systems for hybrid cars," J. Power Sources, vol. 127, pp. 8-15, Mar. 2004.
- [83] R. M. Moore, K.H. Hauer, S. Ramaswamy, and J. M. Cunningham, "Energy utilization and efficiency analysis for hydrogen fuel cell vehicles," J. Power Sources, vol. 159, pp. 1214-1230, Sept. 2006.
- [84] P. Fontela, A. Soria, J. Mielgo, J. F. Sierra, J. de Blas, L. Gauchia, and J. M. Martinez, "Airport electric vehicle powered by fuel cell," *J. Power* Sources, vol. 169, pp. 184-193, June 2007.
- [85] B. J. Bowers, J. L. Zhao, M. Ruffo, R. Khan, D. Dattatraya, N. Dushman, J. C. Beziat, and F. Boudjemaa, "Onboard fuel processor for PEM fuel cell vehicles," Int. J. Hydrogen Energy, vol. 32, pp. 1437-1442, July-Aug. 2007.
- [86] J. Ally and T. Pryor, "Life-cycle assessment of diesel, natural gas and hydrogen fuel cell bus transportation systems," J. Power Sources, vol. 170, pp. 401-411, July 2007.